Ionic conduction in layered double hydroxides and application to electrochemical devices

(層状複水酸化物のイオン伝導性評価と電気化学デバイスへの応用)

令和 2 年度　博士論文

北海道大学　大学院

総合化学院総合化学専攻　博士後期課程

無機合成化学研究室

窪　大樹

Index

Chapter 1

General Introduction

1. General Introduction

1.1 Background

In recent years, the energy problem has become more serious with the rapid economic development. The present energy consumption which is dependent on fossil fuels is estimated to be exhausted within a few decades and countermeasures against resource depletion are urgently needed. On the other hand, it is highly likely that global warming is caused by an increase in CO_2 and other greenhouse gases due to human activities, and it has become a problem common to all humanity. These energy and environmental issues are closely intertwined with economic growth, and humanity is now faced with three very difficult and conflicting issues: conservation of the environment, energy supply, and economic growth. In order to solve these problems, the development of clean energy sources that do not emit greenhouse gases and can generate electricity or thermal energy has received attention in recent years. In particular, fuel cells are received attention as one of these clean energy sources. A fuel cell is a type of power generation device that converts fuel and air into electricity. Fuel cells are of interest for the following three reasons.

(1) Fuel cells are highly efficient in converting chemical energy into electrical energy, and an even higher overall fuel use efficiency can be expected from cogeneration, which uses waste heat, or from combined cycle power generation, which uses high-temperature waste heat to power a turbine. Conventional power generation systems (thermal power generation) use combustion to convert the chemical energy in the fuel into thermal energy, which is then converted into mechanical energy and then into electrical energy,

resulting in a low conversion efficiency of less than 50%. The theoretical power generation efficiency of fuel cells (about 70%) is high in comparison.

(2) Fuel cells using hydrogen as fuel do not emit air pollutants such as (NOx) and sulfur oxides (SOx) or carbon dioxide (CO_2), a greenhouse gas, and the only thing emitted is water, which is good for the earth's environment.

(3) Fuel cells have no pistons, turbines, or other mechanical mechanisms, and thus they are low-noise. In addition to these advantages, fuel cells are expected to be a distributed power supply that can be expected to provide a certain degree of power supply even when the power network is shut down by a disaster.

1.2 Type of Fuel cells and advantages of alkaline fuel cells

Fuel cells are classified according to their operating temperature and the type of electrolyte. There are various types of fuel cells, such as Alkaline fuel cells (AFC) using a hydroxide ion conducting materials as electrolyte, solid polymer electrolyte (PEFC, PEMFC) using a proton conducting cation exchange membrane, phosphoric acid fuel cells (PAFC) using high temperature phosphoric acid, solid oxide fuel cells (SOFC) using oxide ion conducting ceramics. In addition to these, there are direct alcohol fuel cells (DAFCs) that are directly fueled by alcohol such as methanol and ethanol.

The PEFC is one of the most promising fuel cells for home and automotive use. PEFCs have the advantages of a low operating temperature of around 80 °C, small size, and high output. PEFCs have already

launched as a household cogeneration system and fuel cell vehicles. However, there are many challenges for the practical application of PEFCs, such as high cost of using highly corrosion-resistant Pt catalyst and perfluorinated polymers (Nafion®) as electrolyte, degradation of the anode catalyst due to CO poisoning, and corrosion of carbon using as the catalyst support at the cathode. Various efforts have been made to resolve these issues [1-5].

There have been many reports on the use of alloy catalysts to reduce the amount of platinum use, especially on Pt-Ru alloy catalysts [6, 7]. Pt-Ru alloy catalysts can reduce the amount of platinum use, and Ru plays a role in oxidizing CO, reducing the effect of CO poisoning and improving the oxidation of fuel. It has been reported to improve the activity of the catalyst. TiOx and metal oxide materials, for example, has been proposed as an alternative material to carbon as a catalyst support. Metal oxide materials are inexpensive, stable under acidic conditions, and this intermediate layer of TiO_2, TiOx, exhibits high electronic conductivity, making it a promising alternative to carbon [8, 9]. However, the leaching of Ru and the difficulty in synthesizing titanium dioxide with a large specific surface area remain challenges, and these alternative materials have not yet been commercialized.

On the other hand, SOFCs have received much attention in recent years as a household fuel cell. In addition, SOFC has the advantage of not requiring a catalyst, the possibility of use of even CO as a fuel due to its high operating temperature of 800~1000 °C. However, it has disadvantages such as long start-up time and low power density per volume due to its high temperature operation. To solve these problems, research

towards low-temperature operation of SOFCs has been actively conducted, and recently, Ding et al. have reported that SOFCs consisting of thin electrolyte films and cathodes with nanostructures operated at low temperatures of 450-600 °C [10]. Further efforts towards low temperature operation should be made in the future due to problems such as interdiffusion of constituent elements at the electrode-electrolyte interface and degradation due to strains and cracks caused by the different thermal expansion coefficients of the cell components [11, 12].

AFCs have many advantages, compared with PEFCs and SOFCs. AFCs were historically used as a power source for space exploration early on. AFCs have received renewed attention in recent years as a solution to the problems in PEFCs and SOFCs as lower operating power supply. Alkaline atmospheres have higher electrochemical reaction rates at the anode and cathode than acidic atmosphere. It is not necessary to use platinum catalysts in AFCs, but non-precious metal catalysts such as Mn, Ni, Ag, etc. can be used in AFCs. Especially for the cathode, carbon materials such as graphene and carbon nanotubes have catalytic activity for the oxygen reduction reaction and can be used as a catalyst in alkaline atmosphere, and also reduce the concern of corrosion compared to in acidic atmosphere. From the above, it is expected to expand the range of electrode material selection in AFCs [13-21]. The alkaline atmosphere also has the advantage of lowering the overvoltage due to the higher oxygen reduction reaction rate compared to the acidic atmosphere [22]. Consequently, non-noble metals or inexpensive metal oxides can be used as catalysts. Furthermore, the range of fuel selection is also wide in alkaline atmosphere, since the oxidation reaction rate of the alcohol

used as fuel is also greater in alkaline atmospheres compared to acidic atmospheres. Ogumi et al. have reported the preparation of AFCs using methanol, ethylene glycol, glycerol, erythritol, and xylitol as fuels, and all of them have been reported to be capable of generating electricity [23]. Asazawa et al. have reported that AFCs using hydrazine as a fuel and non-precious metal catalyst as a catalyst showed a high power output of more than 500 mW cm^{-2}, and Lue et al. have reported that AFCs using methanol as a fuel showed a high power density of 67.5 mW cm^{-2}. Gao et al. have developed highly efficient electrocatalysts for ethylene glycol oxidation for direct alcohol fuel cell using non-noble catalyst [24-27]. However, in these cases, the reaction of alkali metal cations in the alkaline electrolyte with CO_2 in the air causes carbonate precipitation in electrolyte and electrode, which leads to the inhibition of gas diffusion on the electrodes, resulting that the degradation of the cell performance is caused [28-30].

1.3 Electrochemical devices using alkaline electrolyte

Alkaline-type electrochemical devices using Zn, Ni, and Mg are also attracting attention from the perspective of low cost and resources. In particular, zinc is expected to be used in mobile devices due to its economy, safety and lightness of air batteries. Again, however, the following problems have been identified because the electrolyte is an aqueous solution;

(1) Water volatilization degrades the electrolyte,

(2) The alkaline nature of the electrolyte causes zinc oxide to react with carbon dioxide in the air, which

reduces the performance of the electrode, and

(3) dendrites, which are dendritic projections, are generated at the anode, which can be a problem during charging [31-36].

To solve these problems, alkaline-type electrochemical devices using solid electrolytes, which do not contain alkali metal cations and are considered to be less sensitive to the effects of CO_2 in the air, instead of alkaline aqueous solutions, have been especially studied in recent years. Ueda et al. have reported that the layered oxides such as $NaCoO_2$ and $KCoO_2$ have hydroxide ion conductivity, and maximum power densities of more than 60 mW cm^{-2} were observed in non-platinum-catalyzed anodes, carbon-only cathodes, and $NaCoO_2$ fuel cells under humidified conditions [37-39]. Hibino et al. have reported that Sb^{5+}-doped SnP_2O_7 showed high ionic conductivity on the order of 10^{-2} S cm^{-1} under humidification, and an AFC using it as a solid electrolyte showed a maximum power density of more than 70 mW cm^{-2} at 200 °C in the medium temperature range[40-42]. Xu et. al. have proposed new-type electrolyte for dendrite-free Zn-air rechargeable batteries[43]. The solid-state molten hydrate electrolyte is composed of inorganic Zn salt and water and the cell using the electrolyte exhibits a reversible capacity of 1000 mAh g $(catalyst)^{-1}$ over 100 cycles at 30 °C .

However, the solid hydroxide-ion-conductive solid electrolytes still have some problems, such as (1) low hydroxide ion conductivity and (2) difficulty in constructing a good three-phase boundary.

1.4. Layered double hydroxides (LDHs)

The author has focused attention on layered double hydroxides (LDHs) as an ion conducting material. LDHs are anionic clay and the general formula for LDHs is $[M^{II}_{1-x} M^{III}_x(OH)_2][(A^{n-})_{x/n} \cdot mH_2O]$, where M^{II} is a divalent cation such as Ni^{2+}, Mg^{2+}, Zn^{2+}, etc., and M^{III} is a trivalent cation such as Al^{3+}, Fe^{3+}, Cr^{3+}, etc., and A^{n-} is an anion such as CO_3^{2-}, Cl^-, OH^-, etc. In LDHs, divalent cations in the hydroxide layer are replaced with trivalent cation and the replacement of divalent cation with trivalent cation generates a positive charge on the hydroxide layers of LDHs. LDHs consist of the positively charged metal hydroxide layers with anions located in the interlayer space for charge compensation of the cationic layers as shown in Fig.1.

LDHs has many advantages such as anion exchange capacity, variety of compositions, and easy synthesis, and thus LDHs have attracted much attention for various use in a variety of fields, such as catalysts, anion exchange materials and anion conducting materials [44-48]. For example, Besse et al. have reported the ionic conductivity of Zn-Cr-based LDH and Yamazaki et al. have reported the ionic conductivity of Mg-Al-based LDH in the medium temperature range. Ma et al. have reported that LDH single-layer nanosheet exhibited high in-plane conductivities approaching 10^{-1} S cm^{-1} [49-51]. The inorganic chemistry group in Osaka Prefecture University reported hydroxide ion conduction of LDHs and the cell performance of alkaline fuel cell using LDHs as electrolyte [52-54]. Although the ionic conductivity in LDHs has not been well-known yet, LDHs are considered to be a very attractive material for solid electrolytes because of its

high formability, heat resistance and durability. Meanwhile, it has been reported that LDHs containing transition metals has high activity against methanol oxidation and oxygen reaction and may exhibit the electric conductivity [55-60]. Thus, when LDHs are mixed as an ionomer in the electrode layer into the electrocatalytic layer, the use of LDHs containing transition metals may add other functions such as catalytic activity in addition to its effect as an ionomer, which may contribute to further performance improvement.

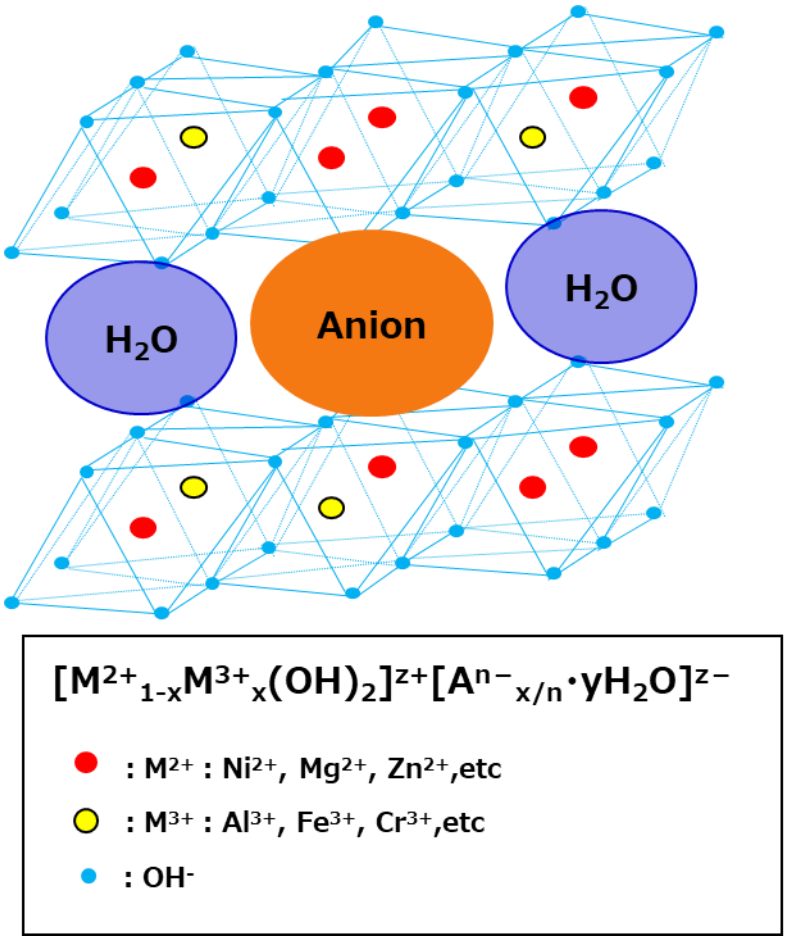

Fig.1 Schematic structure of layered double hydroxide(LDH).

1.5 Aim and outline of the present study

From these perspectives, the present study is concerned with the ionic conduction behavior of LDHs, the application of LDHs to solid electrolytes, and the application of LDHs to ionomers for alkaline fuel cells, with a focus on transition metal-containing LDHs.

This dissertation consists of the following four chapters.

Chapter 1 describes the background and purpose of the study.

In Chapter 2, the ionic conductivity of LDHs was investigated. The effects of interlayer anions and the cationic species of the hydroxide layer on the ionic conductivity of the hydroxide were investigated. In addition to the ionic conductivity, the high entropy LDH was synthesized and its thermal stability was evaluated as reported for the high entropy alloys. In order to investigate the ionic conduction behavior in detail, it is common to replace some of the deuterium in proton conductors to investigate the electrical conductivity and the distribution of the deuterium. Therefore, the ionic conduction pathway in LDHs is investigated by synthesizing LDHs containing D_2O by the reconstruction method and investigating the vibrational mode of O-D, which is considered to be a mobile ionic species, by using FT-IR [61-64].

In Chapter 3, the application of LDHs as an electrolyte and ionomer for alkaline fuel cells was examined; alkaline fuel cells using LDHs as a solid electrolyte were fabricated and the power generation behavior of hydrogen-oxygen fuel cells and direct alcohol fuel cells were investigated. In addition, a thin inorganic solid electrolyte membrane is essential for the fabrication of an AFC with high power. The preparation of thin membranes of the electrolyte was examined by using a support structure. Furthermore,

the effect of the LDHs addition to the catalyst layer on the power generation characteristics of the fuel cell was investigated. Alkaline metal-air batteries were also investigated as other alkaline electrochemical devices [65-67], and their performances were evaluated.

Chapter 4 summarizes this work, and some challenges and future prospects in the development of LDHs as hydroxide ion conductor and application of LDHs electrochemical devices are discussed.

Reference

[1] T. Wilberforce, A. Alaswad, A. Palumbo, M. Dassist, and A. G. Olabi, *Int. J. Hydrogen Energy*, **41** (2016) 16509-16522.

[2] H. Zhang, and P. K. Shen, *Chem. Rev.*, **112** (2012) 2780-2832.

[3] S. Maass, F. Finsterwalder, G. Frank, R. Hartmann, and C. Merten, *J. Power Sources*, **176** (2008) 444-451.

[4] R. Borup, J. Meyers, B. Pivovar, Y. S. Kim, R. Mukundan, N. Garland, D. Myers, M. Wilson, F. Garzon, D. Wood, P. Zelenay, K. More, K. Stroh, T. Zawodzinski, J. Boncella, J. E. McGrath, M. Inaba, K. Miyatake, M. Hori, K. Ota, Z. Ogumi, S. Miyata, A. Nishikata, Z. Siroma, Y. Uchimoto, K. Yasuda, K. Kimijima, and N. Iwashita, *Chem. Rev.*, **107** (2007) 3904-3951.

[5] A. Brouzgou, S. Q. Song, and P. Tsiakaras, *Appl. Catal. B*, **127** (2012) 371-388.

[6] A. S. Arico, P. Creti, H. Kim, R. Mategna, N. Giordano, and V. Antonucci, *J. Electrochem. Soc.*, **143** (12) (1996) 3950-3959.

[7] F. B. Mongeot, M. Scherer, B. Gleich, E. Kopatzki, R. J. Behm, *Sur. Sci.*, **411** (1998) 249-262.

[8] T. Ioroi, Z. Siroma, S. Yamazai, and K. Yasuda, *Adv. Energy. Mater.*, **9** (2019) 1801284.

[9] Z. Zhang, J. Liu, J. Gu, L. Su, and L. Cheng, *Energy Environ. Sci.*, **7** (2014) 2535.

[10] C. Ding, T. Hashida, *Ener. Environ. Sci.*, **3** (2010) 1729-1731.

[11] T. Hibino, A. Hashimoto, T. Inoue, J. Tokuno, S. Yoshida and M. Sano, *Science*, **288** (2000) 2031-2033.

[12] R. Doshi, V. L. Richards, J. D. Carter, X. Wang and M. Krumpelt, *J. Electrochem. Soc*., **146(4)** (1999) 1273-1278.

[13] H. Peng, Q. Li, M. Hu, L. Xiao, J. Lu, L. Zhuang, *J. Power Sources*, **390** (2018) 165-167.

[14] H. Erikson, A. Sarapuu, and K. Tammeveski, *ChemElectroChem*, **6** (2019) 73-86.

[15] E. S. Davydova, F. D. Speck, M. T. Y. Paul. D. R. Dekel, and S. Cherevko, *ACS Catal.*, **9** (2019) 6837-6845.

[16] M. A. A. Rahim, R. M. A. Hameed, M. W. Khalil, *J. Power Sources*, **134** (2004) 160-169.

[17] J. Yang, J. J. Xu, *Electrochem. Commun.*, **5** (2003) 306-311.

[18] N. Wagner, M. Schulze, E. Gulzow, *J. Power Sources*, **127** (2004) 264-272.

[19] A. Nakamura, H. Takahashi, T. Takeguchi, T. Yamanaka, Q. Wang, Y. Uchimoto, and W. Ueda, *ECS Trans*, **33(1)** (2010) 1817-1821.

[20] J. J. Wilkinson, B. Stoffell, C. C. Wilkinson, T. E. Jeffries, M. S. Appold, *Science*, **323** (2009) 764-765.

[21] L. Qu, Y. Liu, J.-B. Baek, and L. Dai, *ACS Nano*, **4(3)** (2010) 1321-1326.

[22] R. S. Jayashree, D. Egas, J. S. Spendelow, D. Natarajan, L. J. Markoski, and P. J. A. Keins, *Electrochem. Solid-State Lett.*, **9(5)** (2006) A252-A256.

[23] K. Matsuoka, Y. Iriyama, T. Abe, M. Matsuoka, Z. Ogumi, *J. Power Sources*, **150** (2005) 27-31.

[24] K. Asazawa, T. Sakamoto, S. Yamaguchi, K. Yamada, H. Fujikawa, H. Tanaka, and K. Oguro, *J.*

Electrochem. Soc., **156(4)** (2009) B509-B512.

[25] P. C. Li, G. M. Liao, S. R. Kumar, C. M. Shih, C. C. Yang, D. M. Wang, and S. J. Lue, *Electrochim. Acta*, **187** (2016) 616-628.

[26] Q. Tan, C. Shu, J. Abbott, Q. Zhao, L. Liu, T. Qu, Y. Chen, H. Zhu, Y. Liu, and G. Wu, *ACS Catal.,* **9** (2019) 6362-6371.

[27] F. Gao, Y. Zhang, O. Song, J. Wang, C. Wang, J. Guo, and Y. Du, *J. Power Sources,* **418** (2019) 186-192.

[28] E. Gulzow, M. Schulze, *J. Power Source,* **127** (2004) 243-251.

[29] G. Merle, M. Wessling, K. Nijmeijer, *J. Mem. Sci.,* **377** (2011) 1-35.

[30] K. Matsuoka, Y. Iriyama, T. Abe, M. Matsuoka, Z. Ogumi, *J. Power Source,* **150** (2005) 27-31.

[31] N. Zhang, F. Cheng, J. Liu, L. Wang, X. Lomg, X. Liu, F. Li, and J. Chen, *Nat. Commun.,* **8** (2017) 405.

[32] J. F. Parker, C. N. Chervin, I. R. Pala, M. Machler, M. F. Burz, J. W. Lomg, and D. R. Rolison, *Science,* **356** (2017) 415-418.

[33] X. Wang, F. Wang, L. Wang, M. Li, Y. Wang, B. Chen, Y. Zhu, L. Zha, L. Zhang, Y. Wu, and W. Huang, *Adv. Mater*., **28** (2016) 4904-4911.

[34] P. Gu, M. Zheng, Q. Zhao, X. Xiao, H. Xue, and H. Pang, *J. Mater. Chem. A*, **5** (2017) 7651.

[35] A. R. Mainar, O. Leonet, M. Bengoechea, I. Boyano, I. de Meatza, A. Kvasha, A. Guerfi, and J. A.

Blazquez, *Int. J. Energy Res.*, **40** (2016) 1032-1049.

[36] D. Lee, J. Fu, M. G. Park, and H. Liu, *Nano Lett.*, **16** (2016) 1794-1802.

[37] T. Takeguchi, H. Takahashi, T. Yamanaka, A. Nakamura, and W. Ueda, *ECS Trans.*, **33(1)** (2010) 1847-1851.

[38] H. Takahashi, T. Takeguchi, T. Yamanaka, T. Kyomen, M. Hanaya, and W. Ueda, *ECS Trans.*, **33(1)** (2010) 1861-1866.

[39] M. Matsuda, T. Murota, H. Takahashi, T. Takeguchi, and W. Ueda, *ECS Trans.*, **33(1)** (2010) 1831-1836.

[40] T. Hibino, Y. Shen, M. Nishida, and M. Nagao, *Angew. Commun.*, **51** (2012) 10786-10790.

[41] T. Hibino, K. Kobayashi, *J. Mater. Chem. A,* **1** (2013) 1134.

[42] T. Hibino, K. Kobayashi, *J. Mater. Chem. A,* **1** (2013) 6934.

[43] C. Y. Chen, K. Matsumoto, K. Kubota, R. Hagiwara, and Q. Xu, *Adv. Energy Mater.,* **9** (2019) 1900196.

[44] EL. Crepaldi, PC. Pavan, JB. Valim, *J. Mater. Chem*., **10**, (1337-1343), (2000).

[45] A.C.S. Alĉantara, P. Aranda, M. Ddader, E. Ruiz-Hitzky, *J. Mater. Chem.*, **20**, (9495-9504), (2010).

[46] X. Guo, F. Zhang, D.G. Evans, X. Duan, *Chem. Commun.,* **46**, (5197-5210), (2010).

[47] F. Song, X. Hu, *J. Am. Chem. Soc.*, **136**, (16481-16484), (2014).

[48] A. Clearfield, M. Kieke, J. Kwan, J.L. Colon, R.C. Wang, *J. Incl. Phenom. Mol. Recog. Chem.*, **11**, (361-378), (1991).

[49] A. D, Roy, J. P. Besse, *Solid State Ionics*, **46** (1991) 95-101.

[50] H. Kim, Y. Yamazaki, J. Kim, T. Kudo, I. Honma, *Solid State Ionics*, **181** (2010) 883-888.

[51] P. Sun, R. Ma, X. Bai, K. Wang, H. Zhu, and T. Sasaki, *Sci. Adv.* **3** (2017) e1602629.

[52] K. Tadanaga, Y. Furukawa, A. Hayashi, M. Tatsumisago, *Adv. Mater.* **22** (2010) 4401-4403.

[53] Y. Furukawa, K. Tadanaga, A. Hayashi, M. Tatsumisago, *Solid State Ionics* **192** (2011) 185-187.

[54] K. Tadanaga, Y. Furukawa, A. Hayashi, M. Tatsumisago, *J. Electrochem. Soc.*, **159(4)** (2012) B368-B370.

[55] Y. Wang, D. Zhang, W. Peng, L. Liu, and M. Li, *Electrochim. Acta,* **56** (2011) 5754-5758.

[56] Y. Wang, D. Zhang, W. Peng, M. Tang, S. Xu, and M. Li, *Electrochim. Acta,* **55** (2010) 4045-4049.

[57] H. Lin, Y. Zhang, G. Wang, and J. Li, *Front. Mater. Sci.,* **6(2)** (2012) 142-148.

[58] V. R. Choudhary, D. K. Dumbre, B. S. Uphade, V. S. Narkhede, J. Mol. Catal. A, 215 (2004) 129-135.

[59] M. Y. Wu, J. M. Wang, J. Q. Zhang, and C. N. Cao, *J. Solid State Electrochem.* **10** (2006) 411-415.

[60] Y. L. Zhao, J. M. Wang, H. Chen, T. Pan, J. Q. Zhang, and C. N. Cao, *Electrochem. Acta* **50** (2004) 91-98.

[61] D. Kubo, K. Tadanaga, A. Hayashi, and M. Tatsumisago, *J. Electroanal. Chem.* **671** (2012) 102-105.

[62] D. Kubo, K. Igarashi, S. Ishiyama, N. C. Rosero-Navarro, A. Miura, M. Higuchi, and K. Tadanaga, *J. Ceram. Soc. Jpn.* **127** (2019) 788-792.

[63] A. Miura, S. Ishiyama, D. Kubo, N. C. Rosero-Navarro, and K. Tadanaga, *J. Ceram. Soc. Jpn.* **128**,

(2020) 336-339.

[64] D. Kubo, K. Tadanaga, A. Hayashi, M. Tatsumisago, *J. Electrochem. Sci. Techn.* (2021) Accepted for publication.

[65] D. Kubo, K. Tadanaga, A. Hayashi, and M. Tatsumisago, *J. Power Sources.* **222** (2013) 493-497.

[66] D. Kubo, K. Tadanaga, A. Hayashi, and M. Tatsumisago, *J. Mater. Chem. A.* **1** (2013) 6804-6809.

[67] D. Kubo, K. Tadanaga, A. Hayashi, and M. Tatsumisago, *Frontiers in Materials* **7** (2020) 117.

Chapter 2

Hydroxide ion conduction in layered double hydroxides and investigation of hydroxide ion conducting mechanism

Chapter 2. Hydroxide ion conduction in layered double hydroxides and investigation of hydroxide ion conducting mechanism

2.1. Introduction

Two-dimensional(2D) materials are interesting material because of their various unique characteristics. Recently, research on 2D materials such as graphene, 2D-hexagonal BN, and transition metal dichalcogenides, oxides and hydroxides with layered structure is rapidly increasing [1-6]. Among these materials, layered double hydroxides (LDHs) have attracted much attention for various use in a variety of fields, such as catalysts, anion exchange materials and anion conducting materials [7-11].

LDHs has attracted much attention as solid-state hydroxide ion conductors because solid-state LDHs which are inorganic materials are expected to have high thermal and chemical stability, and LDHs which contain no alkaline metal should have good durability to CO_2 as electrolyte. Mg-Al LDH intercalated with CO_3^{2-} has been reported to show high hydroxide ion conductivity under high relative humidity (R.H.) and can be used as the electrolyte of the alkaline-type direct ethanol fuel cells (DEFCs) and aqueous ammonia fuel cells [12-14]. LDHs are able to have various compositions, and among LDHs, LDHs containing transition metals are interesting material because of the variety of characteristics [15-17]. Especially in recent years, high-entropy alloys comprising five or more elements in near equimolar ratios have attracted much attention, because their mechanical properties, including ultrahigh fracture toughness at cryogenic

temperatures and excellent specific strength, are particularly attractive [18]. Thus, this strategy has possibility to be applied in LDHs.

For practical application of LDHs as electrolyte in alkaline fuel cells, humidity management and further thermal stability are necessary, therefore, higher ionic conduction under lower humidity and thermal stability are also required and should be improved more. Until now, LDHs interacting with moderate surfactants shows higher conductivity under a dried condition than the conductivity of Mg-Al CO_3^{2-} LDH because of their unique morphology and interaction of water molecules [19, 20]. About thermal behavior, it is reported that the thermal behavior of Mg-Fe LDH is affected by molar ratio (Mg/Fe) [21], indicating that the thermal stability is possible to control to change their composition.

To improve the hydroxide ion conduction in LDHs, the hydroxide ion conducting mechanism is necessary to understand. Recently, Sun *et al.* have reported that the hydroxide ion conduction in LDHs is anisotropic, and in-plane hydroxide ion conductivity is much higher than cross-plane conductivity [22]. Nevertheless, few reports have described investigations of ionic conductivities and ionic conduction of LDHs.

In this study, the ionic conductivity of LDHs as a solid electrolyte was examined. Using the co-precipitation method, Mg–Al LDH and Ni-Al LDH intercalated with CO_3^{2-} (Mg–Al CO_3^{2-} LDH and Ni-Al CO_3^{2-} LDH) were prepared. LDHs intercalated with Cl^-, OH^-, and dodecyl sulfate (DS) anion ($CH_3(CH_2)_{11}OSO^{3-}$) which is an organic anion known to be intercalated easily in LDHs, were prepared using anion exchange process and re-constructing process, and their ionic conductivities were investigated.

Then, high ion conductivity in high-entropy oxide solid electrolytes [23] motivates exploration of new layered hydroxides as electrolytes by the high-entropy strategy. A high-entropy layered hydroxide (HELH) in which five cations were distributed homogeneously was synthesized for the first time, and its ionic conductivity was determined.

In addition to these studies, Mg-Al CO_3^{2-} LDH (H_2O) and Mg-Al CO_3^{2-} LDH (D_2O), in which deuterium water was introduced as interlayer water molecules, were prepared for the investigation of hydroxide ion conduction mechanism. The Mg-Al system was used for this purpose because this system is the most basic composition used for LDHs studies. The transport number and ion conducting species of LDHs were investigated using the water vapor concentration cell. To investigate the carrier generation source in LDHs, the electrochemical properties for Mg-Al LDHs-related compounds, $Mg(OH)_2$, $MgCO_3$ and $Al_2(CO_3)_3$, were examined. In addition, the DC polarization behavior of Mg-Al CO_3^{2-} LDH(D_2O) was examined to discuss the ion conducting path.

2.2. Experimental

2.2.1. Preparation of LDHs

LDHs intercalated with CO_3^{2-} were prepared by using the co-precipitation method reported by Miyata

[24]. $Ni(NO_3)_2 \cdot 6H_2O$ or $Mg(NO_3)_2 \cdot 6H_2O$ and $Al(NO_3)_3 \cdot 9H_2O$ were dissolved in deionized water in a molar ratio of 3 : 1 (Ni or Mg : Al). The mixture was dropped into 0.3 M Na_2CO_3 solution with stirring at 80 °C. The reaction mixture pH was adjusted to 10 by the addition of 2 M NaOH solution and the mixture was aged at 80 °C for 17 h. Then, the resulting green precipitates were filtrated, washed with distilled water, and dried at 80 °C.

Ni-Al LDH intercalated with Cl^- (Ni-Al Cl^- LDH) was prepared by using an anion exchange process with Ni-Al CO_3^{2-} LDH as the starting materials [25]. First, Ni-Al CO_3^{2-} LDH powders were added to an aqueous solution containing 0.005 M HCl and 5 M NaCl with stirring at room temperature under N_2 flow. After stirring for 24 h, the resulting suspension was filtered and washed with deionized water under N_2 flow. The remaining precipitates were collected and immediately dried under vacuum.

Ni-Al LDH intercalated with OH^- (Ni-Al OH^- LDH) was prepared using restructuring process with Ni-Al CO_3^{2-} LDH as the starting materials [28]. First, Ni-Al CO_3^{2-} LDH powders were calcined at 500 °C for 5 h to form a mixed nickel-aluminum oxide solid solution. Then, the mixed oxide was added to deionized water under N_2 flow. After stirring at room temperature for 24 h, the resulting suspension was filtered and washed with deionized water under N_2 flow. The remaining precipitates were dried under vacuum. Mg-Al LDH intercalated with dodecyl sulfate anion was also prepared using the reconstruction process. Mg-Al CO_3^{2-} LDH was calcined at 500 °C for 5 h. Then the obtained oxide was dispersed into the 0.1 M sodium dodecyl sulfate solution. Before adding the oxide, the solution was kept at 90 °C with N_2 bubbling at the

rate of 100 mL min^{-1} for 30 min to remove dissolved CO_2 from the water. The reaction mixture was aged overnight at 80 °C. The precipitates were centrifuged, washed with decarbonated water, and dried in a vacuum.

Mg-Al CO_3^{2-} LDH (D_2O) was prepared through the reconstructing process. Mg-Al CO_3^{2-} LDH obtained by the co-precipitation process was calcined at 500 °C for 5 h to form a mixed magnesium-aluminum oxide. Then, the mixed oxide powders were dispersed in 4M Na_2CO_3-D_2O under N_2 flow. The mixed oxide was rehydrated in 4M Na_2CO_3- D_2O. The solution was stirred at R.T. for 24 h under N_2 flow condition. After stirring, the obtained powders were filtered under a N_2 flow and dried in vacuum.

2.2.2. Characterization of LDHs

X-ray diffraction (XRD) measurements were performed to identify crystalline phases. Presence of CO_3^{2-} or interlayer D_2O in the sample was confirmed using Fourier transform infrared (FT-IR) spectra. The KBr pellet technique was used for IR measurements. Differential thermal analysis and thermogravimetry (DTA-TG) were conducted using a thermal analyzer (thermo plus TG-8120; Rigaku Corp.), with a heating rate of 10 °C min^{-1} in air. The respective morphologies of the prepared LDHs were observed using a field-emission-type scanning electron microscope (FE-SEM, JSE-6300F; JEOL).

The electrical conductivities of Ni-Al LDH were investigated using impedance data in a frequency range of 1-8 x 10^6 Hz. Pellets of Ni-Al LDH for electrical conductivities were obtained by cold pressing under 200 MPa. Gold was sputtered as the electrodes on both sides of the pelletized Ni-Al LDH. The electronic

conductivity of Ni-Al CO_3^{2-} LDH was also investigated by DC polarization technique.

2.2.3. Water Vapor Concentration Cell

Conducting ion species was investigated using a water vapor concentration cell. The reaction and construction of the water vapor concentration cell have been detailed a previous paper [26]. Ni-Al CO_3^{2-} LDH, an anion exchange membrane (A202; Tokuyama Corp.) and a cation exchange membrane (Nafion 117; DuPont) were used as the electrolyte. The membranes or pelletized Ni-Al CO_3^{2-} LDH were sandwiched with a pair of Pt-loaded carbon sheets. The Pt loading amount of carbon sheet is 1.9 mg/cm^2. The electromotive force (EMF) of a cell was measured at 50 °C by exposing a flow of humidified N_2/O_2 gas to one side of the cell and dried N_2/O_2 gas to the other side.

2.3. Results and discussion

2.3.1. The effect of interlayer anion on hydroxide ion conduction

Figure 2.3.1.1 shows XRD patterns of Ni-Al LDHs intercalated with CO_3^{2-}, Cl^- and OH^-. The XRD patterns of each sample showed characteristic 003, 006 reflections attributed to the layered structure of LDHs. The basal spacing of the obtained LDHs changed as anion species changed, indicating that an interaction between hydroxide layer and intercalated anion was changed with the kind of anions. FT-IR

spectra were measured for the obtained Ni-Al LDHs to confirm the exchange of intercalated anion. Ni-Al CO_3^{2-} LDH showed a strong band at 1370 cm^{-1}, which is attributed to C-O asymmetric stretching vibration of CO_3^{2-}. On the other hand, the intensity of the band of 1370 cm^{-1} considerably decreased for LDHs obtained using anion exchange and restructuring processes. These results indicate that Ni-Al LDHs intercalated with Cl^- and OH^- were obtained.

Electrical properties of Ni-Al LDHs were determined using the impedance spectroscopy. The Nyqust plots of Ni-Al LDHs under 80 % relative humidity showed a high frequency arc and a low frequency tail. Temperature dependence of ionic conductivities for Ni-Al LDHs intercalated with CO_3^{2-}, Cl^- and OH^- under 80% relative humidity is shown in Fig. 2.3.1.2. Among them, the conductivity of Ni-Al CO_3^{2-} LDH is the highest at 80 °C under 80% relative humidity (1.3×10^{-2} S cm^{-1}), and that of Ni-Al OH^- LDH is the lowest under the same conditions (1.6×10^{-4} S cm^{-1}). These results suggest that interlayer anions themselves may not be the conducting ion species, but the difference of the conductivity for Ni-Al LDHs is related to the interaction between interlayer anions and water.

XRD patterns of the Mg-Al CO_3^{2-} LDH and Mg-Al DS LDH are shown in Fig. 2.3.1.3. The XRD patterns of both samples were attributed to the layered structure of LDHs. The peaks at around 11° and 23° can be indexed as Mg-Al CO_3^{2-} LDH [18], and 3.5° and 7° as Mg-Al DS LDH [19]. These results indicate that $CO_3^{2-}$and DS anion are intercalated in both LDHs.

Figure 2.3.1.4 presents the FT-IR spectra of Mg-Al CO_3^{2-} LDH and Mg-Al DS LDH. Mg-Al DS LDH

prepared using the reconstruction process showed peaks at 2920 and 2852 cm^{-1} attributed to C–H stretching vibration of the alkyl chain of DS anion [27], and 1203 and 1058 cm^{-1} attributed to S=O stretching vibration of DS anion [20]. These results support the XRD result showing that DS anion was intercalated to LDH. The absorption band at 1370 cm^{-1} for both samples corresponds to C–O antisymmetric stretching of CO_3^{2-} [29], which shows that Mg-Al DS LDH have a trace of CO_3^{2-} as the interlayer anion. Additionally, the peak at 3470 cm^{-1} is assigned to the OH^- group vibration of hydroxide layer. The peak at 1630 cm^{-1} is based on H_2O bending vibration of interlayer water [29].

TG-DTA was measured to investigate the thermal behavior of Mg-Al CO_3^{2-} LDH and Mg-Al DS LDH. Figure 2.3.1.5 shows TG curves of the samples, which were kept at 80 °C, 30%RH overnight before measurement. In Mg-Al CO_3^{2-} LDH, the weight loss at temperatures between room temperature and 250 °C can be assigned to the loss of the adsorbed water and interlayer water of LDHs. The weight loss at higher temperatures is assigned to the elimination of H_2O from OH groups in the inorganic layer and CO_2 from CO_3^{2-} ions [31]. Particularly, the weight loss under 120 °C is attributed to the surface water loss [31]. The weight loss of Mg-Al CO_3^{2-} LDH under 120 °C was 3.1 mass%. That of Mg-Al DS LDH was 6.3 mass%, which indicates that intercalation of DS anion enhances the amount of adsorbed surface water. In Mg-Al CO_3^{2-} LDH, the weight loss between 120 °C and 250 °C assigned to the interlayer water was 12.3 mass%. The interlayer water of Mg-Al DS LDH was not measured because the organic portion of DS anion intercalated in LDHs is removed between 150 °C and 300 °C [27]. For that reason, the ratio of interlayer

water of Mg-Al DS LDH cannot be compared with that of Mg-Al CO_3^{2-} LDH. The weight loss at temperatures higher than 300 °C, assigned to the elimination of H_2O from OH groups in the inorganic layer and CO_2 from CO_3^{2-} ions, is 24.7 mass% for Mg-Al CO_3^{2-} LDH and 13.1 mass% for Mg-Al DS LDH. The small weight loss of Mg-Al DS LDH is probably attributable to the fact that Mg-Al DS LDH contains only a trace amount of carbonate anion. Table 2. 3. 1. 1 presents the weight loss between room temperature and 120 °C, which is attributed to adsorbed water, for the samples exposed to different degrees of humidity before TG measurements. The weight loss of Mg-Al DS LDH was twice as much as that of Mg-Al CO_3^{2-} LDH at all relative humidities. The weight loss of both samples increased along with the enhancement of relative humidity. The temperature dependence of the conductivities at 80%RH is depicted in Fig. 2.3.1.6. Both Mg-Al CO_3^{2-} LDH and Mg-Al DS LDH were found to have rather high ionic conductivity.

Figure 2.3.1.7 shows ionic conductivities of samples measured at 80 °C, 30–80%RH. At all humidities except for 80 °C, 80%RH, the ionic conductivity of Mg-Al DS LDH was higher than that of Mg-Al CO_3^{2-} LDH. The difference is notable, especially at low humidity. The ionic conductivity of Mg-Al CO_3^{2-} LDH was 1.1×10^{-4} S cm^{-1}, whereas that of Mg-Al DS LDH is 7.6×10^{-4} S cm^{-1} at 80 °C, 30%RH. The difference is probably attributable to the amount of adsorbed water. The amount of the adsorbed surface water of Mg-Al DS LDH was much greater than that of Mg-Al CO_3^{2-} LDH, as confirmed by TG-DTA measurements. The adsorbed surface water is likely to play an important role in hydroxide ion conduction.

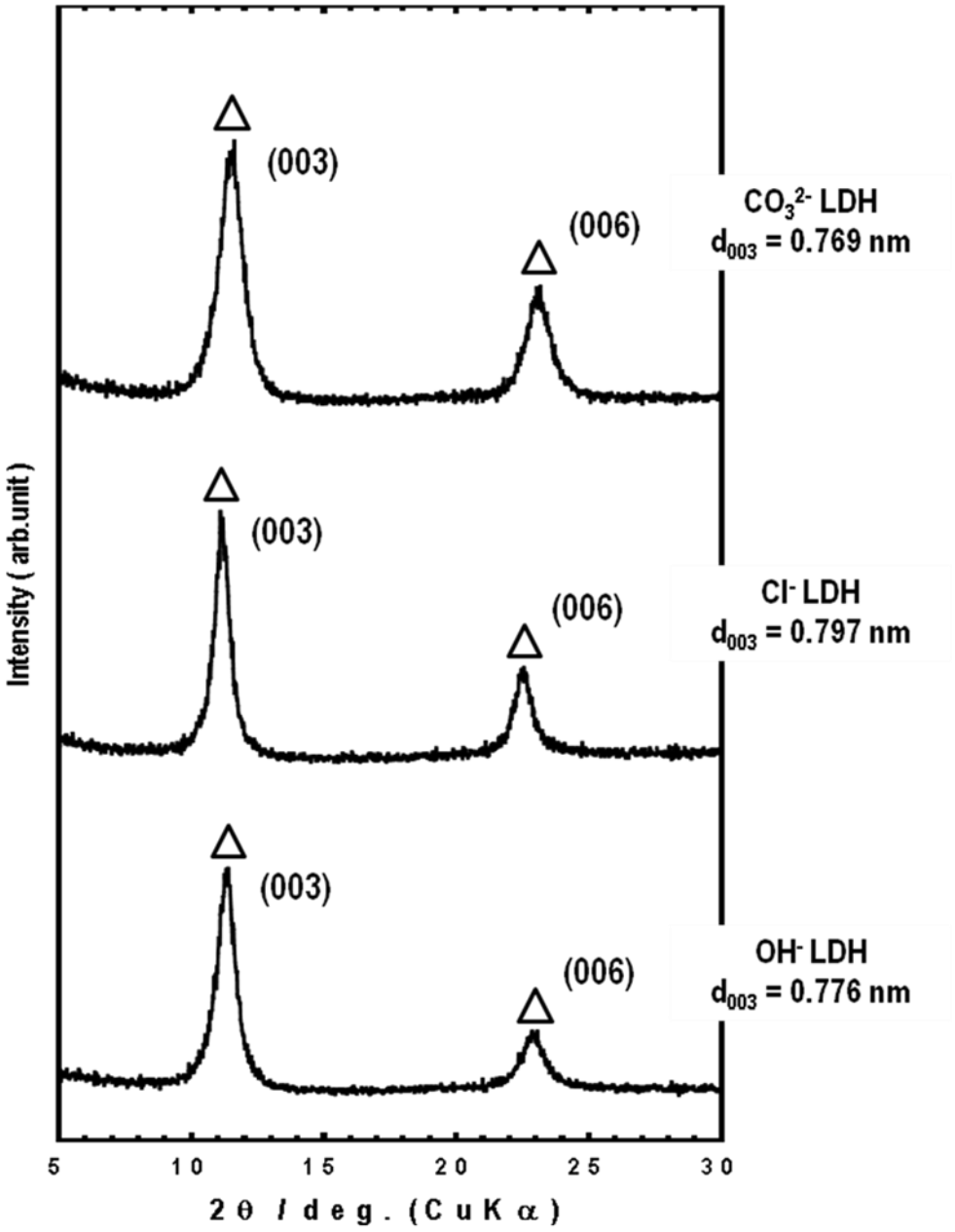

Fig.2.3.1 1 XRD patterns of the obtained Ni-Al LDHs intercalated with CO_3^{2-}, Cl^- , OH^-.

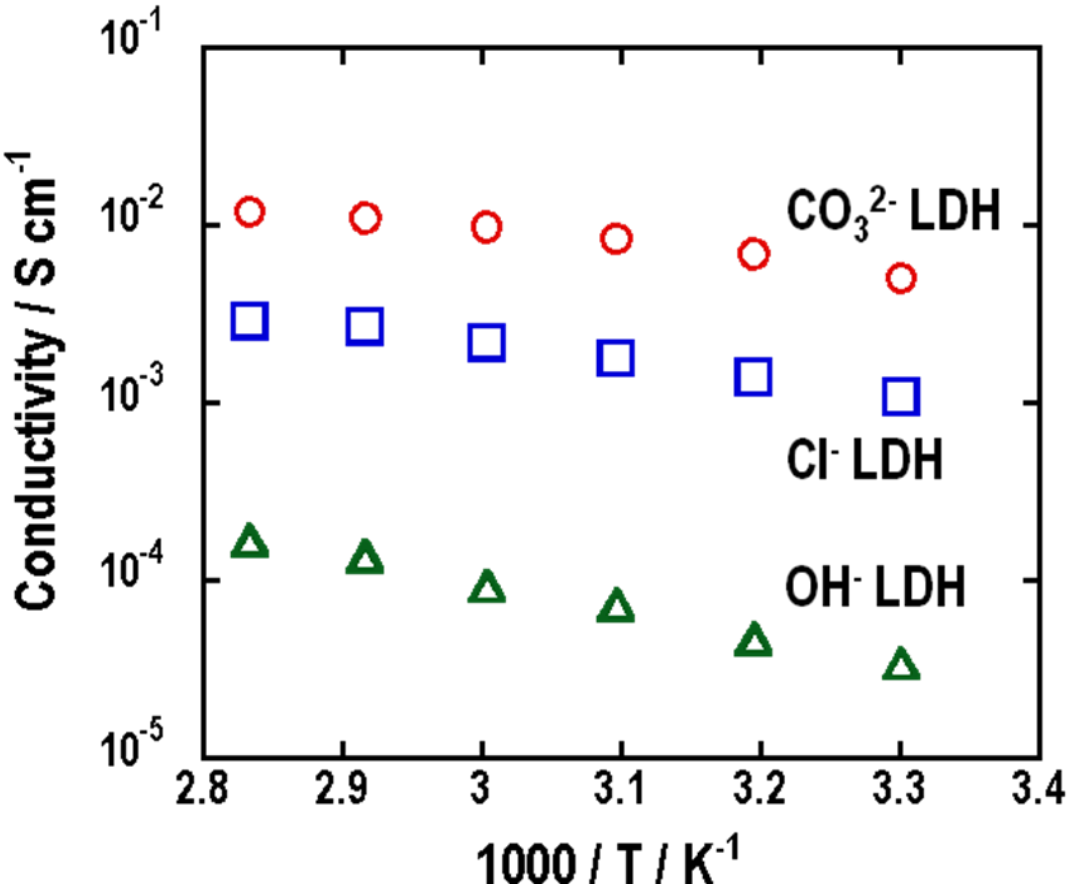

Fig. 2. 3. 1. 2 Temperature dependence of the ionic conductivity of Ni-Al LDHs intercalated with CO_3^{2-}, Cl^- and OH^-.

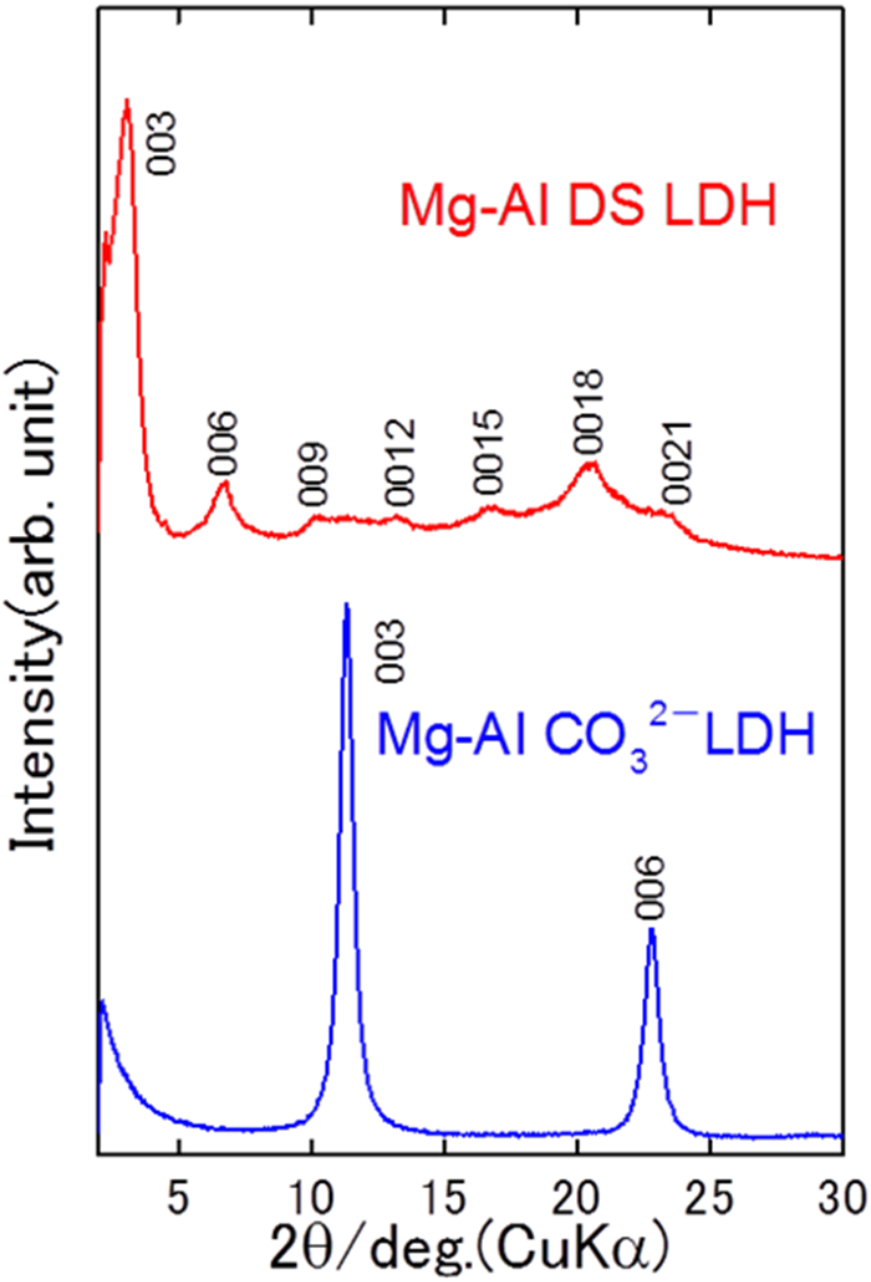

Fig. 2. 3. 1. 3　XRD patterns of the obtained Mg-Al LDHs intercalated with CO_3^{2-}, DS.

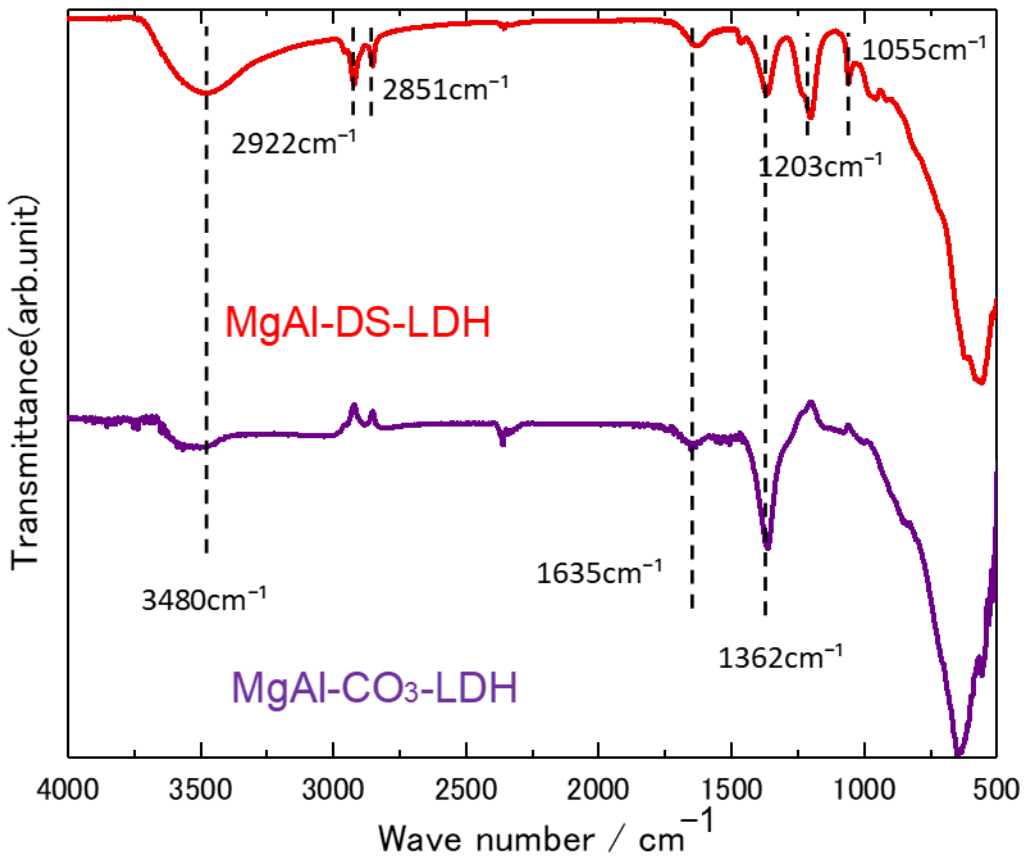

Fig.2. 3. 1. 4 FT-IR spectra of Mg-Al CO_3^{2-} LDH and Mg-Al DS LDH.

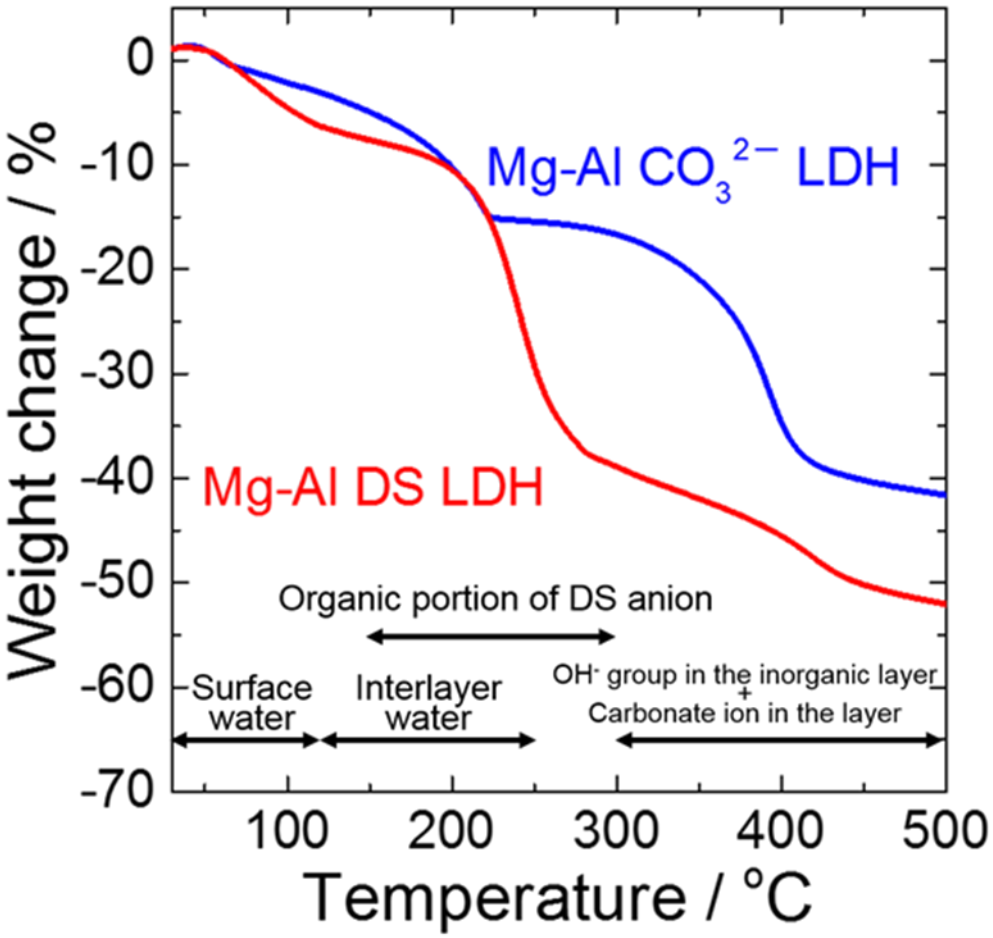

Fig.2. 3. 1. 5 TG curves of Mg-Al CO_3^{2-} LDH and Mg-Al DS LDH.

Table. 2. 3. 1. 1

Weight loss between room temperature and 120 °C of Mg-Al CO_3^{2-} LDH and Mg-Al DS LDH respectively kept at 30%, 50%, and 70% RH.

Relative humidity	30%	50%	70%
Mg-Al CO_3^{2-} LDH	3.1 %	3.3 %	3.6 %
Mg-Al DS LDH	6.3 %	6.7 %	7.2 %

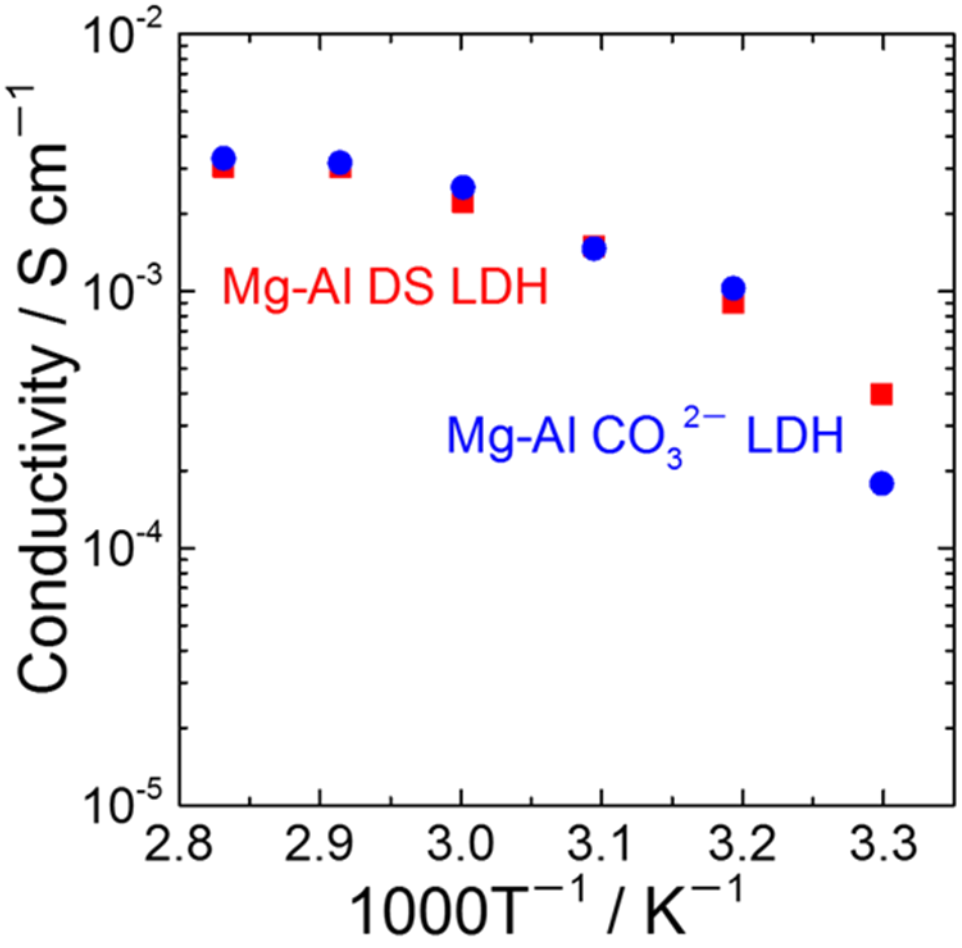

Fig.2. 3. 1. 6 Temperature dependence of the ionic conductivity at 80% RH of Mg-Al CO_3^{2-} LDH and Mg-Al DS LDH.

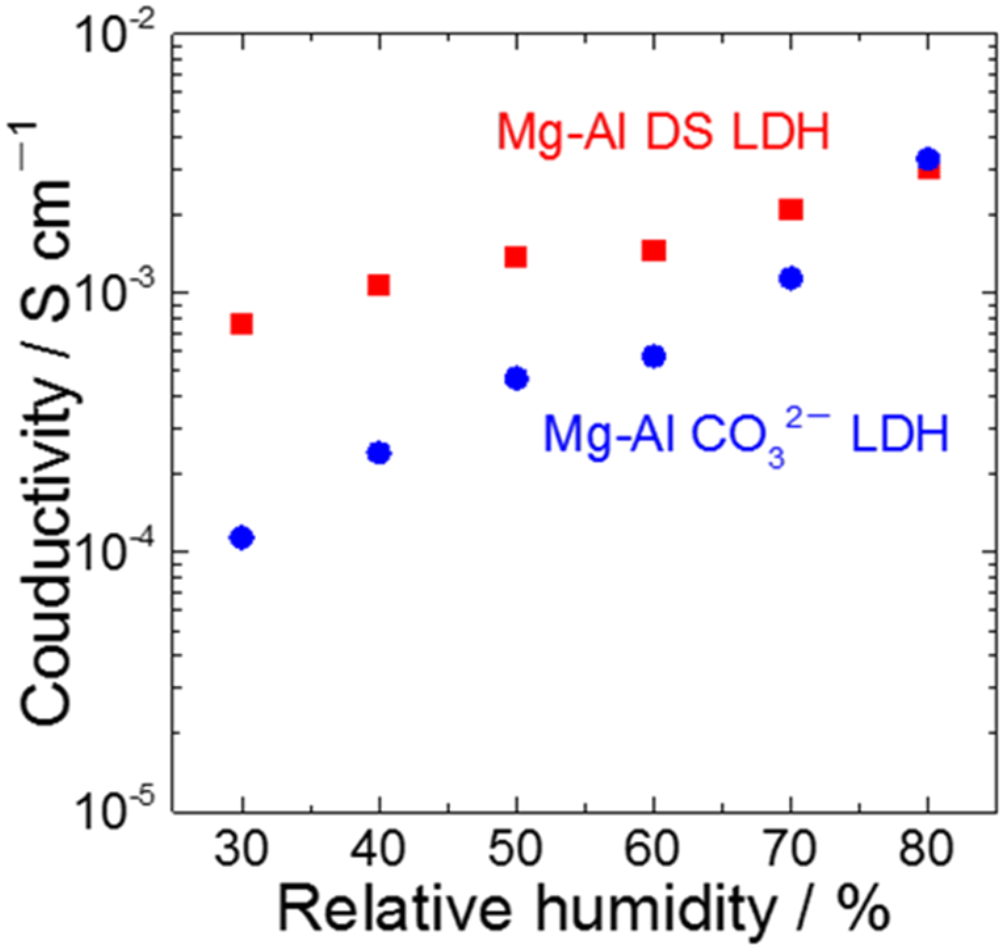

Fig.2. 3. 1. 7 Humidity dependence of the ionic conductivity at 80 ºC of Mg-Al CO_3^{2-} LDH and Mg-Al DS LDH.

2.3.2. The effect of cation of hydroxide layer on hydroxide ion conduction

The hydroxide ion conduction in LDHs is deeply related to the type of interlayer anion intercalated for the compensation of hydroxide layer. Therefore, the hydroxide layer which interacted with interlayer anion is also related to the hydroxide ion conduction. In addition to this, in recent years, high-entropy alloys, which are the alloys comprising five or more elements in near equimolar ratios is highly attracted for unique characteristics (high thermal stability and excellent specific strength). In this section, the high-entropy LDH (HELH) was synthesized and confirmed the improvement the thermal stability and hydroxide ion conduction.

Figure 2.3.2.1 shows the X-ray diffraction pattern of the synthesized HELH and its structural model. The main peaks were indexed as a hexagonal cell with the lattice parameters of a = 0.30553(6) nm and c = 2.2966(11) nm. The c-axis was shorter than that of Mg-Al LDH, as determined by the 003 diffraction peak (c = 2.34 nm). Considering the ionic radii of transition metals (Co, Ni and Zn) larger than those of Mg and Al, smaller amount of water and interlayered anions can account for shorten c-axis. Small and sharp impurity peaks were indexed as wurtzite ZnO, although the origin of two other broad peaks at 28.86° and 33.28° was not clear. It is likely that ZnO and other impurities are thermodynamically relevant to HELH, and further optimization of synthesis condition may achieve selective synthesis of HEDH [32].

The molar ratio of Mg:Al:Co:Ni:Zn was 1:1.00:0.996:0.993:1.00, which was close to the composition of the precursor solution used for its synthesis. The HELH comprised divalent Mg, Ni, Zn cations and trivalent

Al cation. The X-ray absorption spectrum of Co-K edge was close to divalent $Co(NO_3)_2$, indicating the valence of Co is close to two (Figure 2.3.2.2). Divalent Co would accompany less interlayered CO_3^{2-} when compared with trivalent Co to keep charge neutrality.

The scanning transmission electron microscopy (STEM) image showed hexagonal platelet crystals having a size of 300 nm (Figure 2.3.2.3). Energy dispersive X-ray spectrometry (EDX) mapping of each element showed a homogeneous distribution of these platelet crystals.

Figure 2.3.2.4 shows the thermogravimetric (TG) curves of HELH and some LDHs. The first and second weight losses finished at 212 and 385 °C, respectively. These weight losses corresponded to the elimination of absorbed/interlayer water and the decomposition of HELH into oxides with the evolution of gases, respectively. It is worth noting that a qualitative understanding of different LDHs is difficult since each LDH has different species of cations, anions and water. Nonetheless, a small mass loss after heating suggested a relatively small amount of water and interlayered CO_3^{2-} compared to the other LDHs. This is also supported by its short c-axis and divalent Co ion.

There was no significant improvement of its thermal stability as a result of increasing the entropy of its cation site. Since it is a common strategy to produce complex oxides and high-entropy oxide by heating hydroxides [33, 34], the product after heating of HELH is likely to be complex oxide(s) stabilized by high-entropy effect. Assuming the reaction of this HELH into a high-entropy oxide upon heat treatment in air, the entropy gain of reactant, HELH, can be canceled by that of product, high-entropy oxide. Thus, it would

be difficult to design HELH with high thermal stability via high entropy effect.

Figure 2.3.2.5 shows the temperature dependence of conductivity. The AC impedance measurements were conducted under relative humidity of 50% and 80%. The increase in temperature and relative humidity enhanced the total electrical conductivity (as measured by the AC impedance) up to 10^{-3} S cm^{-1}. The electrical conductivity measured by the DC polarization technique was 2×10^{-5} S cm^{-1} at 80 °C under 80% relative humidity. This electrical conductivity was approximately two orders of magnitude lower than the total electronical conductivity. Thus, it was concluded that ionic conduction was dominant in this HELH. The ionic conductivity of HELH was lower than that of Mg-Al LDH under 50 and 80% relative humidity. Nonetheless, the humidity dependence of conductivities on HELH was small.

Although HELH would have various local structure on 2D plain because of high-entropy cation site with five kind of metals, this HELH does not show the significant advantage of its ion conductivity. Even though the origin of conductivity is still under debate, the conductivity may be not dominantly affected by its local structure but lower contents of CO_3^{2-} and absorption water. The possible effect of impurity phase(s) on the ion conductivity cannot be denied.

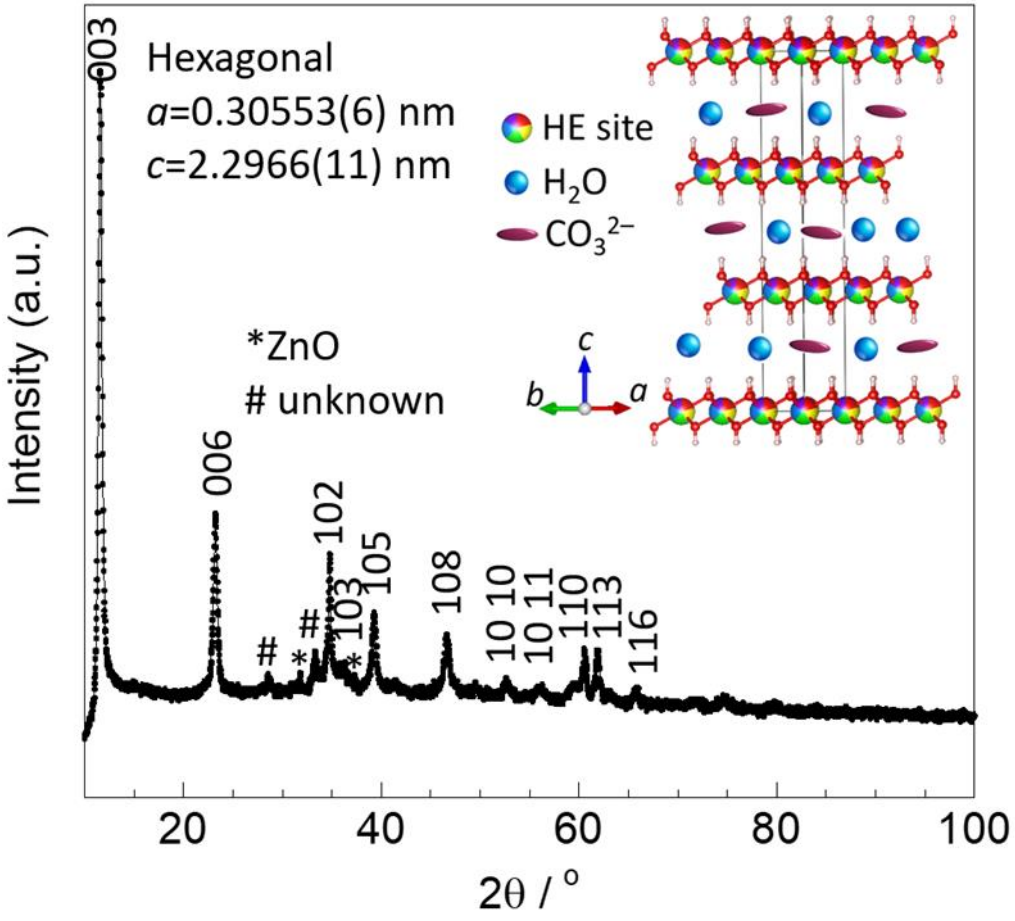

Fig.2. 3. 2. 1 X-ray diffraction pattern of the synthesized HELH.

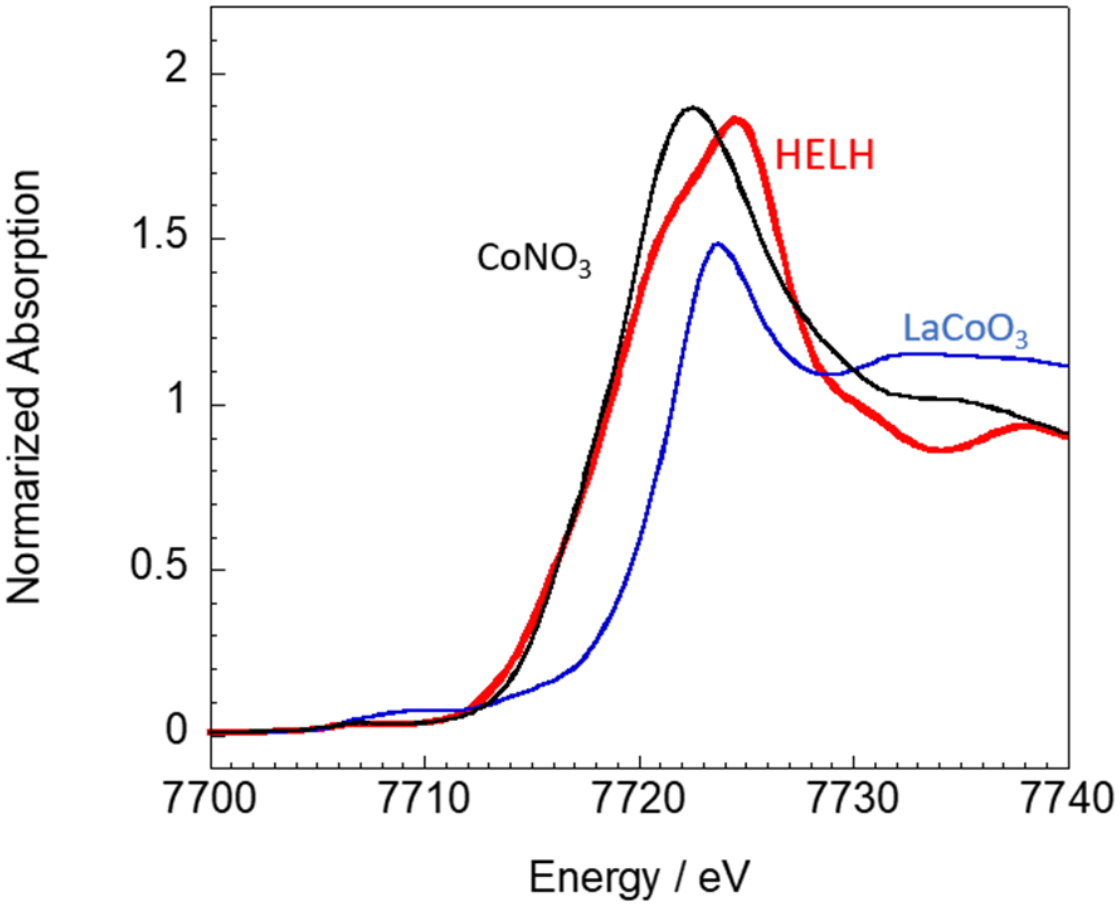

Fig.2. 3. 2. 2 X-ray absorption spectrum of Co-K edge in HELH.

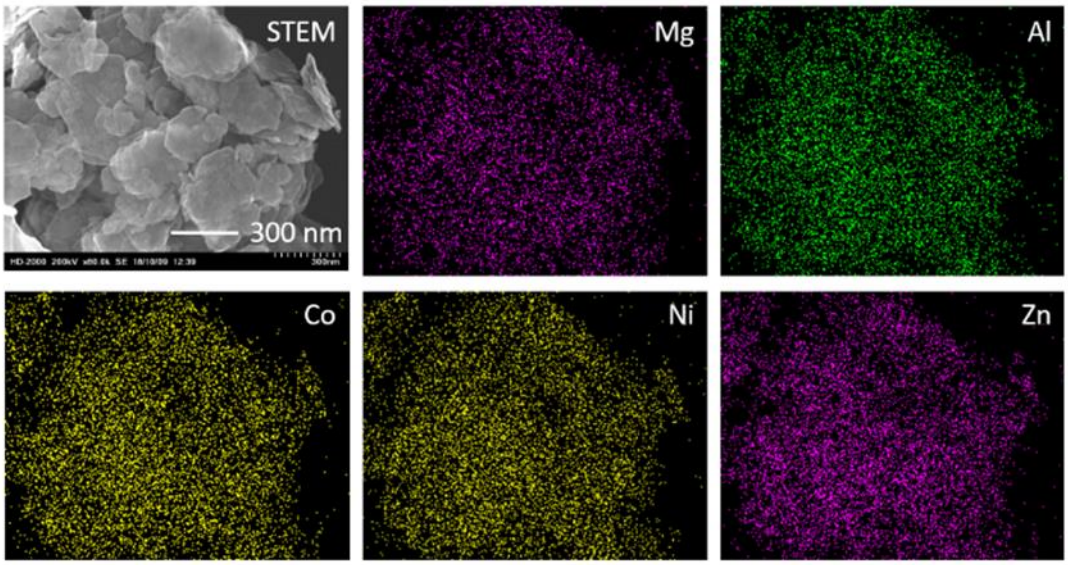

Fig.2. 3. 2. 3 STEM image and corresponding EDX mappings of the synthesized HELH.

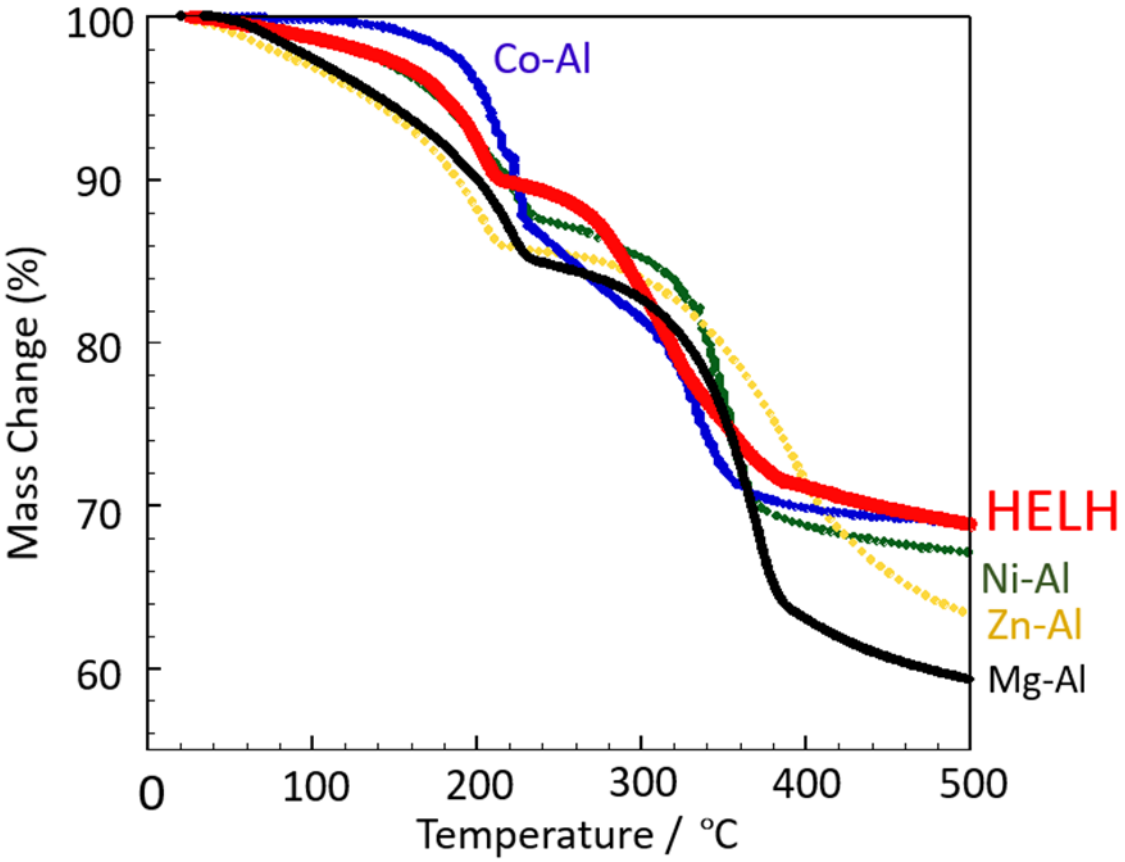

Fig.2. 3. 2. 4 TG curves of HELH at a heating rate of 10 K min^{-1} in air. Mg-Al LDH (Mg:Al = 3:1), Ni-Al LDH (Ni:Al = 2:1), Co-Al LDH (Co:Al = 2:1), and Zn-Al LDH (Zn:Al = 3:1) are shown for comparison.

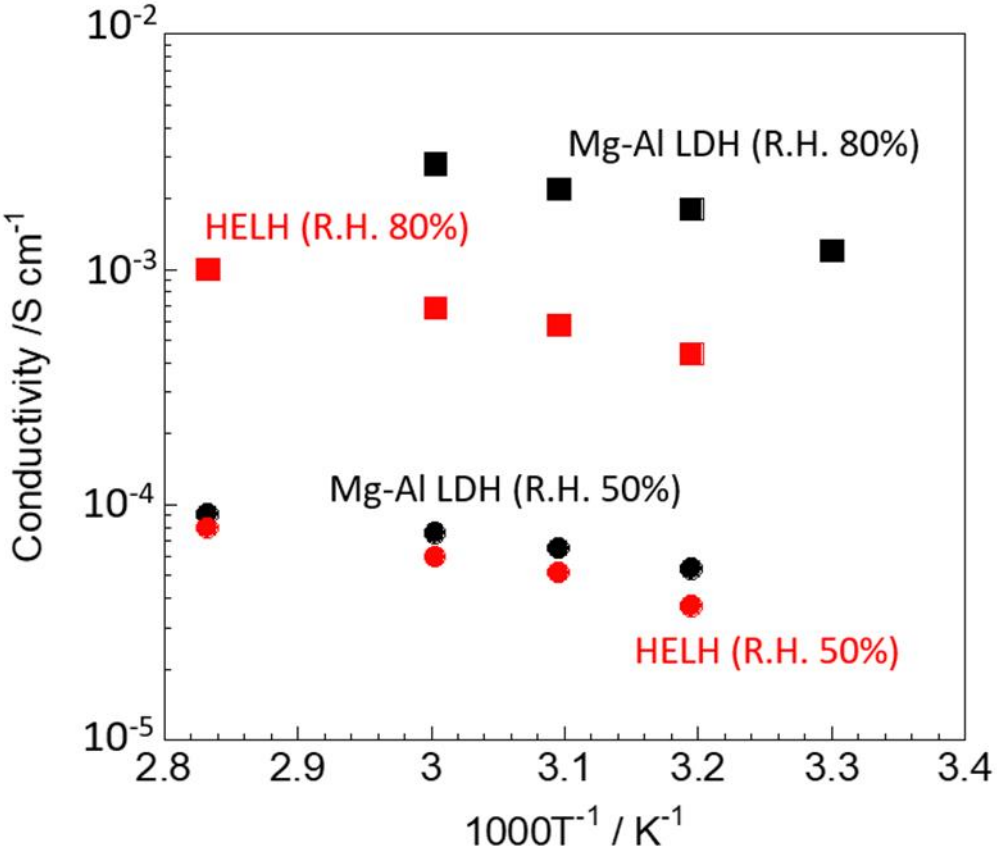

Fig.2. 3. 2. 5 Temperature dependence of conductivity of HELH and Mg-Al LDH (Mg:Al = 3:1) under different relative humidity (R.H.).

2.3.3. Investigation of the hydroxide ion conducting mechanism in LDHs

Figure 2.3.3.1 shows XRD patterns of Mg-Al CO_3^{2-} LDH (H_2O), mixed magnesium-aluminum oxide obtained by calcining Mg-Al CO_3^{2-} LDH (H_2O) at 500 °C, and restructured Mg-Al CO_3^{2-} LDH (D_2O). After the sample is calcined at 500 °C, the characteristic 003, 006 reflections based on the layered structure was disappeared, indicating that the layered structure is collapsed by calcination. The XRD patterns of Mg-Al CO_3^{2-} LDH (H_2O) and Mg-Al CO_3^{2-} LDH (D_2O) showed characteristic 003, 006 reflections. The basal spacing of Mg-Al CO_3^{2-} LDH (D_2O) is slightly larger than that of Mg-Al CO_3^{2-} LDH (H_2O), indicating that interlayer water was replaced with deuterium oxide, which is larger than water molecule.

Figure 2.3.3.2 shows TG-MS spectra of Mg-Al CO_3^{2-} LDH (D_2O) after drying at 100 °C. The weight loss at temperatures below 100 °C is assigned to the loss of the absorbed water on LDHs [30]. The weight loss at temperatures from 100 °C to 250 °C is assigned to the loss of interlayer water in LDHs, and the weight loss at higher temperature is assigned to the elimination of H_2O from OH groups in the inorganic layer and CO_2 form CO_3^{2-}. The TG-MS spectra for Mg-Al CO_3^{2-} LDH (D_2O) showed a good correlation with previous DTA-TG results. Weight loss attributed to D_2O (m/z=20) was observed from 100 °C to 250 °C and at temperatures above 250 °C. Weight loss attributed to CO_2(m/z=44) was observed at temperatures above 250 °C. On the other hand, weight loss attributed to H_2O (m/z=18) was not observed, indicating that interlayer water molecule in Mg-Al CO_3^{2-} LDH (H_2O) was replaced with D_2O and hydroxy groups in LDHs were OD groups. Thus, formation of Mg-Al CO_3^{2-} LDH (D_2O) was confirmed.

Temperature dependence of ionic conductivity for Mg-Al CO_3^{2-} LDH under 80%R.H. with H_2O and D_2O is shown in Fig. 2.3.3.3. In the measurement under D_2O, the chamber was humidified with D_2O. The ionic conductivity of Mg-Al CO_3^{2-} LDH under H_2O condition showed 2.7×10^{-3} S cm^{-1} at 80 °C. On the other hand, the ionic conductivity of Mg-Al CO_3^{2-} LDH under D_2O condition showed 2.4×10^{-3} S cm^{-1} at 80 °C. The ionic conductivity ratio is 1:0.91 (in H_2O : in D_2O). In previous reports, the ionic conductivity of LDHs is reported to depend on its their hydration state. The hydroxide ion conduction in LDHs needs humidified conditions and is supposed to be based on the Grotthuss mechanism through the water in the atmosphere. If LDHs are a proton conducting material, the ionic conductivity ratio is the same of the molecular amount: the ratio should be 1 : 0.5 (H^+ : D^+). On the other hand, if LDHs are hydroxide ion conducting material, the ionic conductivity ratio should be 1: 0.94 (OH^-: OD^-), which is in good agreement with the observed conductivity ratio. Thus, this result strongly suggests that Mg-Al CO_3^{2-} LDH is hydroxide ion conductor.

To investigate the hydroxide ion transport number, the water vapor concentration cell using Mg-Al CO_3^{2-} LDH (H_2O) as electrolyte was fabricated. As stated in previous reports, the water vapor concentration cell results proved that Mg-Al CO_3^{2-} LDH is hydroxide ion conductor [27], and the all solid-state alkaline fuel cell using Mg-Al CO_3^{2-} LDH as electrolyte was operated [14, 27]. However, the hydroxide ion transport number of LDHs has not been discussed so far. Thus, the transport number of LDHs was determined by the water vapor concentration cell with different water-vapor pressure.

The reactions for the anion (OH^-) conductor at the electrodes of water vapor concentration cell are described as follows [27].

Wet side : $2H_2O + O_2 + 4e^- \rightarrow 4OH^-$ (1)

Dry side : $4OH^- \rightarrow 2H_2O + O_2 + 4e^-$ (2)

In case that above reaction proceeds, the following Nernst equation is consisted.

$E=RT/2F \cdot \ln(pH_2O^{I}/pH_2O^{II})$ (3)

The relative humidity in dry side is controlled at 10 %R.H., and then, the EMF of the cell at each water vapor partial pressure was measured by changing the relative humidity in wet side.

Partial pressure dependence of the measured and theoretical EMF of the water vapor concentration cell using Mg-Al CO_3^{2-} LDH as electrolyte is shown in Fig. 2.3.3.4. The measured EMF of the cell showed the same trend as the theoretical EMF of the Nernst equation. The transport number is calculated by the proportion of the measured EMF to the theoretical EMF. The hydroxide ion transport number of Mg-Al CO_3^{2-} LDH is estimated to be from 0.91 to 0.95, indicating that the dominant conducting ion species of Mg-Al CO_3^{2-} LDH are hydroxide ion.

To investigate the source of hydroxide ions in LDHs, the ionic conductivity of the Mg-Al LDH-related compounds ($Mg(OH)_2$ (brucite, layered structure), $MgCO_3$ (spherical powder), $Al_2(CO_3)_3$ (spherical powder), and the mixture of $Mg(OH)_2$ and $Al_2(CO_3)_3$ with Mg/Al=3) was measured. Temperature dependence of ionic conductivity of these compounds is shown in Fig. 2.3.3.5. The conductivity of

$Mg(OH)_2$ and $MgCO_3$ was below the measurement limit (less than 10^{-10} S cm^{-1}) under 80%R.H., suggesting that simple metal hydroxides with layered structure or carbonate salts with the basic element do not have conducing ion species. On the other hand, $Al_2(CO_3)_3$ and the mixture of $Mg(OH)_2$ and $Al_2(CO_3)_3$ showed rather high ionic conductivity of the order of 10^{-4} S cm^{-1} under 80%R.H., indicating that $Al_2(CO_3)_3$ is an ion conducting material and related to the generation of carrier.

The water vapor concentration cell using these compounds as electrolyte was fabricated and measured EMF of these cells. Figure 2.3.3.6 shows the EMF for the water vapor concentration cell using these compounds as electrolyte. The EMF of the cell using the cation exchange membrane is positive, whereas that of the cell using the mixture of $Mg(OH)_2$ and $Al_2(CO_3)_3$, and the anion exchange membrane as well as Mg-Al CO_3^{2-} LDH is negative, indicating that $Al_2(CO_3)_3$ is an anion conducting material and the interaction between $Al_2(CO_3)_3$ and water in the atmosphere generates hydroxide ion as below reaction.

$$CO_3^{2-} + H_2O \rightarrow HCO_3^- + OH^- \quad (4)$$

Mg-Al CO_3^{2-} LDH consists of cationic hydroxide layers and carbonate anion located in the interlayer space for charge compensation of the positively charged hydroxide layers. The located carbonate anion could generate hydroxide ion carrier in Mg-Al CO_3^{2-} LDH.

On the other hand, Mg-Al CO_3^{2-} LDH shows higher hydroxide ion conductivity of the order of the 10^{-3} S cm^{-1} under 80%R.H. than that of the mixture of $Mg(OH)_2$ and $Al_2(CO_3)_3$. In this experiment, the specific surface area and molar ratio of Mg/Al (Mg/Al=3), which are related to the amount of carrier, were almost

the same. Therefore, the structural difference between Mg-Al CO_3^{2-} LDH and the mixture of $Mg(OH)_2$ and $Al_2(CO_3)_3$ should be attributed to the difference in hydroxide ion conduction: $Mg(OH)_2$ has layered structure like LDHs but has no carrier. $Al_2(CO_3)_3$ has no layered structure but has ion conducting carrier. Mg-Al CO_3^{2-} LDH has both layered structure and ion conducting carrier.

To examine the conduction path in LDHs, DC polarization test was performed. To reduce the effects of adsorbed water molecule on the surface, Mg-Al CO_3^{2-} LDH(D_2O) was dried at 100 °C for 1 h in advance. DC (0.5V) was applied to the pelletized Mg-Al CO_3^{2-} LDH (D_2O), and IR spectra were measured for the polarized Mg-Al CO_3^{2-} LDH(D_2O) powders. The IR spectra of the power at around the positive electrode and the negative electrode are shown in Fig. 2.3.3.7. The band in the range from 2500 cm^{-1} to 2700 cm^{-1} is attributed to O-D-stretching [35]. The band in the range from 550 cm^{-1} to 800 cm^{-1} is attributed to Mg-O and Al-O-stretching. The absorbance of O-D-stretching bands and Mg-O and Al-O-stretching bands are shown in Table 2.3.3.1. The absorbance attributed to O-D-stretching band for Mg-Al CO_3^{2-} LDH(D_2O) at the positive electrode surface is larger than that before polarization. The absorbance attributed to O-D-stretching band for Mg-Al CO_3^{2-} LDH(D_2O) at the negative electrode surface is smaller than that before polarization. These results show that OD^- ions are moved by the DC polarization. Because the adsorbed water molecules on the surface was removed in advance, the surface conduction can be ignored in this experiment, and the interlayer with D_2O and CO_3^{2-} should be the only ion conduction path. Thus, the DC polarization result indicates that deuterium hydroxide ions move through the interlayer

of Mg-Al CO_3^{2-} LDH(D_2O), probably by the Grotthus mechanism with D_2O in the interlayer. The high hydroxide ion conduction in LDHs must be because of not only the attribution of the surface conduction but also the interlayer conduction.

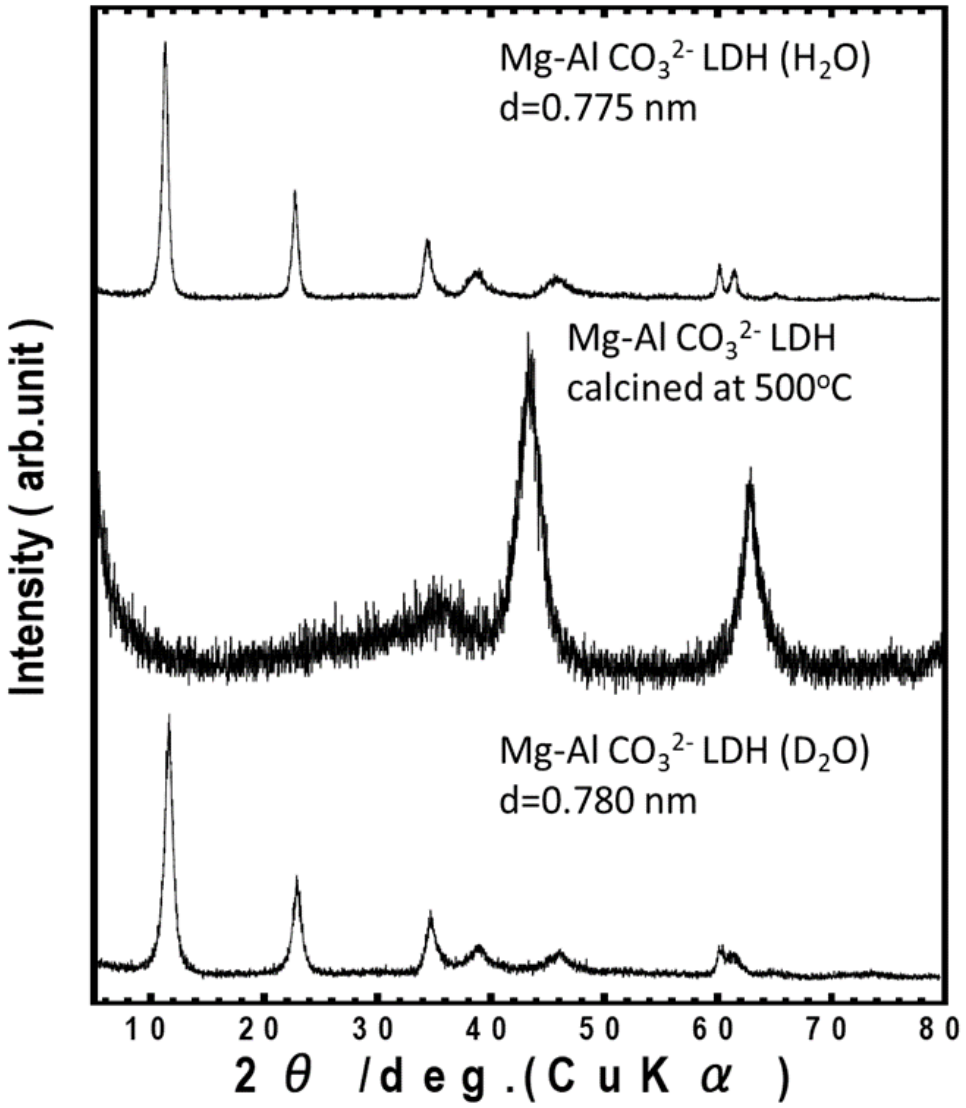

Fig. 2. 3. 3. 1 XRD patterns of Mg-Al CO_3^{2-} LDH(H_2O), Mg-Al CO_3^{2-} LDH (H_2O) calcined at 500°C and Mg-Al CO_3^{2-} LDH(D_2O) obtained by reconstructing calcined Mg-Al CO_3^{2-} LDH in 4M Na_2CO_3 −D_2O.

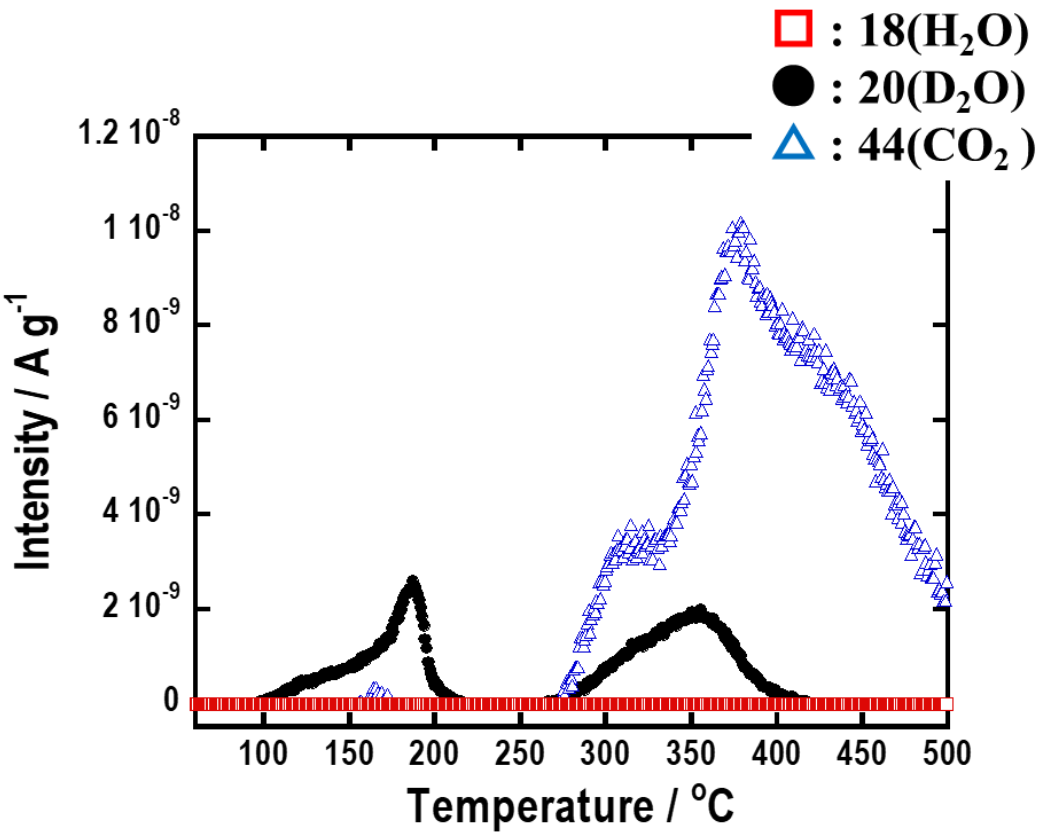

Fig. 2. 3. 3. 2　MS spectra of Mg-Al CO_3^{2-} LDH(D_2O).Square(□):H_2O, Circle(●): D_2O, Triangle(△): CO_2.

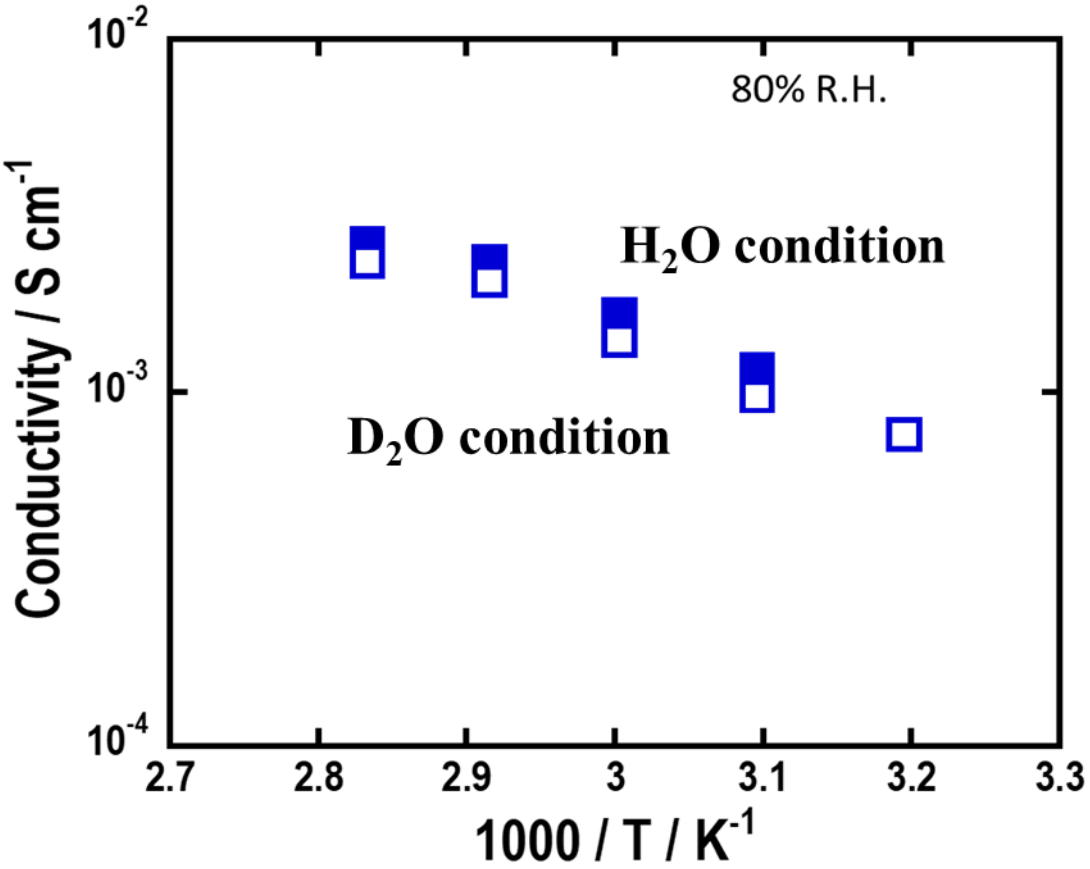

Fig. 2. 3. 3. 3　Temperature dependence of ionic conductivity of Mg-Al CO_3^{2-} LDH under H_2O(■) and D_2O (□) humidified condition.

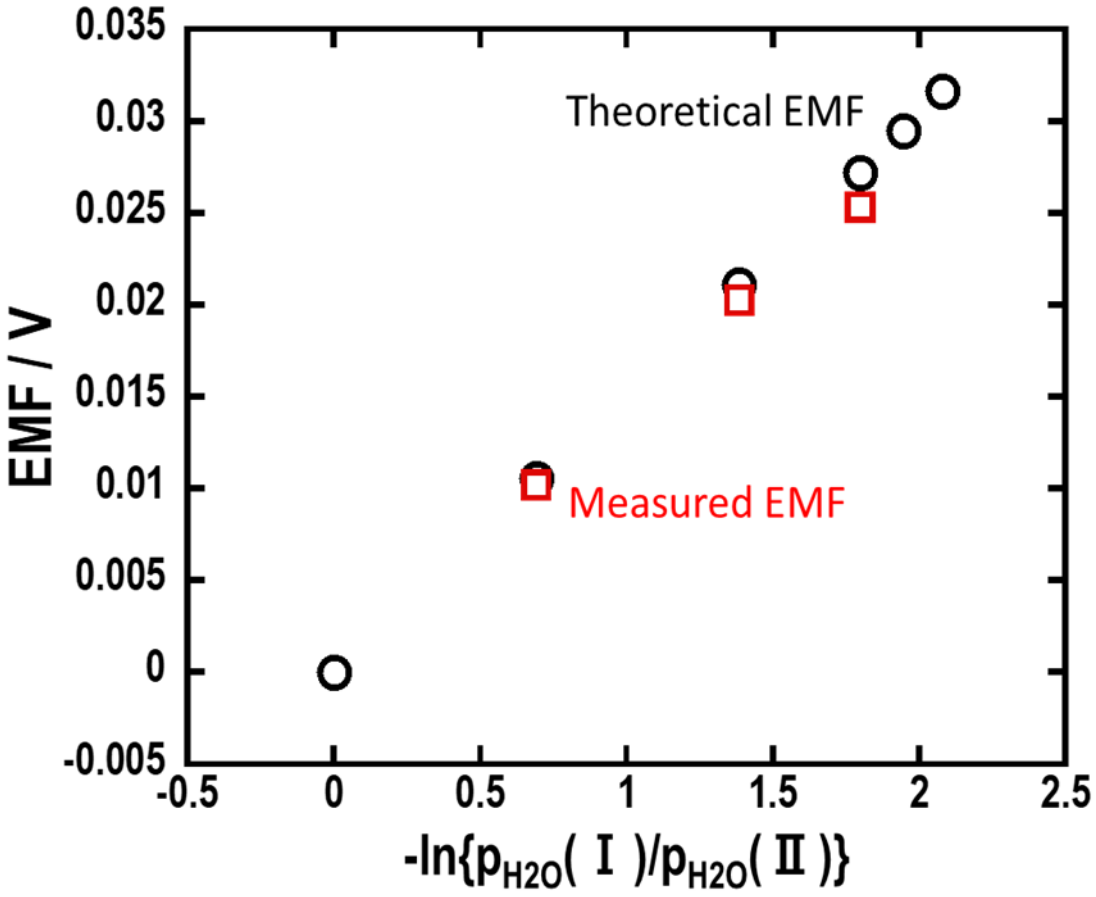

Fig. 2. 3. 3. 4 Partial pressure dependence of water vapor concentration cell using Mg-Al CO_3^{2-} LDH as electrolyte. (pH_2O^{I}: water vapor partial pressure at dry side, pH_2O^{II}: water vapor partial pressure at wet side)

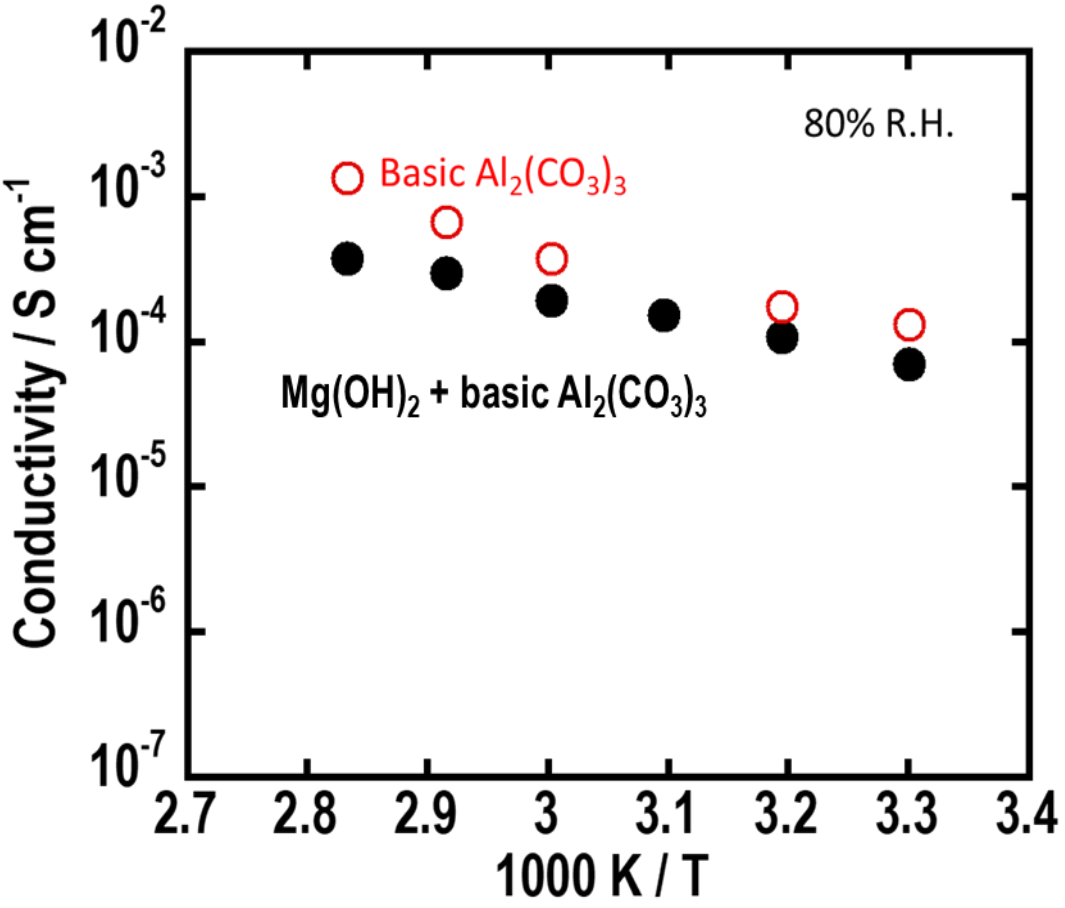

Fig. 2. 3. 3. 5 Temperature dependence of the ionic conductivity of $Al_2(CO_3)_3$ and the mixture of $Mg(OH)_2$ and $Al_2(CO_3)_3$ under 80%R.H..

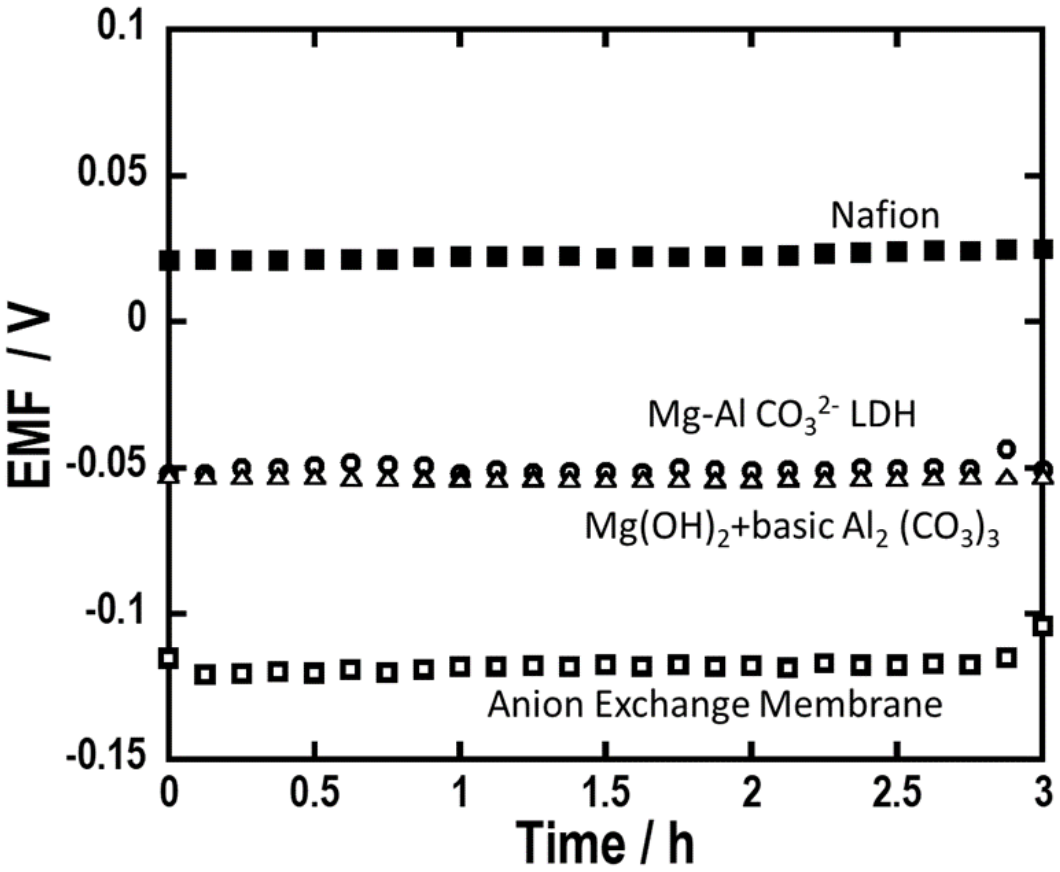

Fig. 2. 3. 3. 6　Variation of electromotive force(EMF) under 80%R.H.. (■:Nafion, ○:Mg-Al CO_3^{2-} LDH, △:$Mg(OH)_2$+basic $Al_2(CO_3)_3$, □:Anion Exchange Membrane).

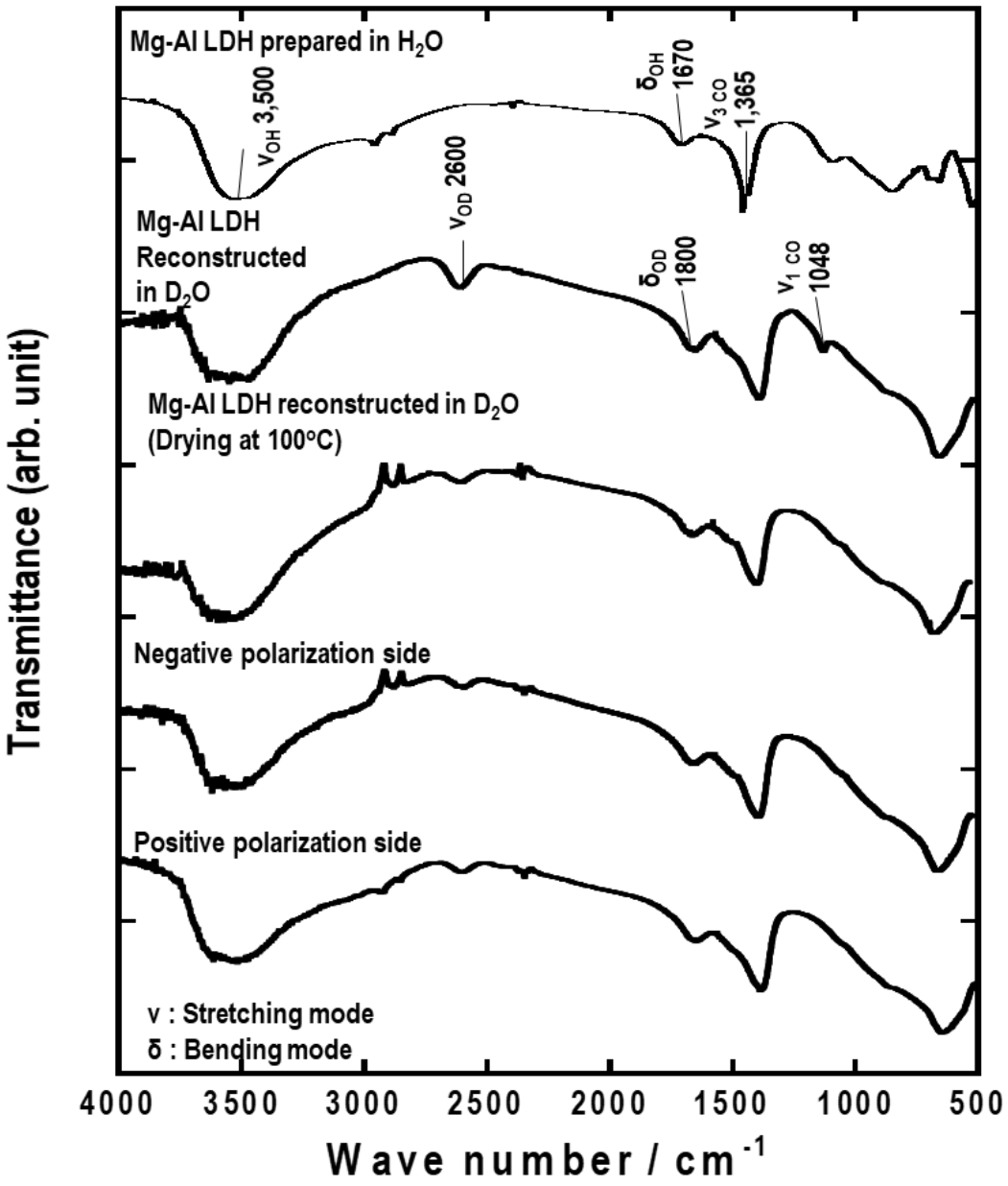

Fig. 2. 3. 3. 7 IR spectra of Mg-Al CO_3^{2-} LDH(H_2O), Mg-Al CO_3^{2-} LDH(D_2O), and Mg-Al CO_3^{2-} LDH(D_2O) before and after DC polarization.

Table. 2. 3. 3. 1

Absorbance for O-D stretching band and Mg-O, Al-O stretching band of Mg-Al CO_3^{2-} LDH(D_2O) before and after DC polarization.

	Absorbance (O-D)	**Absorbance (Mg-O, Al-O)**	**Abs(O-D)/Abs(Mg-O, Al-O)**
Mg-Al LDH reconstructed in D_2O (before DC polarization)	0.027	0.478	0.057
Positive electrode side (after DC polarization)	0.030	0.482	0.062
Negative electrode side (after DC polarization)	0.026	0.484	0.052

2.4. Summary of Chapter 2

In this chapter, various type of LDHs was prepared and the hydroxide ion conduction in LDHs were examined. The ionic conductivity was found to be affected by the interaction forces between the host cation layer and the interlayer anion. Mg-Al LDH intercalated with DS anions showed higher ionic conductivity than Mg-Al LDH intercalated with CO_3^{2-} under lower humidity. HEHL was synthesized and evaluated thermal stability. Although the thermal stability of LDHs was not be improved, HEHL with a low amount of interlayer water showed lower ionic conductivity than Mg-Al LDH intercalated with CO_3^{2-}, indicating that the interlayer water is related to the ionic conduction in LDHs. The ionic conductivity of LDHs was also found to be affected by the amount of the interlayer water by using D_2O. The DC polarization measurements confirmed the movement of D_2O between the layers. Therefore, in addition to surface conduction, the ionic conduction mechanism of LDHs was found to be interlayer conduction.

Reference

[1] X. Huang, Z. Zeng and H. Zhang, *Chem. Soc. Rev.*, **42** (2013) 1934.

[2] D. Chen, L. Tang and J. Li, *Chem. Soc. Rev.*, **39** (2010) 3157-3180.

[3] K. F. Mak and J. Shan, *Nat. Photonics*, **10** (2016) 216-226.

[4] K.S. Novoselov, A.K. Geim, S.V. Morozov, D. Jiang, Y. Zhang, S.V. Dubonos, I.V. Grigorieva, A. A. Firsov, *Science*, **306** (2004) 666-669.

[5] W. Choi, N. Choudhary, G. H. Han, J. Park, D. Akinwande and H. Lee, *Materials Today*, **20** (2017) 116-130.

[6] Y. Lin and J. W. Connell, *Nanoscale*, **4** (2012) 6908.

[7] J. Zhang, J. Liu, L. Xi, Y. Yu, N. Chen, S. Sun, W. Wang, K. M. Lange and B. Zhang, *J. Am. Chem. Soc.*, **140** (2018) 3876-3879.

[8] L. Zeng, T. S. Zhao, *Nano Energy*, **11** (2015) 110-118.

[9] Q. Wang, D. O'Hare, *Chem. Rev.*, **112** (2012) 4124-4155.

[10]. Z. Liu, R. Ma, M. Osada, N. Iyi, Y. Ebina, K. Takada, T. Sasaki, *J. Am. Chem. Soc.*, **128** (2006) 4872-4880.

[11] Y. Li, M. Gong, Y. Liang, J. Feng, J. Kim, H. Wang, G. Hong, B. Zhang, H. Dai, *Nat. Commun.*, **4** (2013) 1805.

[12] K. Tadanaga, Y. Furukawa, A. Hayashi, M. Tatsumisago, *Adv. Mater.* **22** (2010) 4401-4403. [13] Y.

Furukawa, K. Tadanaga, A. Hayashi, M. Tatsumisago, *Solid State Ionics* **192** (2011) 185-187.

[14] S. Ishiyama, N. C. Rosero-Navarro, A. Miura, K. Tadanaga, *Mater. Res. Bull.*, **119** (2019) 110561.

[15] Y. Yang, L. Dang, M. J. Shearer, H. Sheng, W. Li, J. Chen, P. Xiao, Y. Zhang, R. J. Hamers, and S. Jin, *Adv. Energy Mater.*, **8** (2018) 1703189.

[16] Z. Cai, X. Bu, P. Wang, J. C. Ho, J. Yang, and X. Wang, *J. Mater. Chem. A*, **7** (2019) 5069-5089.

[17] R. Patel, J. T. Park, M. Patel, J. K. Dash, E. B. Gowd, R. Karpoormath, A. Mishra, J. Kwak, and J. H. Kim, *J. Mater. Chem. A*, **6** (2018) 12-29.

[18] E. P. George, D. Raabe, and R. O. Ritchie, *Nat. Review Mater.*, **4** (2019) 515–534.

[19] P. Zhang, S. Sago, T. Yamaguchi, G. M. Anilkumar, *J. Power Sources,* **230** (2013) 225-229.

[20] J. P. Maria, R. de M. Bruno, N. Spyridon, C.F. Fabio, C.T. Ana, *J. Nanopart Res.*, **15** (2013) 1-14.

[21] O. P. Ferreira, O. L. Alves, D. X. Gouveia, A. G. Souza Filho, J.´A. C. de Paiva, and J.´M. Filho, *J. Solid State Chem.*, **177** (2004) 3058-3069.

[22] P. Sun, R. Ma, X. Bai, K. Wang, H. Zhu, and T. Sasaki, *Sci. Adv.*, **3** (2017) e1602629.

[23] D. Bérardan, S. Franger, A. K. Meena and N. Dragoe, *J. Mater. Chem. A,* **4** (2016) 9536-9541.

[24] S. Miyata, *Clays Clay Miner.,* **23** (1975) 369-375.

[25] N. Iyi, T. Matsumoto, Y. Kaneko, K. Kitamura, *Chem. Mater.,* 16 (2004) 2926-2932.

[26] F. Kooli, C. Depege, A. Ennaqadi, A. deRoy, J.P. Besse, *Clays Clay Miner.*, **45**, (92-98), (1997).

[27] K. Tadanaga, Y. Furukawa, A. Hayashi, M. Tatsumisago, *Adv. Mater.,* 22 (2010) 4401-4403.

[28] A. Clearfield, M. Kieke, J. Kwan, J.L. Colon, R.C. Wang, *J. Incl. Phenom. Mol. Recog. Chem.*, **11** (1991) 361-378.

[29] W. Yang, Y. Kim, P.K.T. Liu, M. Sahimi, T.T. Tsotsis, *Chem. Eng. Sci.,* **57** (2002) 2945-2953.

[30] K. Tadanaga, Y. Furukawa, A. Hayashi, M. Tatsumisago, *J. Electrochem. Soc.*, **159**, (B368-B370), (2012).

[31] P. Zhang P., T. Yamaguchi, B.N. Nair, K. Miyajima, G.M. Anilkumar, *RSC Adv.,* **4**, (41051-41058), (2014).

[32] T. D. Nguyen, Q. T. Phuong Bui, H. Q. Huy Phan, C. X. Thang, L. T. Bao Tran, L. X. Tien and L. G. Bach, *J. Mater. Sci. and Surf. Eng.,* **4** (2016) 488-491.

[33] M. H. Lee, Y. J. Kang, S. T. Myung and Y. K. Sun, *Electrochim. Acta*, **50** (2004) 939948.

[34] V. I. Sachkov, R. A. Nefedov and I. V. Amelichkin, *IOP Conf. Ser.: Mater. Sci. Eng.*, **597** (2019) 012005.

[35] J.T. Kloprogge, L. Hickey, R. L. Frost, *J. Mater. Sci.*, **21**, 603-605 (2002).

Chapter 3

Application of layered double hydroxides to electrochemical devices

Chapter 3. Application of layered double hydroxides to electrochemical devices

3.1. Introduction

In electrochemical devices using alkaline electrolytes, such as fuel cells and metal–air batteries, cost effective and environmentally friendly designs are expected [1–7]. These electrochemical devices using alkaline electrolyte are known to be lower temperature-operating type and show high performance because of the faster kinetics for oxygen reduction reaction (ORR). Especially in recent years, a new concept of integrating a fuel cell and an electrolyzer together has been introduced to realize periodic energy storage and conversion with reduces cost and increased energy density. This kind of device is so-called reversible fuel cells [8]. The metal-air batteries are also aimed to convert into rechargeable batteries. These batteries are expected as next-generation batteries with high energy density because of their use of oxygen in the air. However, for a rechargeable battery using an alkaline electrolyte, several problems exist such as the reversibility of the oxygen electrode reaction (oxygen reduction reaction (ORR) and oxygen evolution reaction (OER)) in a reversible air electrode and the formation of solid state K_2CO_3 in the electrolyte or electrode–electrolyte interface generated through a reaction between KOH in an aqueous solution and carbon dioxide in the air. The solid-state carbonates precipitated in the air electrode inhibit the diffusion of oxygen, block electrolyte pathways, reduce the effective area for the reaction, and result in expansion and destruction of the electrode structure [2, 9-12]. Therefore, to solve above issues, electrolytes with no alkali

metal cation are required.

Then, the performance of the reversible air electrode must be improved to support the practical use of rechargeable metal–air batteries. About the improvement of the air electrode, an anion exchange membrane (AEM)-type air electrode has been proposed [13]. In the AEM-type air electrode, an AEM is placed at the interface between a catalyst layer of an air electrode and an aqueous alkaline electrolyte. The AEM is expected to suppress the permeation of cations (K^+) in the alkaline electrolyte into the air electrode and inhibition of the carbonate precipitation at the electrode–electrolyte interface, thereby reducing degradation of the reversible air electrode. However, the formation of triple-phase boundary regions in the air electrode is difficult because the electrode–electrolyte interface is a solid–solid one in the AEM-type air electrode. Therefore, a hydroxide ion conducting ionomer to form favorable triple-phase boundary regions in the air electrode are necessary to transport OH^- ions effectively. For alkaline type batteries, many researchers are working to prepare novel hydroxide ion conducting ionomers. However, ionomers with sufficient high hydroxide ion conductivity and chemical durability (alkali resistance, carbon dioxide resistance etc.) have not been developed to date [14, 15].

As shown in the previous chapter, some of LDHs show with high hydroxide ion conductivity, and thus LDHs can be applied to electrolytes and ionomer in alkaline electrochemical devices. LDHs are also widely studied and applied to various fields as catalysts, active materials in electrochemical capacitors or electrodes of dye-sensitized solar cells [16-20].

In this chapter, application of LDHs to electrolytes, ionomer or electrocatalysts in the air electrodes of electrochemical devices is described. As the application to electrolyte of the electrochemical devices, alkaline-type direct ethanol fuel cell and H_2-O_2 fuel cell are studied. As the application of LDHs to catalytic layer of the air electrodes in the electrochemical devices, oxygen reduction reaction (ORR) / oxygen evolution reaction (OER) activity of the catalyst layers containing LDHs as an ionomer was firstly evaluated by a half-cell using anion exchange membrane. Then the catalyst layers are applied to air electrodes of direct ethanol fuel cells and zinc-air batteries.

First, alkaline-type direct ethanol fuel cell (DEFC) and H_2-O_2 fuel cell, using LDHs prepared by co-precipitation method as solid electrolyte, were fabricated and evaluated at various temperatures. Especially, to improve the H_2-O_2 fuel cell performance using LDHs as electrolyte, self-standing Mg-Al LDH thin membrane was prepared using a glass paper as a support and the H_2-O_2 fuel cell using Mg-Al LDH thin membrane as electrolyte was fabricated.

Second, the catalyst layers with and without LDHs as an ionomer were prepared and the oxygen reduction reaction (ORR) / oxygen evolution reaction (OER) activity of the prepared catalyst layers was evaluated by a half-cell using the prepared catalyst layers and an anion exchange membrane. In addition, to evaluate how LDHs affected the triple phase boundary (TPB) regions in the catalyst layers and cell performances, DEFCs using the prepared catalyst layers were fabricated and evaluated.

Third, transition-metal-containing LDHs are expected to show catalytic activity in catalytic layer. Ni-Fe

CO_3^{2-} LDH was prepared and the electrochemical properties of Ni-Fe CO_3^{2-} LDH were examined as an electrode material because an electrode material is desirable to show higher electronic conductivity along with ionic conductivity. To investigate the effects of the LDH addition to the reversible air electrode of the rechargeable metal–air battery, the reversible air electrode composed of a α-MnO_2 catalyst, Ni-Fe LDH and a carbon material were fabricated and ORR and OER activity were evaluated. After a rechargeable zinc–air battery was fabricated, the electrochemical performance and stability of the reversible air electrode were examined.

3.2. Experimental

3.2.1. Preparation of LDHs

Ni-Fe LDH intercalated with CO_3^{2-} were also prepared by using the co-precipitation method as in section 2.2.1. $Ni(NO_3)_2 \cdot 6H_2O$ and $Fe(NO_3)_3 \cdot 9H_2O$ were dissolved in deionized water in a molar ratio of 3 : 1 (Ni : Fe). The mixture was dropped into 0.3 M Na_2CO_3 solution with stirring at 80 °C. The reaction mixture pH was adjusted to 10 by the addition of 2 M NaOH solution and the mixture was aged at 80 °C for 17 h. Then, the resulting yellow precipitates were filtrated, washed with distilled water, and dried at 80 °C. As for Mg-Al LDH and Ni-Al LDH, the one prepared in section 2.2.1 were used.

3.2.2. Fabrication of LDH thin membrane for electrolyte in H_2-O_2 fuel cell

Thin Mg-Al LDH membrane was fabricated using the Mg-Al LDH re-dispersed solution and a glass paper.

The obtained Mg-Al LDH powder by the co-precipitation method was re-dispersed into distilled water. Then, glass paper provided by Nippon Sheet Glass Co. Ltd., (C-glass fibers, nominal thickness of 50 μm, about 90% porosity) was immersed into the Mg-Al LDH re-dispersed solution. The immersion into the solution was not held. After removal from the solution, with withdrawal speed of 3 mm s^{-1}, the glass paper with LDH precipitates was dried at 50 °C for 1h. This immersion-drying procedure was repeated five times because the dense Mg-Al LDH thin membrane was not obtained by the immersion less than five times. Consequently, the crystals were deposited in the inside and surface of the glass paper, and the self-standing Mg-Al LDH thin membrane was obtained. The thickness of the Mg-Al LDH thin membrane was measured by a micrometer with the error of 5% or less. The membrane was pressed from both sides before the conductivity and fuel cell evaluations. Pelletized Mg-Al LDH powder electrolyte was also prepared for comparison, by mixing Mg-Al LDH powder and 5 wt% polytetrafluoroethylene (PTFE) or 10 wt% PTFE as binder for pellet molding. The thickness of Mg-Al LDH thin membrane with the glass paper was about 150 μm and that of pelletized Mg-Al LDH powder was about 250 μm.

3.2.3. Fabrication of DEFCs

A passive-type DEFC was fabricated using pelletized LDH powder as an electrolyte. The anode and cathode electrodes with non-Pt catalysts (Hypermec; ACTA S.p.A.) on nickel form and carbon cloth were

used respectively. The amount of loaded non-Pt catalysts is 1.9 mg cm^{-2}. The pelletized LDH powder was sandwiched with the two electrodes and the gold-plated current collectors that were attached with cell fixtures. An aqueous solution of ethanol and potassium hydroxide was used as fuel and the cathode was exposed to air. Polarization performances were measured using potentiostat and galvanostats (Autolab, PGSTAT30) at 50-80 °C.

3.2.4. Fabrication of H_2-O_2 fuel cell

To evaluate the fuel cell performance of the Mg-Al LDH thin membrane as electrolyte, a H_2-O_2 fuel cell was fabricated using the pelletized Mg-Al LDH powder or Mg-Al LDH thin membrane as electrolyte as shown in Fig. 3.2.4.1. The anode electrode catalyst was prepared by mixing Pt/C (EC-20-10-10; Electrochem Inc.), Mg-Al CO_3^{2-} LDH and PTFE as a binder with a weight ratio of 1:1:0.6. The cathode electrode catalyst was prepared by mixing Pt/C, Ni-Al CO_3^{2-} LDH and PTFE with the same ratio as anode electrode catalyst. Catalysts were loaded on a carbon sheet by painting the catalyst ink. In this study, the loading amount of Pt was 1.9 mg cm^{-2}, the LDH loading amount as ionomer was the same amount as the Pt catalyst. Then, these electrolytes were sandwiched with the prepared catalyst layers on carbon sheet. The cell performance was measured at 60 °C by exposing a flow of 25 mL min^{-1} humidified H_2 gas to anode side and 50 mL min^{-1} humidified air to cathode side.

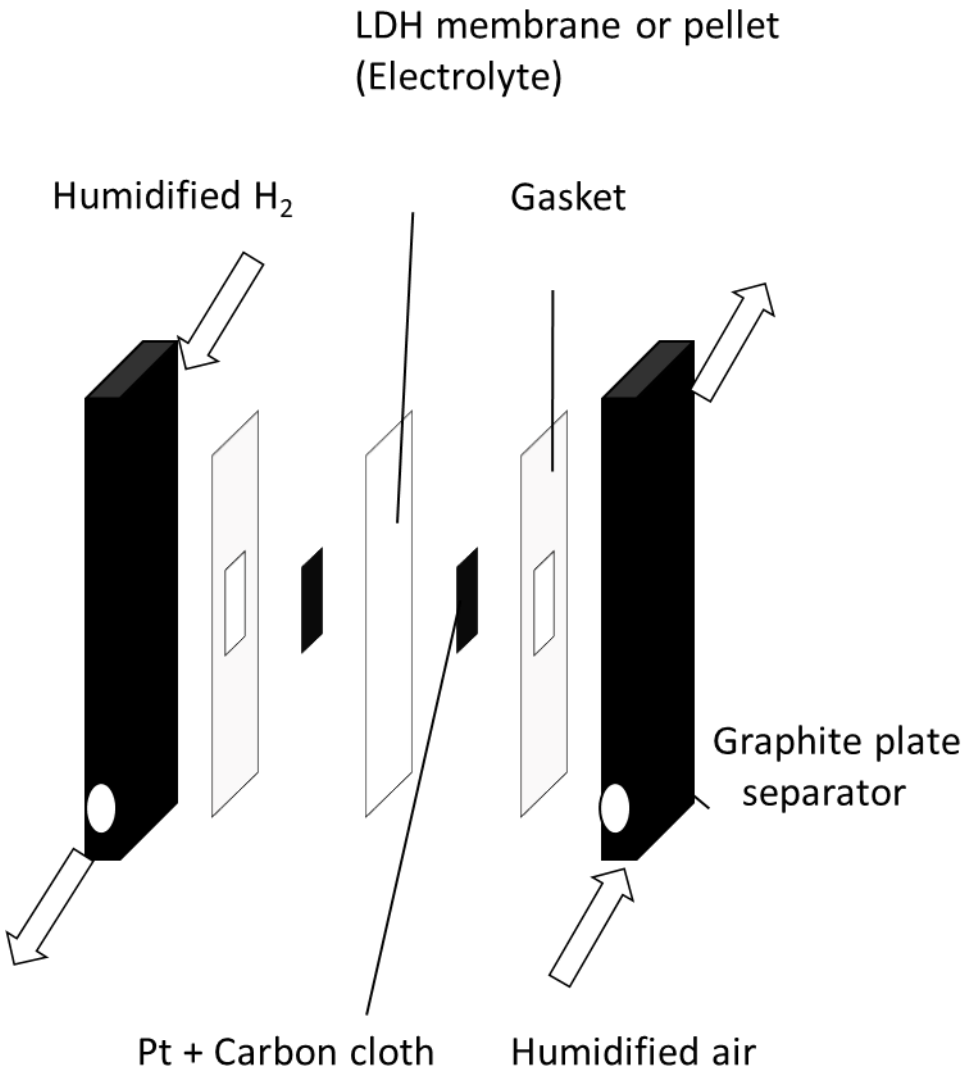

Fig.3.2.4. 1 Schematic illustration of H_2−O_2 fuel cell.

3.2.5. Evaluation of the ORR and OER activity of catalyst layers with LDHs

Effects of LDHs to the TPB regions in catalyst layers were evaluated using a half cell using an AEM (AHA; Tokuyama Corp.) as presented in Fig. 3.2.5.1 [21]. The catalyst inks were prepared by mixing Pt/C (EC-20-10-10; Electrochem Inc.), LDH and PTFE as a binder with a weight ratio of 1 : 1 : 0.6. The optimum amount of ionomer should depend on the Pt catalyst loading in the catalyst layer. In the study on the influence of Nafion loading on performance of PEFC, the optimum amount of Nafion ionomer is reported to be about 0.8-1.1 mg cm^{-2} in the case of Pt loading amount of 0.4 mg cm^{-2} [22, 23]. Although LDH crystals are rather easy to change shape and size, a formation of favorable contact interface with other electrode materials is rather difficult, compared with Nafion ionomer. In this experiment, the Pt loading amount is 1.9 mg cm^{-2}, the loading amount of LDH as ionomer was over 3.8-5.2 mg cm^{-2} for increasing TPB regions. Catalyst layers were formed by pasting catalyst ink on a carbon cloth (EC-CC1-T). ORR activity of fabricated electrodes in this way was evaluated in three electrode cell with 1 M KOH solution, and Hg/HgO electrode and Ni plate as reference and counter electrode, respectively. With the half cell, steady-state polarizations were measured at 5 mV s^{-1} in a potential range from -1.0 V to 0.2 V (v.s. Hg/HgO).

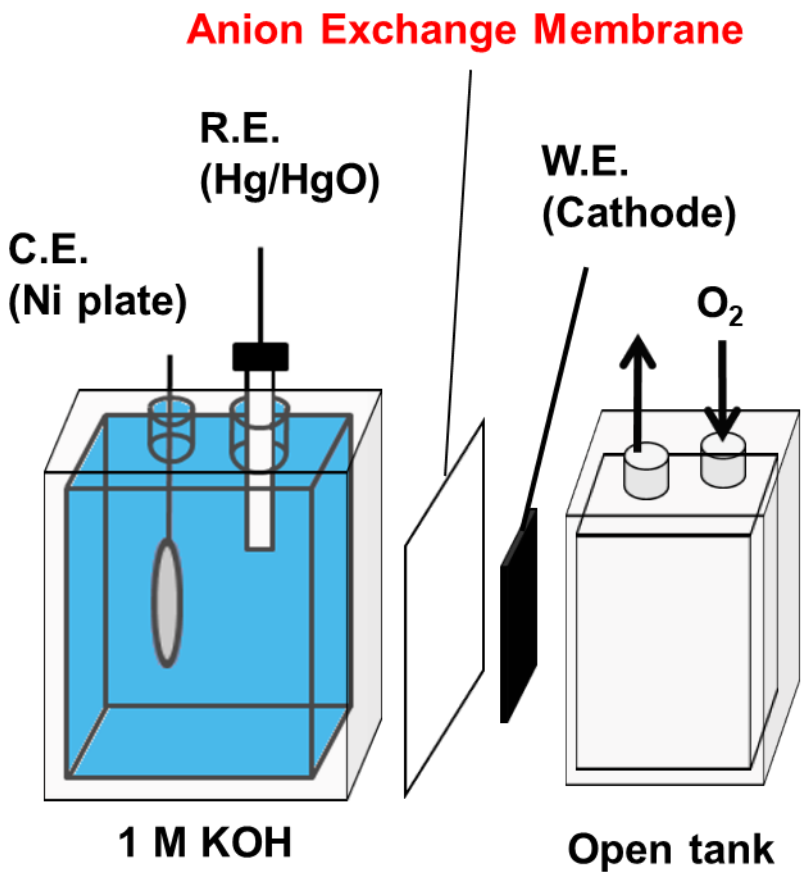

Fig. 3. 2. 5. 1 Schematic representation of half-electrode electrolyte assembly.

3.2.6. Preparation of α-MnO_2 and fabrication of Zn-air secondary battery

α-MnO_2 as a bi-functional catalyst for ORR and OER was prepared using a hydrothermal treatment [24]. $Mn(SO_4) \cdot 5H_2O$ and $KMnO_4$ were dissolved in deionized water in a molar ratio of 5 : 13. The mixed solution was stirred magnetically to form a homogeneous mixture, which was transferred into a Teflon-lined stainless steel autoclave with subsequent heat treatment of 140 °C for 2 h. The obtained precipitation was filtered and washed with distilled water, and then dried at 80 °C for 6 h. The XRD pattern of the precipitation was indexed as that of α-MnO_2, which showed that α-MnO_2 can be prepared.

Then, for a rechargeable metal–air battery, a reversible air electrode using α-MnO_2 as a catalyst was fabricated in the same way described above. The catalyst ink was prepared by mixing the prepared α-MnO_2, Ni-Fe CO_3^{2-} LDH, Vulcan carbon as a conductive additive, and PTFE as a binder with a weight ratio of 1: 10: 2: 0.6. The ratio of Ni-Fe CO_3^{2-} LDH and Vulcan carbon was decided such that these materials have almost identical volume to percolate ionic and electronic conducting paths in the catalyst layer homogeneously. As described above, the catalyst inks were pasted on the carbon cloth. The electrochemical properties of the prepared reversible air electrode were investigated using the half cell. Electrochemical tests and the electrochemical impedance spectroscopy measurements of the prepared reversible air electrode were conducted at room temperature using a charge–discharge measuring device (BTS-2004; Nagano Co. Ltd.) and an impedance analyzer (PGSTAT30; Autolab). Charge–discharge performance was assessed respectively at current densities of 10 mA cm^{-2} (400 mA g^{-1}) and cut-off capacity of 400 $mAhg^{-1}$. The

observed capacity was normalized by the weight of the catalyst. Impedance measurements of the air electrode during discharging were conducted from 100 kHz to 0.01 Hz at -0.3 V (vs. Hg/HgO). A rechargeable zinc–air battery was fabricated using the cell described above. The prepared reversible air electrode for a positive electrode, a zinc pellet prepared by pressed zinc powders at 500 MPa for a negative electrode, and a 1 M KOH aqueous solution saturated ZnO for an electrolyte were used in the rechargeable zinc–air battery. The polarization curves of the rechargeable zinc–air battery were then examined using a potentiostat and galvanostat (PGSTAT30; Autolab) at room temperature.

3.3 Results and discussion

3.3.1. Evaluation of the performance of the DEFC using LDHs as electrolyte

Alkaline-type DEFC using Ni-Al CO_3^{2-} LDH as an electrolyte was fabricated as one of the applications. Figure 3.3.1.1 shows the cell performance for a passive-type DEFC using Ni-Al CO_3^{2-} LDH as an electrolyte at 50-80 °C. The open circuit voltage of the cell was about 0.82 V, indicating that crossover of ethanol to the cathode side is sufficiently small. The maximum power density was 70 mW cm^{-2} at 80 °C. These results that Ni-Al CO_3^{2-} LDH worked as an electrolyte of DEFC supports that Ni-Al CO_3^{2-} LDH is a hydroxide ion conducting material.

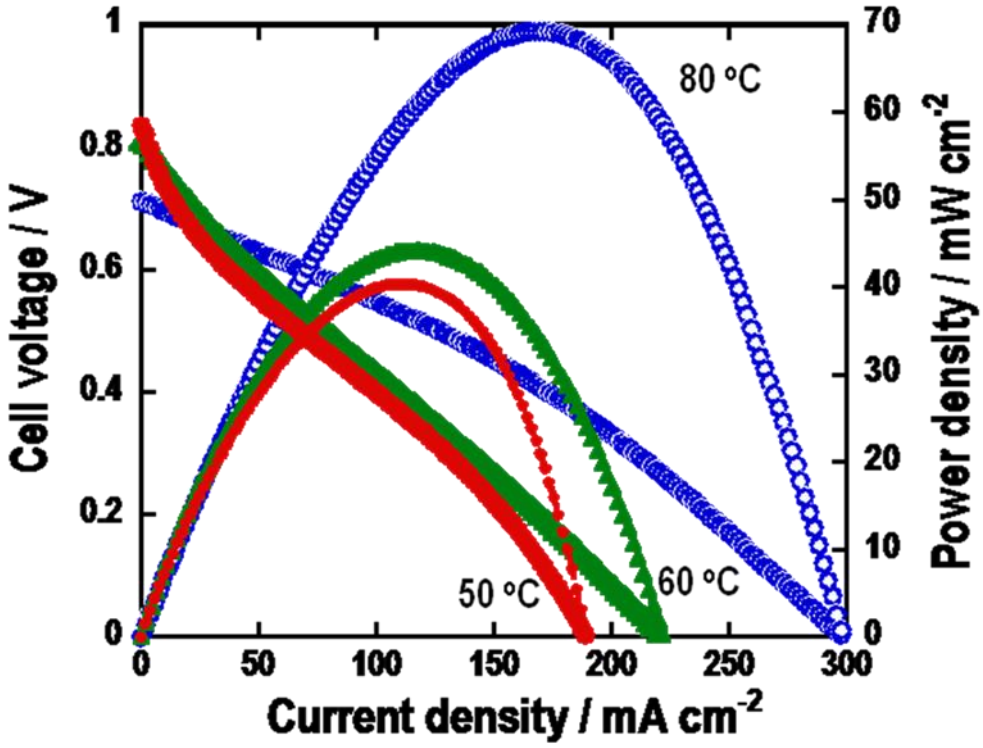

Fig. 3. 3. 1. 1 Performance of the DEFC using Ni-Al LDH intercalated with CO_3^{2-} at various temperatures.

3.3.2. Characterization of Mg-Al LDH thin membrane

Figure 3.3.2.1 shows XRD patterns of the Mg-Al CO_3^{2-} LDH powder obtained by coprecipitation method. The XRD patterns of the sample showed characteristic 003, 006, 0012, etc. reflections attributed to the layered structure of LDHs.

Figure 3.3.2.2(a) shows scanning electron microscope (SEM) image of cut-surface of the glass paper used in this study. The glass paper is non-woven fabric and consists of glass fibers with a diameter of about 5 μm and 0.5 μm. Figure 3.3.2.2(b) shows the image of the obtained Mg-Al LDH thin membrane. Mg-Al LDH particles were confirmed to be deposited on the inside of the glass paper. The deposited Mg-Al LDH crystals in the inside of the glass papers are physically attached with the glass fibers.

Figure 3.3.2.3 show surface SEM images of Mg-Al LDH thin membrane with the glass paper support and the pelletized Mg-Al LDH powder. The surface of the pelletized LDH powder (Fig. 3.3.2.3(b)) is rather smooth. This may be because shape and size of LDH crystals are rather easy to be changed by pressing. On the surface of the pelletized sample, the presence of mixed PTFE binder is also confirmed. However, some cracks are present on the surface. On the other hand, in Mg-Al LDH thin membrane (Fig. 3.3.2.3(a)), Mg-Al CO_3^{2-} LDH powder was deposited on glass paper, and LDH hexagonal particles were well oriented parallel to the plane of glass paper. The characteristic morphology of Mg-Al LDH thin membrane electrolyte and the pressure bonding in fabrication of membrane-electrolyte assembly for fuel cell are expected to result in dense structure and high gas barrier property.

Electrical properties of the pelletized Mg-Al LDH powder and Mg-Al LDH thin membrane were determined using the impedance spectroscopy. The temperature dependence of the ionic conductivities under 80% relative humidity for the pelletized Mg-Al LDH powder and Mg-Al LDH thin membrane is shown in Fig. 3.3.2.4. The ionic conductivity of Mg-Al LDH thin membrane is almost the same as that of the pelletized Mg-Al LDH powder. Mg-Al LDH on glass paper seems to connect each other. Thus, the moderate difference of the conductivity may be because of the decrease of the grain boundary resistance.

Alkaline-type H_2-O_2 fuel cells using the pelletized Mg-Al LDH powder with PTFE binder and Mg-Al LDH thin membrane as electrolyte were fabricated. Figure 3.3.2.5 shows the cell performance for the alkaline-type H_2-O_2 fuel cell under 80% relative humidity. The H_2-O_2 fuel cell using Mg-Al LDH thin membrane as electrolyte showed open circuit voltage (OCV) of more than 0.9V, indicating that the thin membrane with well-oriented Mg-Al LDH crystals has high gas barrier property. The H_2-O_2 fuel cell using Mg-Al LDH thin membrane as electrolyte showed higher cell performance than the cell using pelletized Mg-Al LDH powder. The maximum power density of the H_2-O_2 fuel cell using Mg-Al LDH thin membrane was about 5 times higher than that using pelletized Mg-Al LDH powder. The effect of PTFE content in the pelletized electrolyte on the cell performance is much smaller at the same experiment. Therefore, the improvement of the cell performance must be because of the smaller thickness in the Mg-Al LDH thin membrane. The better performance should mainly be attributed to the lower resistance of the electrolyte. For detail analysis of the high cell performance using Mg-Al LDH thin membrane as electrolyte, the

impedance spectra under the cell working condition were measured. Figure 3.3.2.6 shows the impedance plot under the cell working condition. The intercept in high frequency range is electrolyte resistance because this value is almost proportional to the thickness of the electrolytes. The circle in low frequency range is attributable to the overlap of activation overpotential and concentration overpotential [25, 26]. The impedance plot of H_2-O_2 fuel cell using Mg-Al LDH thin membrane as electrolyte shows that electrolyte resistance is small compared to the pelletized Mg-Al LDH powder. The circle in the H_2-O_2 fuel cell using Mg-Al LDH thin membrane as electrolyte in low frequency range is rather small, indicating that the concentration overpotential is also lowered.

The glass paper is proved to be very effective support for making thin electrolyte membranes for fuel cells. Thin membrane with smaller thickness or larger area can be prepared by using an appropriate glass paper. This procedure can also be applied to a separator of other all solid-state electrochemical cells, such as all solid-state lithium batteries, by using powder of solid electrolytes.

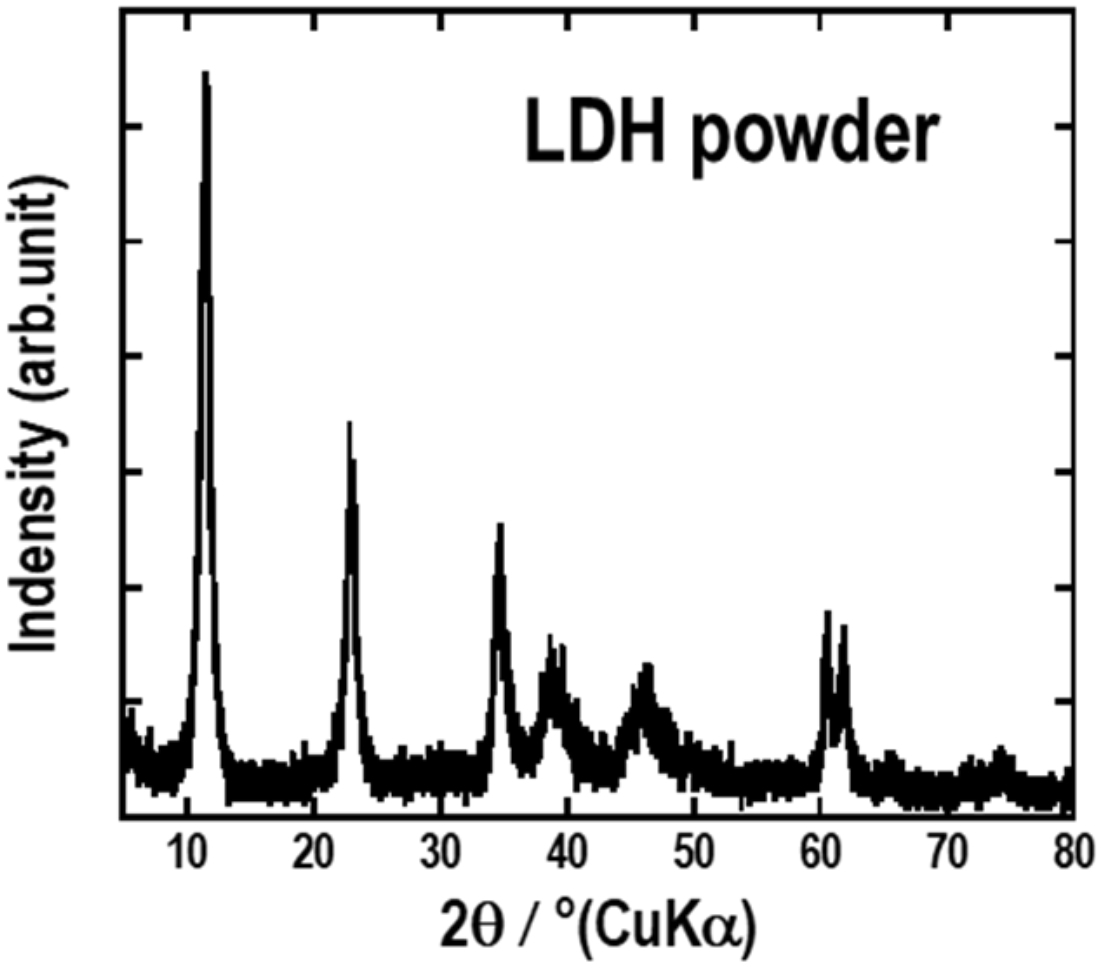

Fig.3. 3. 2. 1 XRD patterns of the obtained Mg-Al LDH intercalated with CO_3^{2-}.

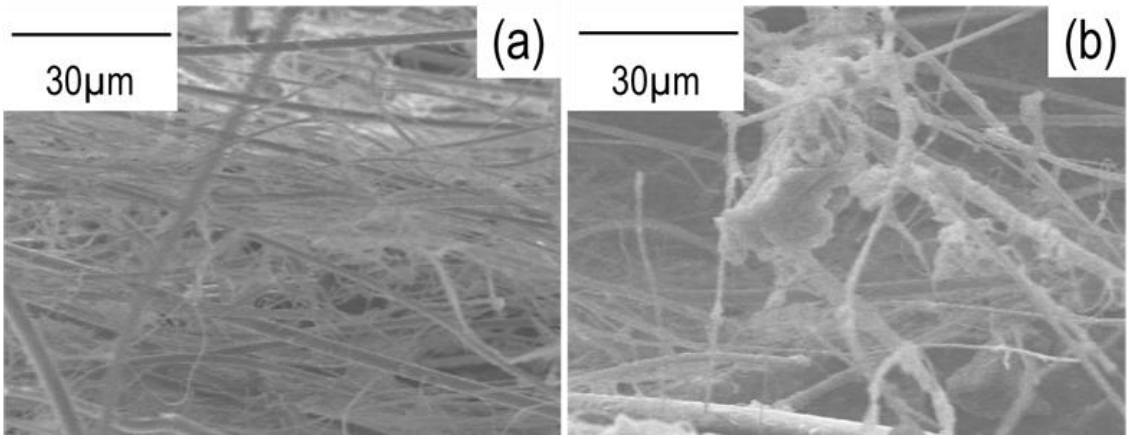

Fig. 3. 3. 2. 2 Cross-section SEM images of the glass paper (a) and the obtained Mg-Al LDH membrane (b).

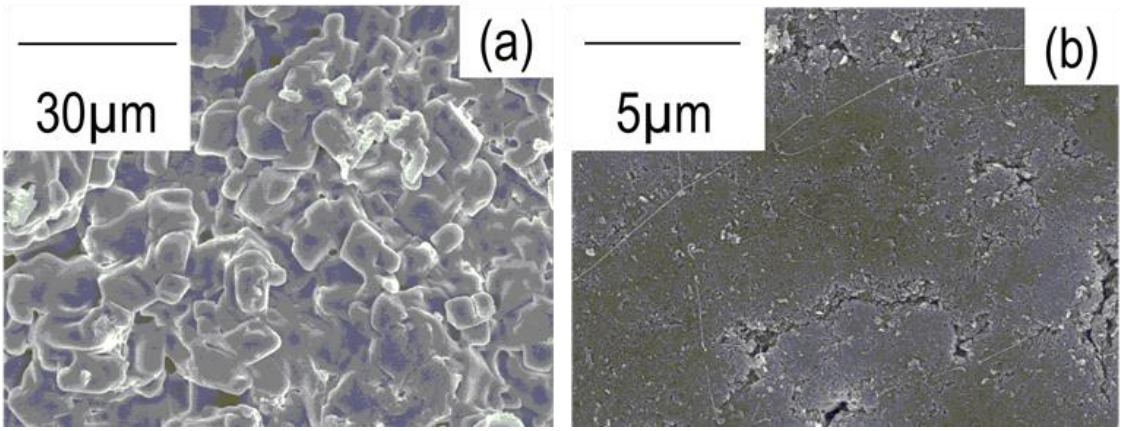

Fig. 3. 3. 2. 3 Surface SEM images of Mg-Al LDH thin membrane (a) and pelletized Mg-Al LDH powder (b) with 10% PTFE binder.

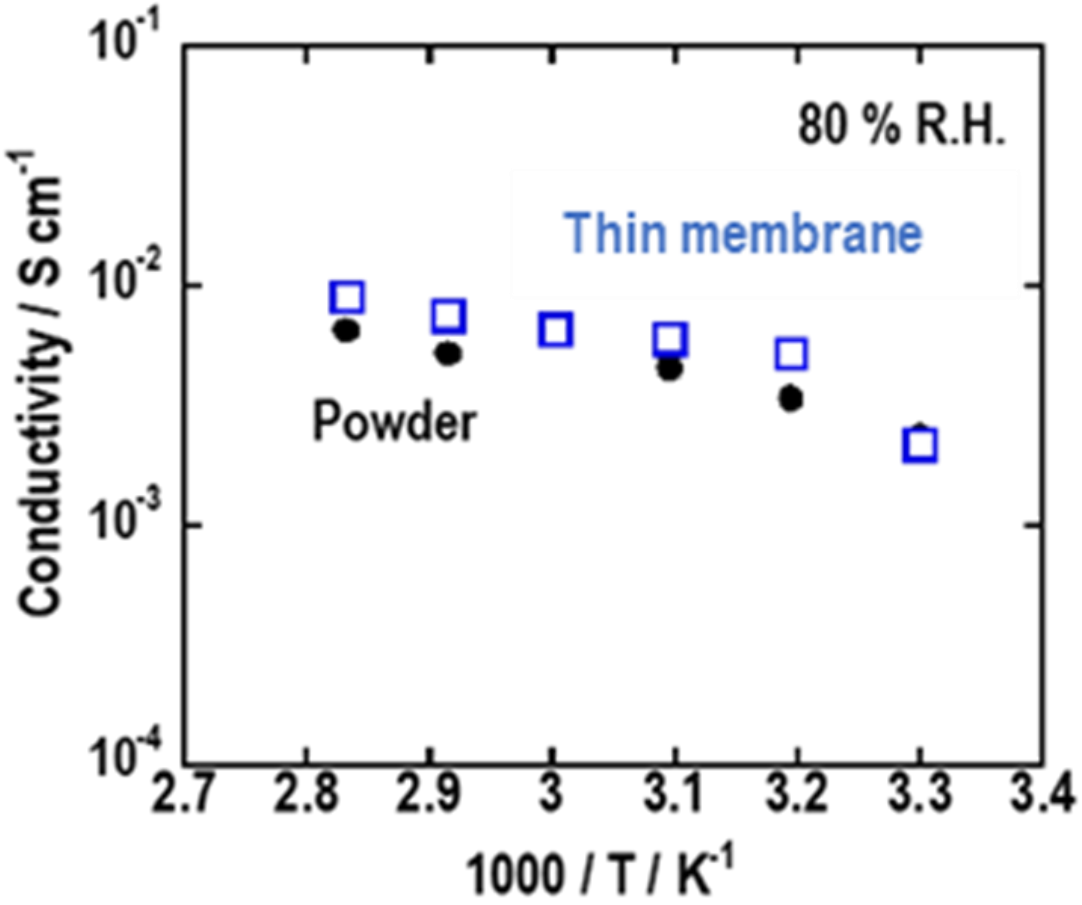

Fig. 3. 3. 2. 4 Temperature dependence of the ionic conductivity of Mg-Al LDH thin membrane and pelletized Mg-Al LDH powder.

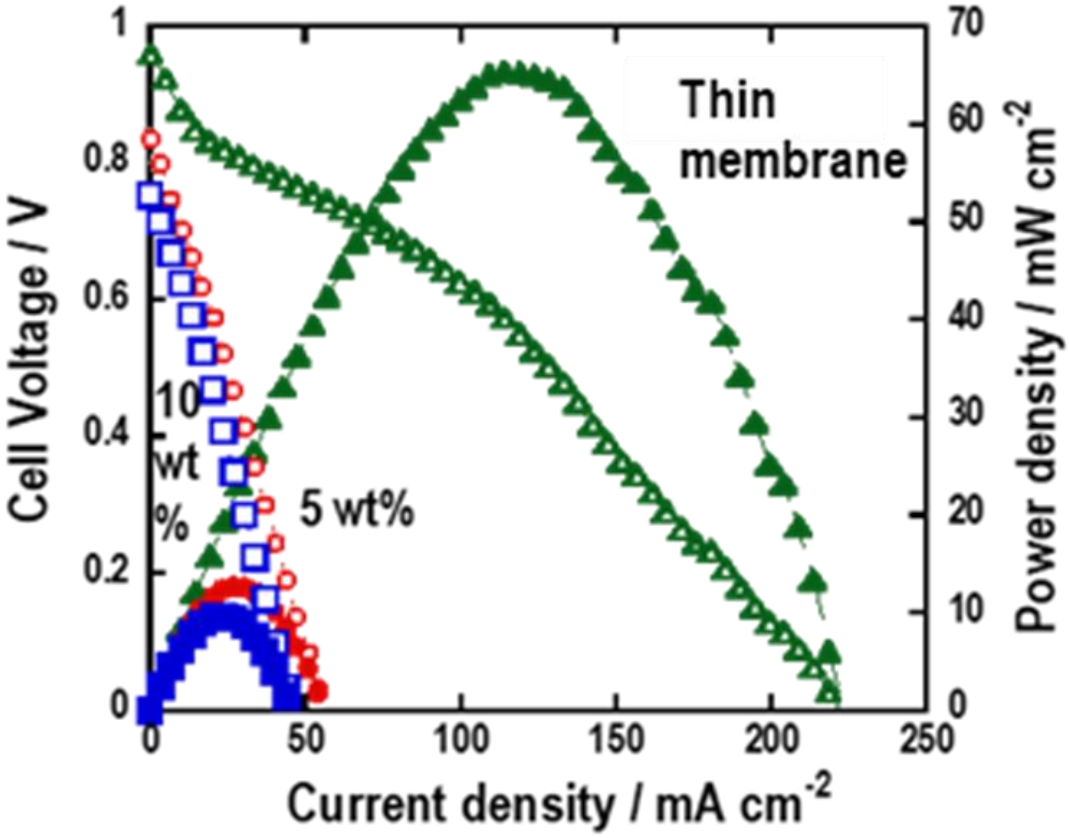

Fig. 3. 3. 2. 5 Performance of H_2–O_2 fuel cells using Mg-Al CO_3^{2-} LDH thin membrane (without PTFE) using the glass paper as support medium, and Mg-Al CO_3^{2-} LDH pellet containing 5, 10 wt.% PTFE as a binder.

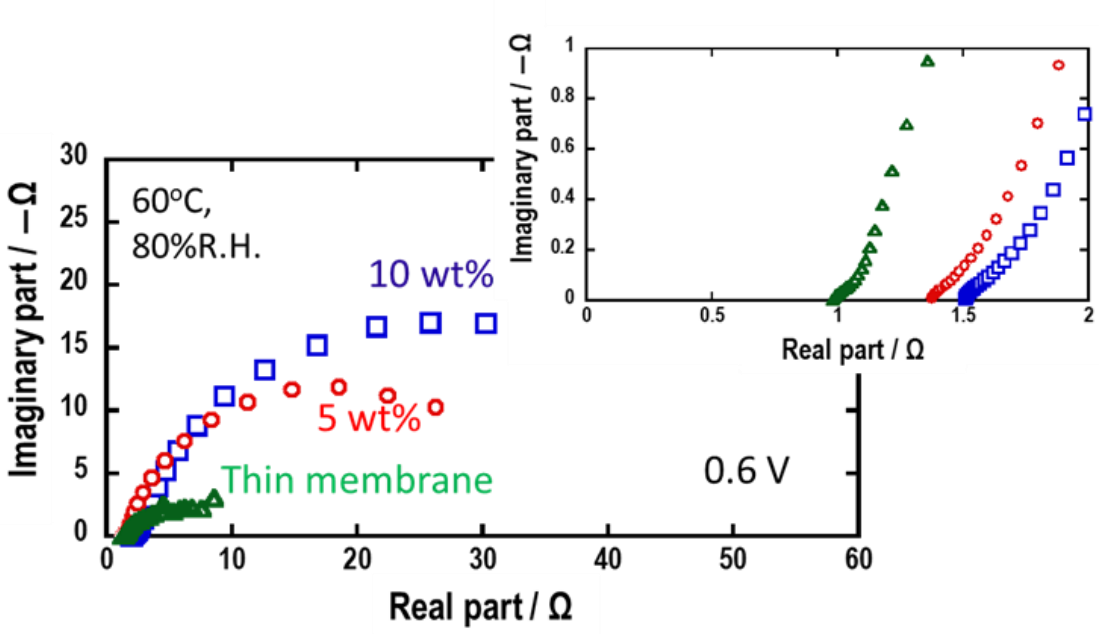

Fig. 3. 3. 2. 6 Nyquist plots of H_2–O_2 fuel cells using Mg-Al CO_3^{2-} LDH thin membrane using the glass paper as support medium and Mg-Al CO_3^{2-} LDH pellet containing 5, 10 wt.% PTFE as a binder at 0.6 V.

3.3.3. Effect of LDHs addition as an ionomer to catalytic layer and evaluation of DEFC cell performance using catalytic layer with LDHs

To investigate the effect of LDHs addition as an ionomer to the catalyst layer, the ORR respective activities of catalyst layers composed of Pt/C only, Pt/C + Mg-Al CO_3^{2-} LDH, Pt/C + Ni-Al CO_3^{2-} LDH, and Pt/C + Ni-Fe CO_3^{2-} LDH were evaluated. The steady state polarization curves of the half cell using the prepared air electrodes with different catalyst layers are shown in Figure 3.3.3 1. Current density for ORR below 0 V (vs. Hg/HgO) in the catalyst layers with LDHs is higher than that without LDHs. The air electrode with Ni-Fe CO_3^{2-} LDH shows the highest ORR current density of all. In this experiment, the Ni-Fe CO_3^{2-} LDH addition to the catalyst layer is even more effective than the Ni-Al CO_3^{2-} LDH addition to the catalyst layer, although Ni-Fe CO_3^{2-} LDH provides lower ionic conductivity than Ni-Al CO_3^{2-} LDH. The result suggests that the electronic conductivity of an ionomer mixed to the catalyst layer is extremely important. An electrode material with both high ionic and electronic conductivity is desirable to form more favorable triple-phase boundary regions. Therefore, Ni-Fe CO_3^{2-} LDH with high ionic and electronic conductivity functions more effectively as an ionomer.

In subsequent experiments, the Ni-Fe CO_3^{2-} LDH, which mostly contributed to the improvement of the air electrode performance, was used as an ionomer. Steady state polarization curves of the prepared reversible air electrodes are shown in Fig. 3.3.3.2. Reversible air electrode with α-MnO_2 as catalyst shows higher ORR current density at -0.8 V(vs. Hg/HgO), higher OER current density at 0.8 V(vs. Hg/HgO), an

increase in onset potential for ORR to -0.10 V(vs. Hg/HgO) and a decrease in onset potential for OER to +0.5 V(vs. Hg/HgO), compared to that without α-MnO_2 . These results show that α-MnO_2 has catalytic activity for ORR and OER. The addition of Ni-Fe CO_3^{2-} LDH to the catalyst layer of the reversible air electrode using α-MnO_2 as catalyst decreased the Tafel slope of the polarization curves, indicating that Ni-Fe CO_3^{2-} LDH formed more favorable triple-phase boundary regions and facilitated the electrode reactions (ORR and OER). Furthermore, the addition of Ni-Fe CO_3^{2-} LDH to the catalyst layer of the reversible air electrode shifted the onset potential slightly for ORR and OER. The LDHs containing transition metal are electroactive materials, and electrocatalytic activity of the LDHs is expected. In fact, some reports have described that the LDHs containing transition metal display good electrocatalytic activity for methanol oxidation and OER via an internal redox in LDHs [27, 28]. It is also reported that LDHs containing iron showed a good H_2O_2 decomposition activity [29]. An ORR on MnO_2 is produced via a two-electron pathway producing H_2O_2 ions [30, 31]. Therefore, Ni-Fe CO_3^{2-} LDH can function as electrocatalysts to decompose the produced H_2O_2, and the addition of Ni-Fe CO_3^{2-} LDH to the catalyst layer of the reversible air electrode must contribute to improve the catalytic activity for oxygen electrode reaction, and facilitate the oxygen electrode reaction. Actually, the reversible air electrode without catalysts was prepared and examined using steady-state polarization. Ni-Fe CO_3^{2-} LDH showed the electrocatalytic activity as shown in Fig. 3.3.3.3.

To understand the effects of the addition of Ni-Fe CO_3^{2-} LDH to the catalyst layer in the reversible air

electrode, the electrochemical impedance was measured during the air electrode discharge at -0.3 V (vs. Hg/HgO). Figure 3.3.3.4 presents impedance profiles of the air electrodes at -0.3 V (vs. Hg/HgO). Nyquist plots of the air electrodes show a semicircle in the low frequency region. In previous impedance studies of rechargeable metal–air batteries, two semicircles at high-frequency and low-frequency regions were reported as contributing respectively to the solid–electrolyte interface resistance and the charge transfer resistance [32]. In the present experiment, the electrode – liquid electrolyte interface resistance at the high frequency region is exceedingly small: the resistance is regarded as negligible [32, 33]. Consequently, the observed semicircle at low frequency is attributable to the charge transfer resistance. The reversible air electrode with Ni-Fe CO_3^{2-} LDH shows much smaller charge transfer resistance than that without Ni-Fe CO_3^{2-} LDH, indicating that Ni-Fe CO_3^{2-} LDH formed the reactant and product transport path in the reversible air electrode and that it facilitates electrode reactions (ORR and OER).

The charge–discharge curves of the reversible air electrode with and without Ni-Fe CO_3^{2-} LDHs are shown in Fig. 3.3.3.5. Reversible air electrodes show capacity higher than 400 $mAhg^{-1}$, indicating that the catalytic ORR and OER reactions occur in the reversible air electrodes. The addition of Ni-Fe CO_3^{2-} LDH to the catalyst layer of the reversible air electrode increases the discharge potential and slightly decreases the charge potential compared to that without Ni-Fe CO_3^{2-} LDH. The results of the charge–discharge measurements are good agreement with the steady-state polarization measurements (Figure 3.3.3.2). The X-ray diffraction pattern of the LDH in the prepared catalyst layer before and after charge and discharge

experiments had no change, indicating that the oxidative and reductive decompositions of LDHs had not occurred.

Alkaline-type DEFC using anion exchange membrane as an electrolyte and the prepared electrodes was fabricated to confirm the effect of LDHs addition to the catalyst layer. Figure 3.3.3.6 shows the cell performance for the passive-type alkaline DEFCs. Although the complete conversion of ethanol to CO_2 is difficult, the catalytic activity of ethanol is dependent on temperature. Therefore, DEFC performance test was evaluated at relatively high temperature (80 °C). The DEFC using catalyst layers with LDHs showed higher cell performance than the DEFC using catalyst layer without LDHs, in accordance with the obtained results for evaluation of ORR activity. The DEFC using catalyst layers with LDHs showed higher cell performance than the DEFC using catalyst layer without LDHs, in accordance with the obtained results for evaluation of ORR activity. The maximum power density of the DEFC using catalyst layer with Ni-Al CO_3^{2-} LDH was about 2 times higher than that using catalyst layer without LDHs. The better performance was attributed to construction of more favorable TPB regions, which enhanced the electrode reactions and reduced activation overpotential.

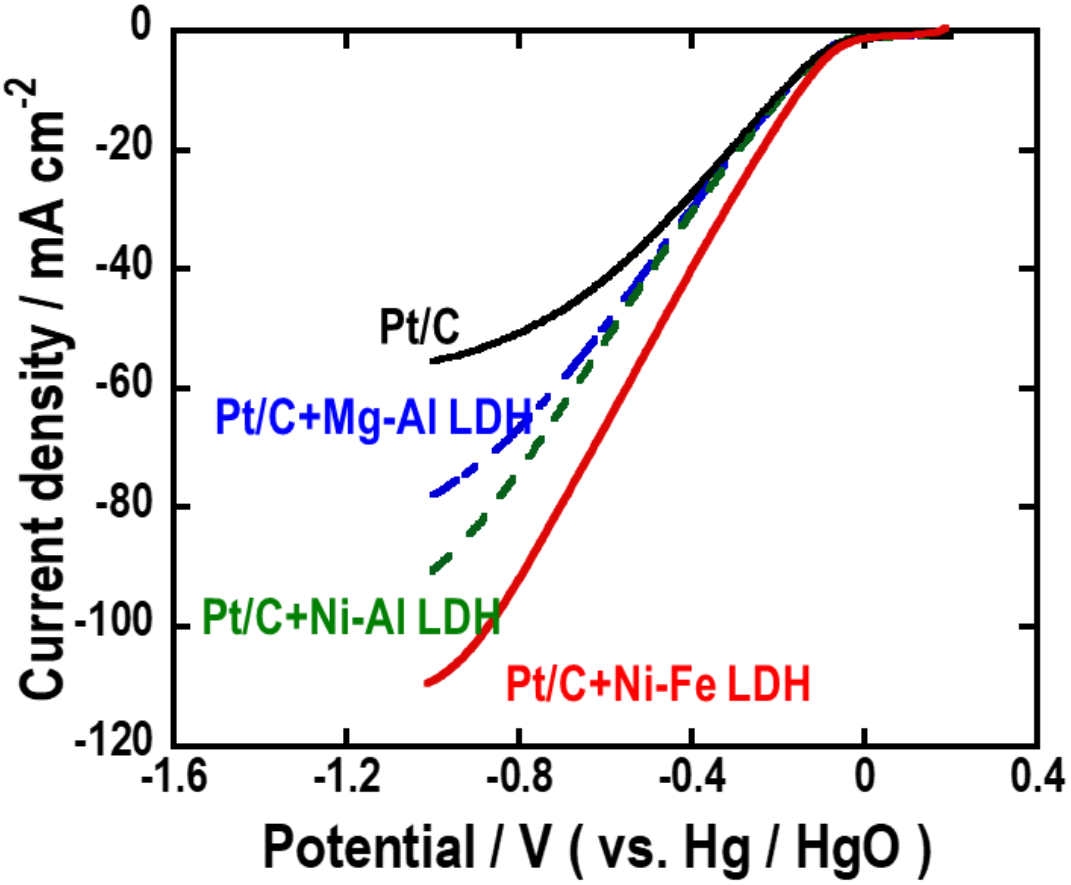

Fig. 3. 3. 3. 1 Steady-state polarization curves for the oxygen reduction reaction activity of the air electrodes with or without LDH.

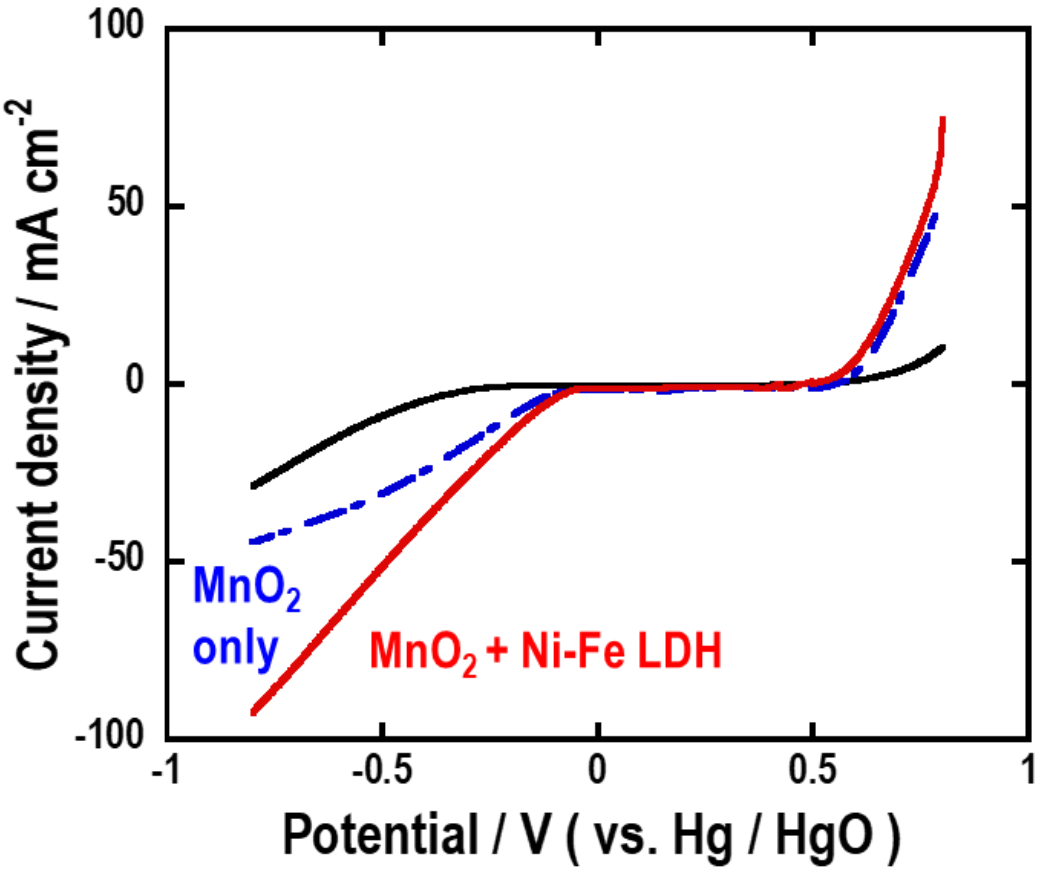

Fig. 3. 3. 3. 2 Steady-state polarization curves for the oxygen reduction reaction activity and oxygen evolution reaction of the reversible air electrodes with or without LDH.

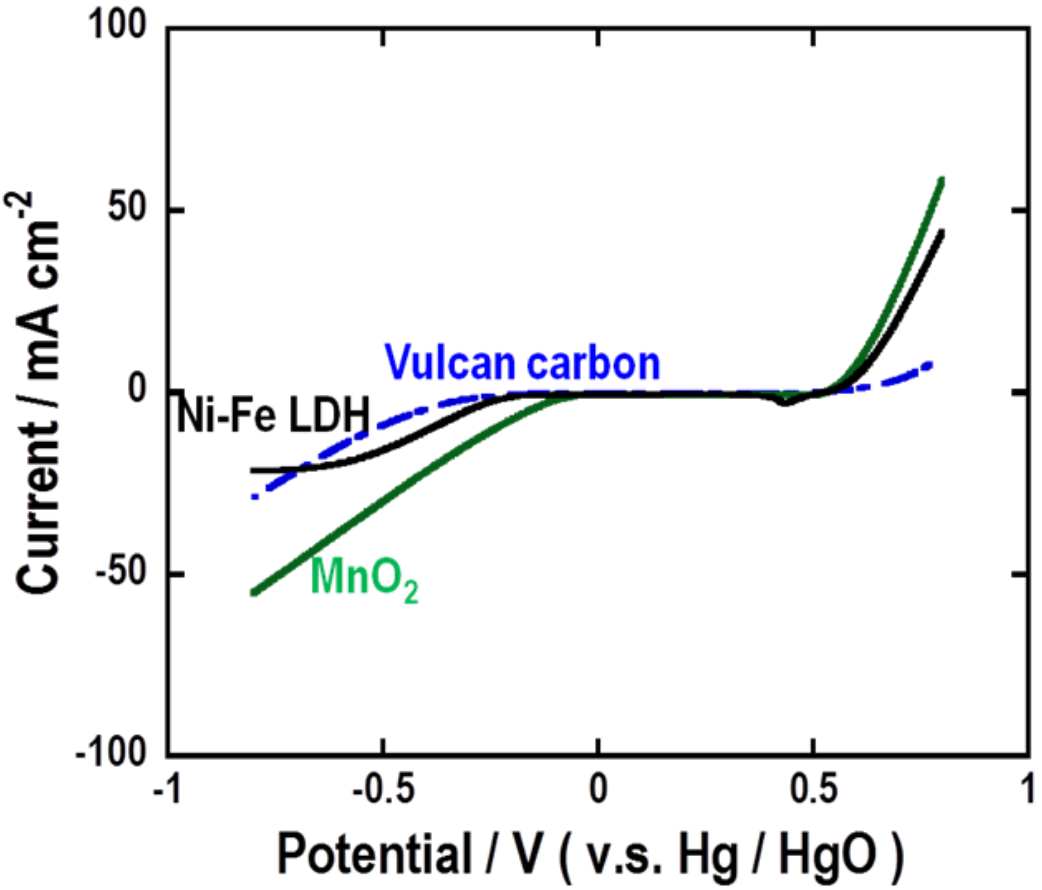

Fig. 3. 3. 3. 3 Steady-state polarization curves for the oxygen reduction reaction activity and oxygen evolution reaction of the reversible air electrodes.

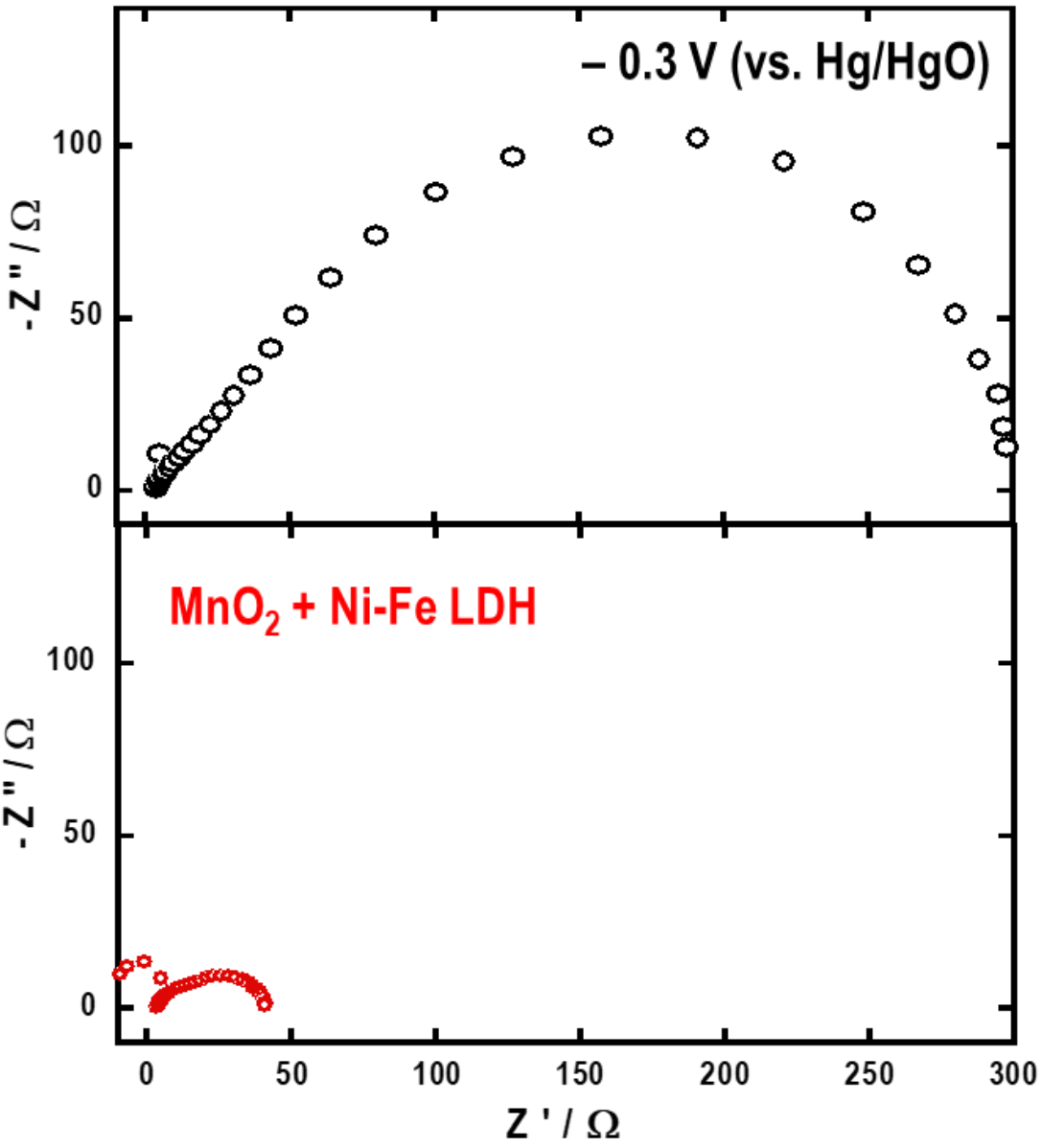

Fig. 3. 3. 3. 4 Impedance profiles of the air electrodes using MnO_2 as a catalyst with or without Ni-Fe CO_3^{2-} LDH.

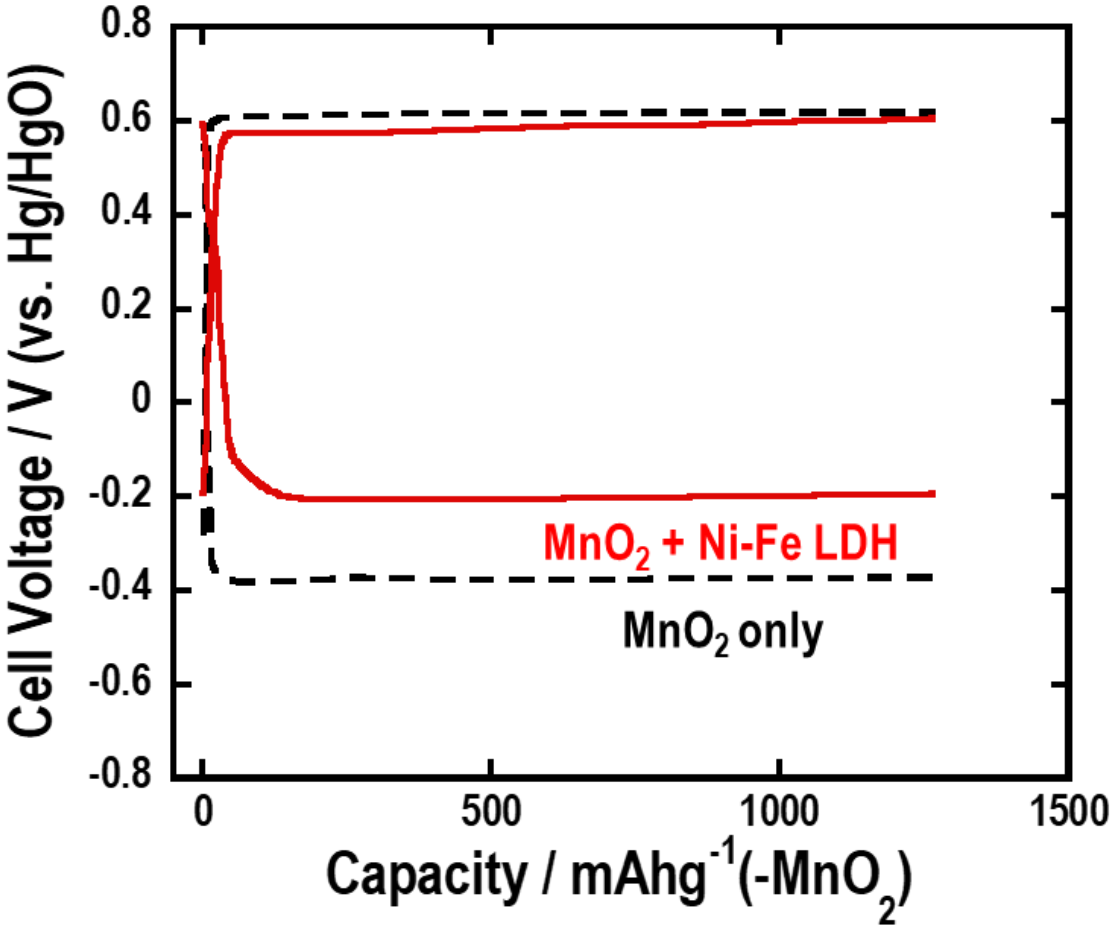

Fig. 3. 3. 3. 5 Charge–discharge curves of reversible air electrodes with or without Ni-Fe CO_3^{2-} LDH.

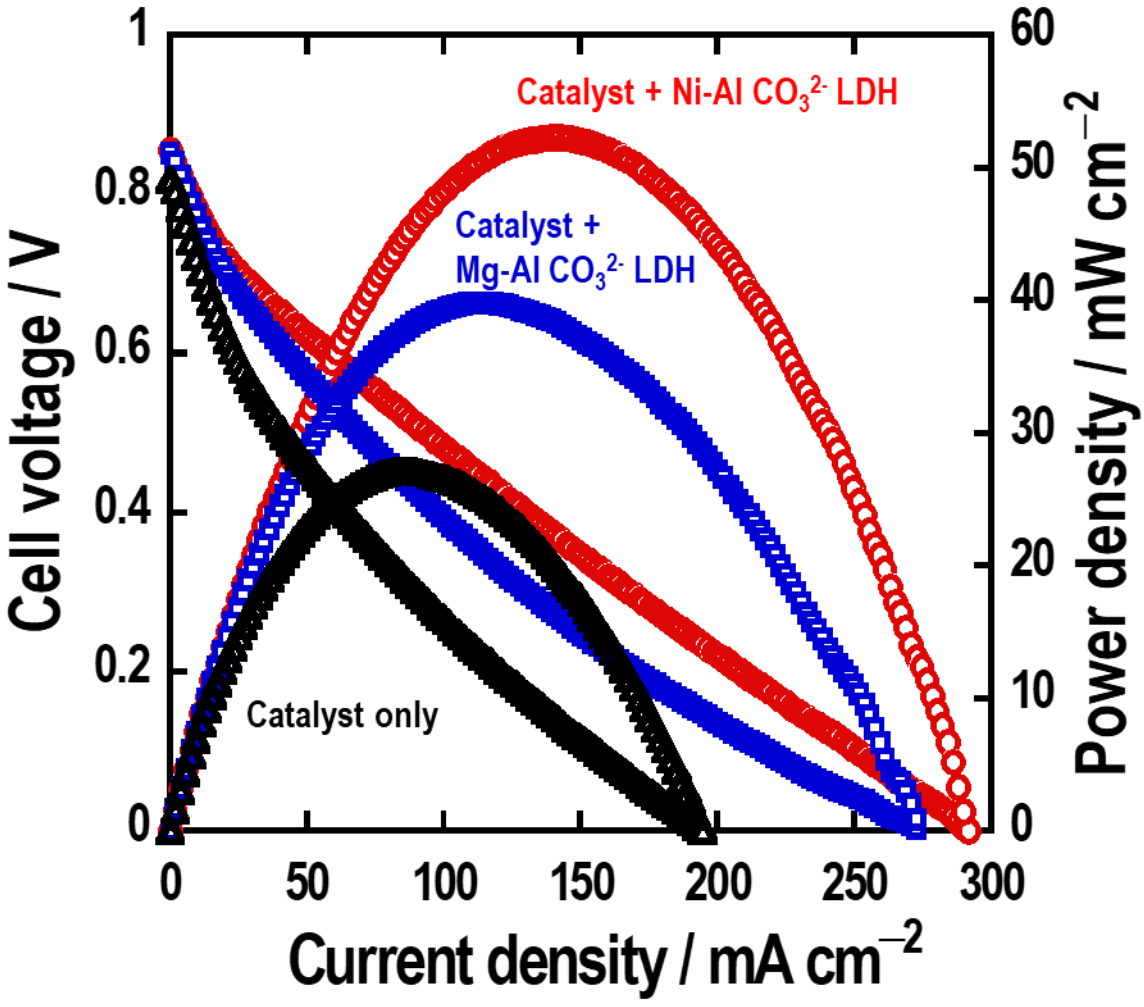

Fig. 3. 3. 3. 6 Performance of the DEFC using the electrodes with LDHs as ionomer or without LDH at 80 ºC.

3.3.4. Evaluation of Zn-Air secondary battery using the AEM-type reversible electrode with Ni-Fe LDH as ionomer

Figure 3.3.4.1 presents the cell performance for the rechargeable zinc–air battery using the reversible air electrodes with or without Ni-Fe CO_3^{2-} LDH as a positive electrode. The cell using the reversible air electrode with Ni-Fe CO_3^{2-} LDH demonstrates a larger charge and discharge current density compared to the cell without Ni-Fe CO_3^{2-} LDH. The result proves a great advantage with respect to improvement of the charge–discharge efficiency and catalyst stability during battery cycling at the constant current density.

To investigate the reversible air electrode stability, a charge–discharge cycle test was performed using the half cell as shown in Fig. 3.3.4.2. A reversible air electrode with Ni-Fe CO_3^{2-} LDH operated stably during 40 cycles. A slight increase of the overpotential is observed over 40 cycles. Because the oxidative decomposition of α-MnO_2 was not confirmed in the experimental potential range, degradation of the reversible air electrode might be accelerated by carbon corrosion [34, 35]. In the steady-state polarization measurement, oxidation and reduction peaks for Ni-Fe CO_3^{2-} LDH decomposition were not observed in the experimental potential range. Consequently, Ni-Fe CO_3^{2-} LDH in the reversible air electrode is expected to remain stable in the reversible air electrode. Transition metals containing LDHs (Ni-Fe CO_3^{2-} LDH) facilitated the ORR and OER in the air electrode with limited influence of CO_2 in the atmosphere. In addition, Ni-Fe CO_3^{2-} LDH exhibits catalytic activity for ORR and OER. Consequently, transition-metal-containing LDHs with mixed conductivity are anticipated as promising materials for use in reversible air

electrodes of rechargeable metal–air batteries.

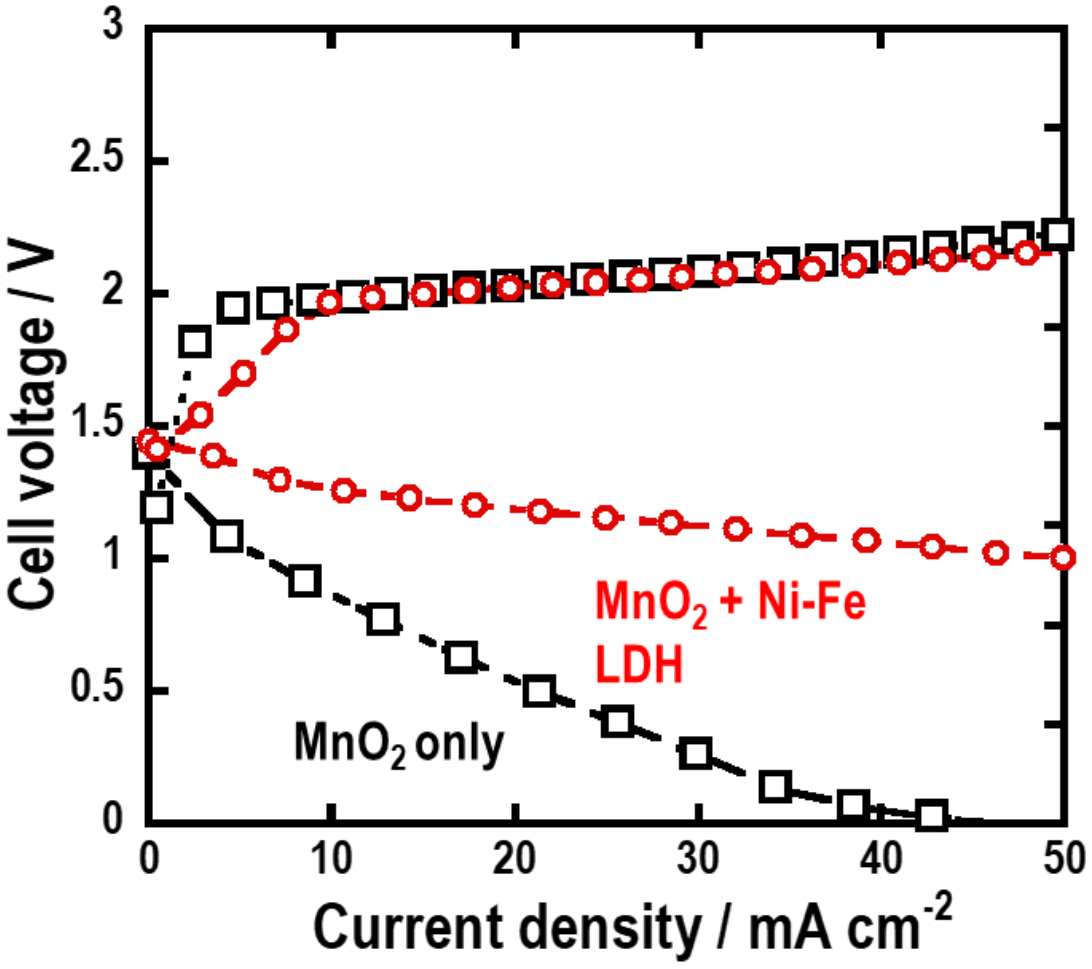

Fig. 3. 3. 4. 1 Performance of the rechargeable zinc–air battery using electrodes with LDH as an ionomer or without LDH, at room temperature.

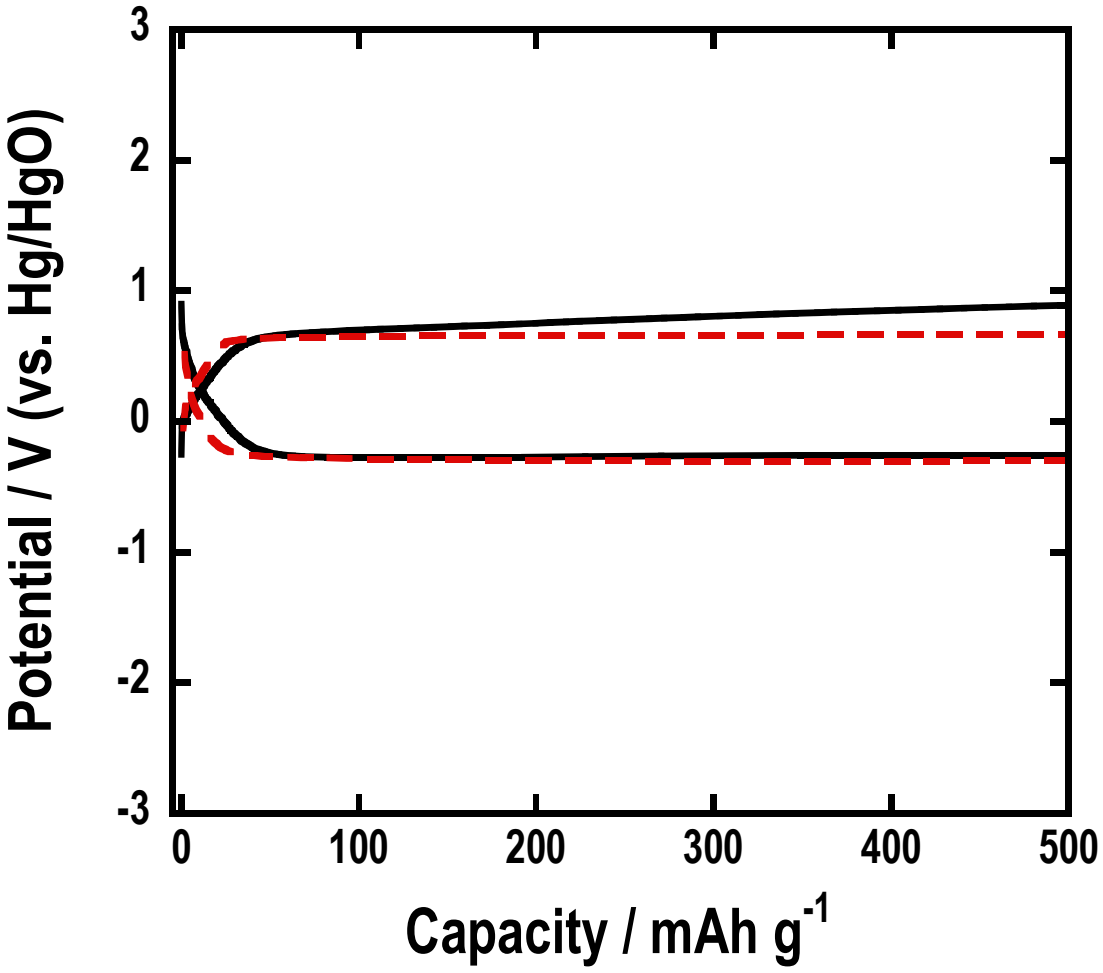

Fig. 3. 3. 4. 2 Charge–discharge cycling performance of the reversible air electrode with Ni-Fe CO_3^{2-} LDH as an ionomer. One discharge and charge is designated as one cycle. The reversible air electrode cycled 40 times.

3.4. Summary of Chapter 3

DEFC using LDHs as electrolyte was fabricated and evaluated the cell performance. The DEFC using LDHs as electrolyte was able to operate under 80% R.H.

Self-standing Mg-Al LDH thin membranes were prepared using a glass paper as support. The H_2-O_2 fuel cell with using the Mg-Al LDH thin membrane as the separator showed high OCV, indicating that Mg-Al LDH thin membrane has high gas barrier property. The H_2-O_2 fuel cell showed higher cell performance compared with the H_2-O_2 fuel cell using the pelletized Mg-Al LDH powder. These results indicate that the glass paper is very effective support for making thin Mg-Al LDH electrolyte membrane.

Ni-Fe CO_3^{2-} LDH showed high hydroxide ion conductivity of the order of 10^{-3} S cm^{-1} and exhibited higher electronic conductivity (7×10^{-5} S cm^{-1}) than that of Mg-Al CO_3^{2-} LDH or Ni-Al CO_3^{2-} LDH. The air electrode using Ni-Fe CO_3^{2-} LDH with high ionic and electronic conductivity showed the best performance of all other air electrodes prepared in this study, indicating that Ni-Fe CO_3^{2-} LDH formed more favorable triple-phase boundary regions and that the electrode reaction in the air electrode was facilitated more effectively. The steady state polarization measurements indicate that Ni-Fe CO_3^{2-} LDH has catalytic activity for ORR and OER. The DEFC using catalytic layer with LDHs and the rechargeable zinc–air battery using the reversible air electrode with Ni-Fe CO_3^{2-} LDH as a positive electrode showed

high performance, and the reversible air electrode of zinc-air rechargeable electrode operated during 40 cycles. These results indicate that the addition of LDHs to catalyst layer hydroxide ion is effective to construction of favorable TPB regions in the catalyst layer. Among various LDHs, Ni-Fe CO_3^{2-} LDH with hydroxide ion conductivity, electric conductivity and catalytic activity is the most promising material as multifunctional ionomer with limited influence of CO_2 for alkaline type batteries.

Reference

[1] J.-S. Lee, S. T. Kim, R. Cao, N.-S. Choi, M. Lie, K. T. Lee, and J. Cho, *Adv. Energy Mater.,* **1** (2011) 34-50.

[2] V. Neburchilov, H. Wang, J. J. Martin, and W. Qu, *J. Power Sources,* **195** (2010) 1271-1291.

[3] A. Ito, L. Zhao, S. Okada, and J. Yamaki, *J. Power Sources,* **196** (2011) 8154-8159.

[4] B. T. Hang, H. Hayashi, S.-H. Yoon, S. Okada, and J. Yamaki, *J. Power Sources,* **178** (2008) 393-401.

[5] C. Li, W. Ji, J. Chen, and Z. Tao, *Chem. Mater.,* **19** (2007) 5812-5814.

[6] Q. Li, and N. J. Bjerrum, *J. Power Sources,* **110** (2002) 1-10.

[7] L. Jorissen, *J. Power Sources,* **155** (2006) 23-32.

[8] M. Chen, L. Wang, H. Yang, S. Zhao, H. Xu, and G. Wu, *J. Power Sources*, **375** (2018) 277-290.

[9] E. Gulzow, and M. Schulze, *J. Power Sources,* **127** (2004) 243-251.

[10] G. Merle, M. Wessling, and K. Nijmeijer, *J. Membrane Sci.,* **377** (2011) 1-35.

[11] K. Matsuoka, Y. Iriyama, T. Abe, M. Matsuoka, and Z. Ogumi, *J. Power Sources,* **150** (2005) 27-31.

[12] S. Gultekin, M. Alsaleh, and A. Alzakri, *Int. J. Hydrogen Energy*, **19** (1994) 181-185.

[13] N. Fujiwara, M. Yao, Z. Siroma, H. Senoh, T. Ioroi, and K. Yasuda, *J. Power Sources*, **196** (2011) 808-813.

[14] A. Kkonovalova, H. Kim, S. Kim, A. Lim, H. S. Park, M. R. Kraglund, D. Aili, J. H. Jang, and H. J.

Kim, *J. Membrane Sci.*, **564** (2018) 653-662.

[15] A. D. Mohanty, S. E. Tignor, J. A. Krause, Y. K. Choe, and C. Bae, *Macromolecules*, **49** (2016) 3361-3372.

[16] H. Sun, Z. Yan, F. Liu, W. Xu, F. Cheng, and J. Chen, *Adv. Mater.,* **32** (2020) 1806326.

[17] Y. Qi, C. Guo, X. Xu, B. Gao, Q. Yue, B. Jiang, Z. Qian, C. Wang, and Y. Zhang, *Sci. Total Environ.*, **715** (2020) 136982.

[18] N. Hirata, K. Tadanaga, and M. Tatsumisago, *Mater. Res. Bull.*, **62** (2015) 1–4.

[19] Z. Gao, J. Wang, Z. Li, W. Yang, B. Wang, M. Hou, Y. He, Q. Liu, T. Mann, P. Yang, M. Zhang, and L. Liu, *Chem. Mater.,* **23** (2011) 3509-3516.

[20] J. H. Lee, J. Chang, J. H. Cha, D. Y. Jung, S. S. kim, and J. M. Kim, *Chem. Eur. J.*, **16** (2010) 8296-8299.

[21] K. Miyazaki, T. Abe, K. Nishio, H. Nakanishi, and Z. Ogumi, *J. Power Sources,* 195 (2010) 6500-6503.

[22] V. A. Paganin, E. A. Ticianelli, and E. R. Gonzalez, *J. Appl. Electrochem.,* 26 (1996) 297-304.

[23] J. M. Song, S. Y. Cha, and W. M. Lee, *J. Power Source,* 94 (2001) 78-84.

[24] L. Mao, D. Zhang, D. Sotomura, K. Nakatsu, N. Koshiba, and T. Ohsaka, *Electrochim. Acta*, **48** (2003) 1015-1021.

[25] T.E. Springer, T. A. Zawodzinski, M. S. Wilson, and S. Gottesfeld, *J. Electrochem. Soc.*, **143** (1996)

587-599.

[26] X. Yuan, H. Wang, J. C. Sun, and J. Zhang, AC impedance technique in PEM fuel cell diagnosis-A review **32** (2007) 4365-4380.

[27] H. Lin, Y. Zhang, G. Wang, and J.-B. Li, *Front. Mater. Sci.* **6(2)** (2012) 142-148.

[28] Y. Wang, D. Zhang, W. Peng, L. Liu, and M. Li, *Electrochim. Acta, **56*** (2011) 5754-5758.

[29] Z. Chen, A. Yu, D. Higgins, H. Li, H. Wang, and Z. Chen, *Nano Lett.* **12** (2012) 1946-1952.

[30] Z. Chen, A. Yu, R. Ahmed, H. Wang, H. Li, and Z. Chen, *Electrochim. Acta*, **69** (2012) 295-300.

[31] H. Arai, S. Muller, and O. Haas, *J. Electrochem. Soc.*, **147** (2000) 3584-3591.

[32] V. R. Choudhary, D. K. Dumbre, B. S. Uphade and V. S. Narkhede, *J. Mol. Catal. A: Chem*., **15** (2004) 129–135.

[33] F. Chang, Y. Su, J. Liang, Z. Tao and J. Chen, *Chem. Mater.*, **22** (2010) 898–905.

[34] F. H. B. Lima, M. L. Calegaro and E. A. TIcianelli, *Electrochim. Acta*, **52** (2007) 3732–3738.

[35] L. Mao, D. Zhang, D. Sotomura, K. Nakatsu, N. Koshiba and T. Ohsaka, *Electrochim. Acta*, **48** (2003) 1015–1021.

Chapter 4

General Conclusions

4. General Conclusions

4.1 General Conclusions

In this dissertation, detailed study of hydroxide ion conduction in layered double hydroxides (LDHs) is described. Application of LDHs to several types of alkaline electrochemical devices is also stated. Because LDHs are inorganic clay materials, these materials and electrochemical devices are expected to have advantages for chemical or thermal stability.

Ionic conduction in LDHs is found to be affected by the composition of LDHs, indicating that the interaction between the host cation layer and the interlayer anions plays important role to the ionic conduction in LDHs. The ionic conduction species of LDHs were evaluated by the water vapor concentration cell. The electromotive force (EMF) of the cell using the anion exchange membrane as well as LDHs is negative. The measured EMF of the cell showed the same trend as the theoretical EMF expected from the Nernst equation. These results prove that the dominant conducting ion species of LDHs are hydroxide ion. Since high hydroxide ion conduction in LDHs need the presence of the absorbed water and interlayer water, the hydroxide ion conduction mechanism is considered to be the Grotthus mechanism using hydrogen bond with water molecules. The investigation of hydroxide ion conduction in LDHs using D_2O showed that the high hydroxide ion conduction in LDHs must be because of not only the attribution of the surface conduction but also the interlayer conduction.

Alkaline-type fuel cells using LDHs as electrolyte were fabricated and evaluated the cell performance.

Direct ethanol fuel cells and H_2-O_2 fuel cells using LDHs as electrolyte were able to operate under 80% R.H. Self-standing Mg-Al LDH thin membrane was prepared using a glass paper as support. The performance of the H_2-O_2 fuel cell using the Mg-Al LDH thin membrane was improved because of the decrease of the electrolyte resistance and the concentration overpotential.

In the air electrode in the half cell, using hydroxide ion conducting LDHs as ionomer, the oxygen reduction reaction (ORR) and oxygen evolution reaction (OER) activities were improved, in comparison with those of the air electrode without LDHs. This indicates that LDHs in the electrodes formed more favorable triple-phase boundary regions and that the electrode reaction in the air electrode was facilitated more effectively. The air electrodes were applied to alkaline-type fuel cells and Zn-air secondary battery. In the Zn-air battery, the air electrode with transition metal containing Ni-Fe CO_3^{2-} LDH as ionomer showed the best performance among all other air electrode.

In conclusion, LDHs intercalated with CO_3^{2-} shows high ionic conductivity under humidifying conditions, and the dominant conducting ion species are hydroxide ions. The ionic conductivity of LDHs were considered to be influenced by the interaction between the host cation layer and the interlayer anion. The interlayer anion and interlayer water, the interlayer water and surface-adsorbed water were considered to be the hydroxide ion conduction pathways. In addition, LDHs can be used as an electrolyte and ionomer for alkaline fuel cells and metal-air batteries, and the use of LDHs can improve the performance of those electrochemical devices.

4.2 Future Prospects

Hydroxide ion conducting LDHs studied in the present study contains carbonate anion in the interlayer, and these LDHs are considered to have high stability against atmospheric CO_2 because LDHs contain carbonate ions in the structure beforehand. The results of each cell performance in the present study do not show any structural or property degradation of LDHs over a long cycle, indicating that LDHs are promising material as a hydroxide ion conductor and a potential solution to the problems of electrochemical devices using alkaline electrolytes.

Further investigation of the factors affecting the electrochemical properties of LDHs will enable us to improve the hydroxide ion conductivity and design the material as a multifunctional material, which will further expand the range of electrochemical device applications using alkaline electrolytes.

List of appended publications

[1] D. Kubo, K. Tadanaga, A. Hayashi, M. Tatsumisago, *J. Electroanal. Chem.*, **671** (2012) 102-105.

[2] D. Kubo, K. Tadanaga, A. Hayashi, M. Tatsumisago, *J. Power Sources*, **222** (2013) 493-497.

[3] D. Kubo, K. Tadanaga, A. Hayashi, M. Tatsumisago, *J. Mater. Chem. A*, **1** (2013) 6804.

[4] D. Kubo, K. Igarashi, S. Ishiyama, N. C. Rosero Navarro, A. Miura, M. Higuchi, K. Tadanaga, *J. Ceramic. Soc. Jpn.* **127** (2019) 788-792.

[5] D. Kubo, K. Tadanaga, A. Hayashi, M. Tatsumisago, *Front. Mater.*, **7** (2020) 117.

[6] A. Miura, S. Ishiyama, D. Kubo, N. C. Rosero Navarro, K. Tadanaga, *J. Ceramic. Soc. Jpn.* **128** (2020) 336-339.

[7] D. Kubo, K. Tadanaga, A. Hayashi, M. Tatsumisago, *J. Electrochem. Sci. Techn* (2021) Accepted for publication.

Acknowledgement

I would like to gratefully and sincerely thank me supervisors Prof. Masahiro Tatsumisago and Prof. Akitoshi Hayashi, Associate Prof. Akira Miura, Associate Prof. Nataly Carolina Rosero-Navarro for their instruction, understanding and patience during my studies, and also for the help they gave me for my dissertation work. In particular, I would like to thank Prof. Kiyoharu Tadanaga for his direct guidance throughout this study. I am grateful to have this opportunity to purse for my PhD in this group. Prof. Tadanaga gave me important instructions in the research and taught me how to be an engineer but also as an independent thinker

I would like to thank laboratory members in Osaka Prefecture University and Hokkaido University for help my study and understanding my thought. Finally, I would like to give my gratitude to may parents, my wife, my brother and my son for their love, encouragement and support.